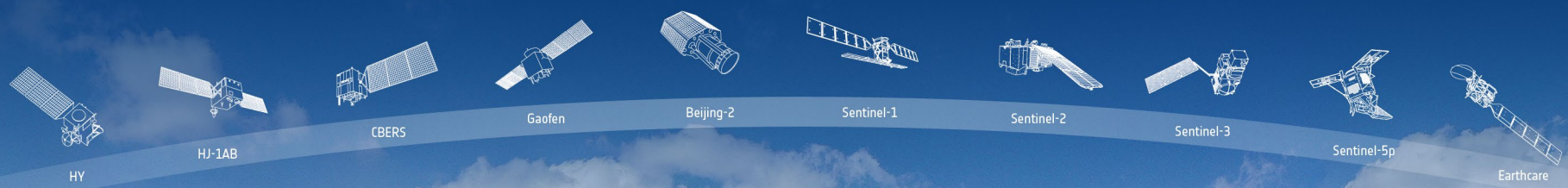
CSTEC
中国科学技术交流中心
China Science and Technology Exchange Center

esa
→ THE EUROPEAN SPACE AGENCY



2025 DRAGON 6 SYMPOSIUM

14-18 JULY 2025

PROJECT ID. 95348

COLLABORATIVE DETECTION OF SURFACE DEFORMATIONS ASSOCIATED WITH NATURAL PHENOMENA AND ANTHROPOGENIC ACTIVITIES WITH MULTI-SOURCE REMOTE SENSING DATA







WEDNESDAY 16 JULY 2025

ID. 95348

PROJECT TITLE:
COLLABORATIVE DETECTION OF SURFACE DEFORMATIONS ASSOCIATED WITH NATURAL PHENOMENA AND ANTHROPOGENIC ACTIVITIES WITH MULTI-SOURCE REMOTE SENSING DATA

PRINCIPAL INVESTIGATORS: CRISTIANO TOLOMEI & LIANHUAN WEI

CO-AUTHORS: S. SALVI, C. BIGNAMI, E. TRASATTI, G. VENTURA, S. ATZORI, F. CINTI, S. LIU, M. AO, G. LIU, X. PAN, X. SHAN, J. YI

PRESENTED BY: CRISTIANO TOLOMEI & LIANHUAN WEI

Project Objectives

- Deformation monitoring associated with industrial activities and volcano dynamics in Liaoning province (Northeastern China). We plan to continue the successful research activities of the previous DRAGON projects, focusing on monitoring the ground motion dynamics at the Fushun open-pit mine and Changbaishan volcano.

- New study site, the **Songliao Basin**, where ground movements caused by both natural phenomena and anthropogenic activities can be investigated using the ground deformation signature. The Songliao Basin is a Mesozoic-Cenozoic continental basin characterized by relevant oil and gas extraction activities.

The main research objectives of the project are to detect, quantify, and study the time evolution of the ground deformation measured using remote sensing data, and characterize the processes and the hazards due to:

- ✓ The anthropogenic activities at Fushun and Songliao Basin (mining and oil/gas extraction);
- ✓ The volcano dynamics at the Changbaishan volcano.

For these sites, we will delimit the areas exposed to natural and anthropogenic ground deformation, providing the necessary information for the prevention and damage mitigation actions to be planned by local Authorities.

Project Objectives

- The methodology to achieve such objectives is the joint analysis of multi-source EO and in situ data: InSAR time-series (MT-InSAR), VNIR optical data series, seismic data, geochemical data, oil/gas extraction data, and their modeling.
- The obtained ground deformation patterns will be validated with leveling and GNSS data, where available, and through cross-comparison between ascending and descending MT-InSAR results.
- We expect to be able to monitor the phenomena using imagery from different sensors and frequency bands (e.g., C, X-, and L-band).

- Based on the detected surface deformation and the possible correlation between volcanic and seismic activity, we will model the degassing and magmatic activity in the volcanic areas and explore the correlation between deformation and the amount of oil/gas extraction or fluid pumping in deep wells.

- The proposed research also plans to carry out training and the exchange of young scientists. For this purpose, we will use funding from this project and will apply for funding at different agencies in both countries.

Data used (first year)

To reach the proposed objectives, the following data were used:

- Sentinel-1 (C-Band) data along both the ascending and descending orbit for the Songliao Basin;
- Sentinel-1 (C-Band) data along both the ascending and descending orbit for the Fushun area.

- In a short time, new SAR data will be used to improve and update the already retrieved results over the study areas.
- Data from COSMO-SkyMed (X-Band) and ALOS-2 (L-Band) will be selected and analyzed.

In-situ data for the Changbaishan volcano

12 real-time transmission seismic stations;

12 real-time transmission GPS stations;

Strain meter:100 samples/s;

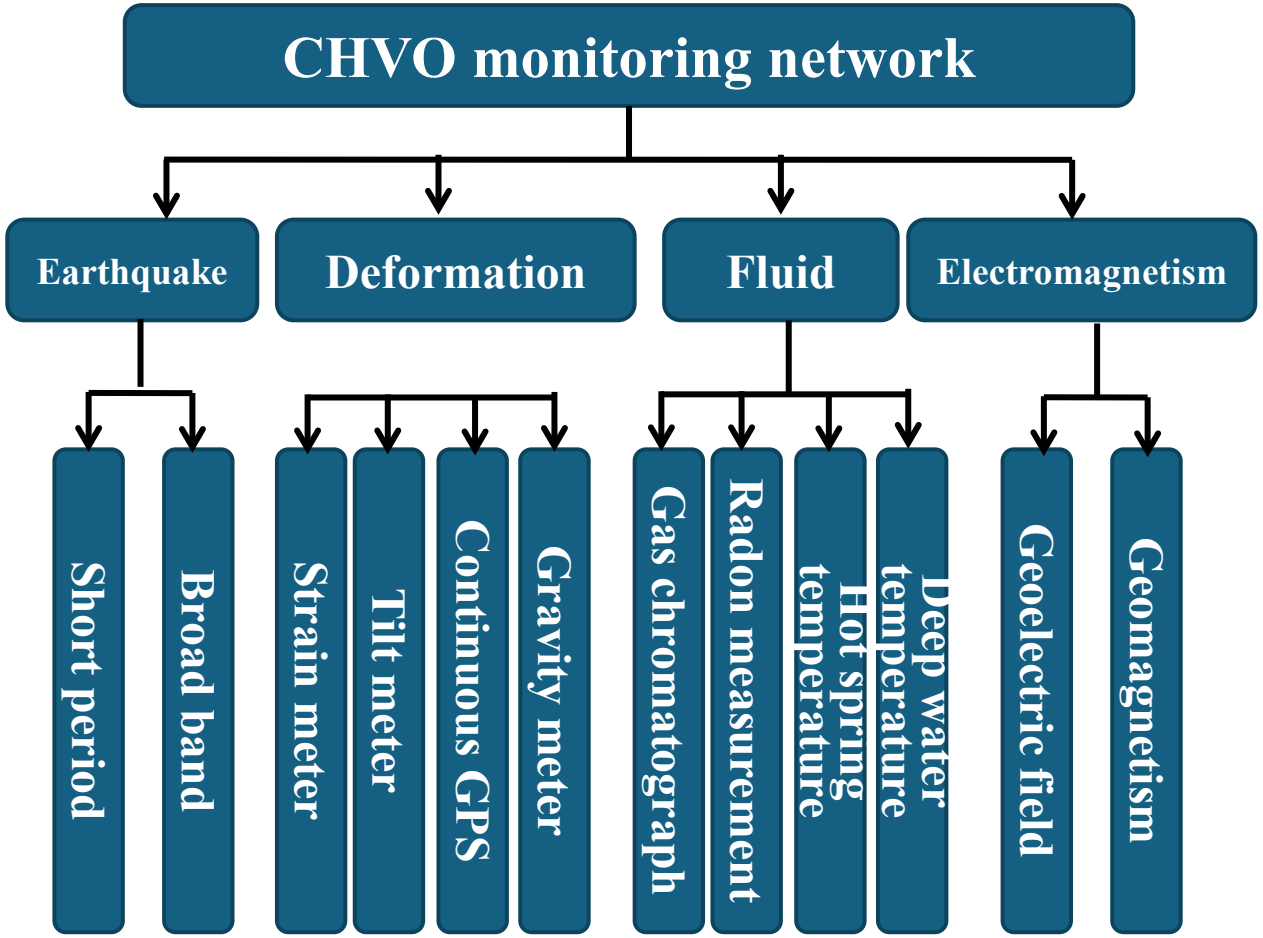
Tilt meter:100 samples/s;

Gravity meter:100 samples/s;

Gases, Radon and Temperatures:2-3 samples/month;

Geoelectric: 100 samples/s;

Geomagnetism: 4 samples/day



Data will be processed

To achieve the project objectives, the following data will be used:

- Archived SLC images from Sentinel-1 IW TOPSAR acquisition mode covering the study areas are required for InSAR time-series analysis.
- The surface morphology changes will be observed through Sentinel-2 MSI Level 1c/2a optical images, and by combination with the MT-InSAR processing outcomes, to analyze the ground deformation from multiple lines of sight.
- High-resolution optical data GF-6 and GF-2 will be used for surface change detection caused by industrial activities and/or geological disasters.

Project Scheduling

The research goals of this proposal will be achieved through the following 3 work phases:

Work phase 1 would last about 9 months.
Preparation of remote sensing data and preprocessing of the data stacks will be carried out. A field survey of the study areas will be conducted, measuring, taking pictures, and analyzing features as evidence of surface changes. A quality check of the seismic, geodetic, and geochemical data available in Changbaishan will be performed to ensure the reliability of the datasets.

Work phase 2: Work phase 2 would last about 24 months.
During this phase, the activities in WP1 and WP2 would be carried out on the following research topics:

i) the retrieval of the 2.5D deformation of landslides from multi-orbit InSAR time-series using precise DEM from laser scanning for slope motion measurements;
ii) the processing, analysis, and fusion of the InSAR products obtained from multiple orbits and different sensors, aiming to retrieve precise 2.5D surface displacement for Changbaishan volcano. Moreover, the derived MT-InSAR data will be validated and interpreted taking into account the seismic, geodetic, and geochemical data for the Changbaishan volcano;
iii) the volcanic modeling with Mogi, Okada, or combined more complex models will be conducted to reveal the magmatic, hydrothermal, geomorphological, and tectonic mechanisms of deformation in the area.

Project Scheduling

Work phase 3 would last about 18 months.

During this work phase, the research team will cooperate to analyze and interpret the relations between the multiple disasters with data modeling and assimilation techniques. A simple model linking two disasters would be initiated at first. Other disasters will be integrated one by one, and eventually refining the previous model could reveal the complex geological processes affecting the study areas, and the causes of surface deformation will be analyzed and explained at the geodynamic level. The refined model could also be used to forecast when and how disasters might happen in the future, providing technical support for disaster prevention and damage reduction.

Dragon 6 EO Data Delivery

Data access (list all missions and issues if any). NB. in the tables please insert cumulative figures (since June 2024) for no. of scenes of high bit rate data (e.g. S1 100 scenes). If data delivery is low bit rate by ftp, insert “ftp”

ESA /Copernicus Missions	No. Scenes
1.Sentinel-1 (Songliao Basin)	742
2.Sentinel-1 (Kambalny volcano)	4
3.Sentinel-1 (Guobu landslid)	160
4.Sentinel-1 (Hainan Province)	220
5.	
6.	
Total:	1126

Issues:We use Sentinel-1 SAR imagery to monitor ground deformation in various geological hazard scenarios. It allows us to detect and track landslides, surface subsidence, mining-induced deformation, and volcanic activity with high temporal resolution. The data supports both long-term monitoring and rapid assessment in complex terrains.

ESA Third Party Missions	No. Scenes
1. COSMO.SkyMed (to be requested)	110
2. ALOS-2 (to be requested)	30
3.SRTM-1 DEM	
4.ALOS World DEM	
5.	
6.	
Total:	140

Issues: With high resolution and all-weather imaging capabilities, Sentinel-1 enables precise deformation monitoring of mining areas using Synthetic Aperture Radar pixel offset tracking and Interferometric SAR (InSAR) techniques. By capturing millimeter-scale ground displacement, it effectively detects subsidence, fault activity, and slope instability in open-pit mines. These data support real-time hazard warning, resource management, and environmental impact assessment, particularly in rugged or hard-to-access terrain.

Chinese EO data	No. Scenes
1.GF-5A/B	20
2.GF-2	6
3.	
4.	
5.	
6.	
Total:	26

Issues:The hyperspectral sensor onboard Gaofen (GF) offers high spectral resolution and wide coverage, enabling detailed identification of surface materials. In mineral exploration, GF data can be used to detect spectral anomalies, identify alteration zones, and distinguish lithological and structural features. It is particularly effective in recognizing ore-related minerals such as muscovite, chlorite, and pyrite, making it valuable for resource surveys, prospecting, and mineral prediction. GF enhances the informatization and automation of exploration, especially in areas with complex terrain or limited field access.

European Young Scientists contributions in Dragon 6

Name	Institution	Poster title	Contribution including period of research
TBD in the 2nd yr	INGV		

Chinese Young Scientists contributions in Dragon 6

Name	Institution	Poster title	Contribution including period of research
Xiaosong Feng	Northeastern University	Phase Gradient Rate-Constrained Minimum Cost Flow Method for Accurate Phase Unwrapping in Large Gradient Deformation Fields	This study proposes the PGR-MCF method, which improves phase unwrapping in high-gradient deformation areas by integrating phase gradient rate constraints into the unwrapping path. The method enhances deformation monitoring accuracy and shows strong adaptability across various InSAR scenarios.
Xiangben Zhang	Northeastern University	Debris flow risk assessment via numerical simulation: A case study in Northeast China	This comprehensive approach effectively generated debris flow risk maps and potential building damage degrees in the absence of detailed building damage information, providing valuable insights for debris flow risk assessment in the eastern Liaoning region.

Overview of Chinese YSs research

ESA-MOST Dragon Cooperation
2025 Dragon 6 Symposium
14–18 July 2025 | Qingdao, China

Phase Gradient Rate-Constrained Minimum Cost Flow Method for Accurate Phase Unwrapping in Large Gradient Deformation Fields (Project ID: 95348)

Xiaosong Feng[1], Lianhuan Wei[1], Meng Ao[1] , Yian Wang[1], Christian Bignami[2], Xiangben Zhang[1], Shiliu Wang[1]

1. School of Resources and Civil Engineering, Northeastern University, Shenyang, 110819, China
2. Istituto Nazionale di Geofisica e Vulcanologia, Rome, 00143, Italy

Abstract: Phase unwrapping (PU) is a key step in Synthetic Aperture Radar Interferometry (InSAR) that significantly affects the accuracy of ground deformation measurements. While widely used, many conventional PU methods—including Minimum Cost Flow (MCF), Snaphu, and recent deep learning-based models such as CNN SQD-LSTM and PUNet—tend to struggle in areas with large deformation gradients. In such regions, the underlying assumption of phase continuity is often violated, leading to substantial phase unwrapping errors and underestimation of deformation signals. To address this limitation, this study proposes a Phase Gradient Rate Constrained Minimum Cost Flow (PGR-MCF) method. The core idea is to incorporate the Phase Gradient Rate (PGR), derived by stacking and fusing time series differential interferograms, as a constraint to guide the unwrapping path construction in the MCF framework. First, high-coherence pixels are selected based on a predefined threshold, and a Delaunay triangulation network is constructed to represent spatial connectivity. The PGR is then calculated to highlight areas of strong deformation gradient. During the unwrapping process, arcs corresponding to high PGR values (above a preset threshold) are assigned zero weight, thereby avoiding paths through regions where phase continuity is likely disrupted. This enables the unwrapping path to propagate from stable, low-gradient regions into the deformation field, improving the reliability of the unwrapped results. Simulation experiments demonstrate that the PGR-MCF method achieves correct unwrapping in 99.5% of high-gradient deformation regions, significantly outperforming conventional methods. In a real-world case study of the Guobu landslide, the proposed method reduces the Root-Mean-Square Error (RMSE) between InSAR-derived and Global Navigation Satellite System (GNSS)-measured deformation time series by over 69% compared to other test methods. Moreover, PGR-MCF produces a more spatially continuous deformation velocity field and successfully delineates internal deformation fronts that are blurred or missed by other algorithms, enhancing the interpretability of landslide dynamics. A major advantage of the PGR-MCF method lies in its ability to effectively handle interferograms with large temporal and spatial baselines, thereby increasing the number of usable unwrapped interferograms for time series analysis. This not only improves deformation monitoring accuracy but also facilitates the use of longer historical SAR datasets for retrospective studies. Additionally, the method is fully data-driven and does not rely on external datasets or prior deformation models, ensuring strong adaptability to different InSAR datasets and diverse environmental conditions. It is particularly suitable for rapid disaster response or large-scale deformation mapping where ancillary data may be unavailable. While the method exhibits robust performance in complex deformation scenarios, one limitation is that unwrapping may fail when the entire boundary of a region exhibits high PGR, preventing reliable phase connection. Nevertheless, the PGR-MCF approach represents a significant advance in phase unwrapping techniques, offering enhanced accuracy, reliability, and physical interpretability in deformation monitoring, particularly in regions with large deformation gradients.

PGR-MCF

In the PGR-MCF method, high-coherence points are first selected based on a predefined coherence threshold (e.g., 0.4), and these points are used to construct a Delaunay triangulation network, thereby establishing an initial spatial framework. Subsequently, the **central difference method** is employed to calculate the **phase gradient** of the interferograms at each pixel. By stacking the phase gradients derived from multiple interferograms, a more stable and accurate **Phase Gradient Rate (PGR)** is obtained.

During processing, two types of phase gradient rates are distinguished based on the temporal baseline: one is obtained from interferograms with the shortest temporal baseline (**short baseline phase gradient rate**), and the other is obtained from all available interferograms (**full temporal baseline phase gradient rate**). Experimental results indicate that the full temporal baseline phase gradient rate generally exhibits a higher signal-to-noise ratio compared to the short baseline phase gradient rate. However, in regions with high deformation gradients, a phenomenon known as "**Gradient Decrease**" may occur. When the unwrapping network crosses pixels affected by this phenomenon, the gradient difference along that arc segment is erroneously estimated, which in turn leads to **phase unwrapping errors.**

To address this issue, the PGR-MCF method employs an intelligent weight suppression strategy. Specifically, the maximum value of the **full temporal baseline phase gradient rate** is established as a threshold; **when the short baseline phase gradient rate of a pixel exceeds this threshold, the weight of the arc segment containing that pixel is set to zero.** This measure effectively excludes areas prone to gradient disappearance, **thereby guiding the unwrapping network to preferentially enter the interior of the deformation field from regions with lower deformation gradients**. As a result, the overall reliability of the phase unwrapping process is significantly enhanced. The technical flowchart of PGR-MCF is shown in Fig 1.

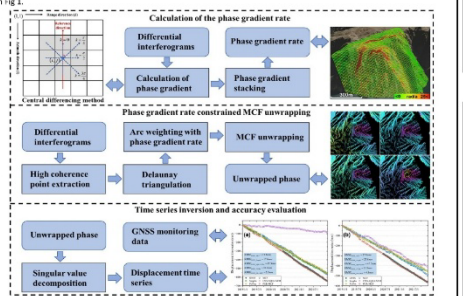


Fig.1 PGR-MCF Technical Flowchart

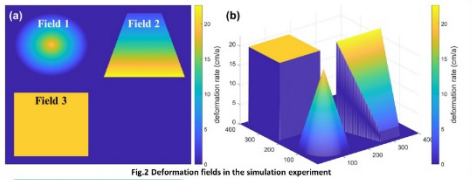


Fig.2 Deformation fields in the simulation experiment

Simulation Experiment

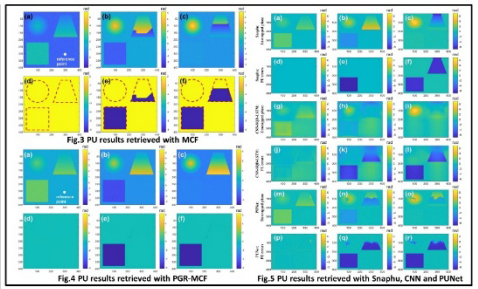


Fig.3 PU results retrieved with MCF

Fig.4 PU results retrieved with PGR-MCF

Fig.5 PU results retrieved with Snaphu, CNN and PUNet

Real Data Experiment (Guobu Landslide)

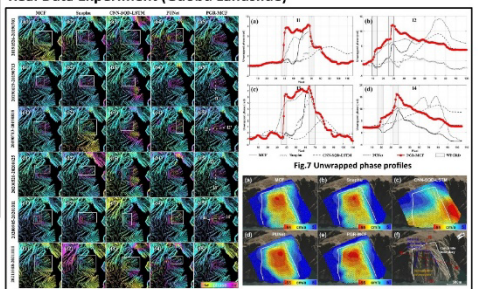


Fig.7 Unwrapped phase profiles

Fig.6 PU results obtained by different unwrapping methods

Fig.8 Deformation rates of the Guobu landslide

After phase unwrapping with different methods, the deformation rates of the Guobu landslide were estimated using Stacking-InSAR (Fig. 8). Positive values indicate movement toward the satellite, and negative values indicate movement away. Among all methods, PGR-MCF yields a more spatially continuous velocity field, especially capturing motions exceeding -50 cm/a in the landslide center—significantly higher than MCF and Snaphu, which underestimate deformation. CNN-SQD-LSTM underestimates the left-side motion and introduces artifacts on the right, likely due to over-smoothing. While PUNet retains the overall pattern, it loses detail in core and edge areas. Notably, PGR-MCF clearly identifies an internal deformation front (blue line in Fig. 8(f)), which is blurred or missed by other methods. This internal boundary separates zones of differing kinematics, offering valuable insights into the landslide's failure mechanism and progression.

Conclusions

This study proposes PGR-MCF, a novel phase unwrapping method that incorporates phase gradient rate (PGR) information into the minimum cost flow framework. By constraining the unwrapping path with PGR extracted from stacked differential interferograms, the method effectively avoids high-gradient regions and improves phase recovery accuracy. Simulation results show over 99.5% correct unwrapping in synthetic high-gradient scenarios. In the Guobu landslide case, PGR-MCF reduces the RMSE between InSAR and GNSS deformation time series by over 69% compared to other methods. PGR-MCF is fully data-driven, requiring no external datasets or prior models, and performs reliably on interferograms with large temporal and spatial baselines. This increases the number of usable interferograms for time series analysis, enhancing deformation monitoring accuracy and robustness. Overall, PGR-MCF offers a reliable and adaptable solution for phase unwrapping in complex deformation areas, with strong potential for improving InSAR-based geohazard analysis.

ESA-MOST Dragon Cooperation
2025 Dragon 6 Symposium
14–18 July 2025 | Qingdao, China

Debris flow risk assessment via numerical simulation: A case study in Northeast China Project ID:95348

Xiangben Zhang[1], Lianhuan Wei[1], Xiaosong Feng[1], Yaxin Xu[1], Meng Ao[1*], Christian Bignama[2], Cristiano Tolomei[2], Shiliu Wang[1], Xingyu Pan[1], Yuan Dai[1], Shanjun Liu[1], Ramesh P. Singh[3]

1. School of Resources and Civil Engineering, Northeastern University, Shenyang, 110819, China
2. Istituto Nazionale di Geofisica e Vulcanologia, Rome, 00143, Italy
3.Schmid College of Science and Technology, Chapman University, Orange, CA, 92866, USA

Abstract: The mountainous area of eastern Liaoning is the only debris flow disaster-prone zone in Northeast China. Houses in this area are predominantly built downstream in the valley along river sides, which are highly susceptible to debris flow hazards. This is particularly evident in the Wudaogou region, where multiple debris flow disasters have occurred during the past decades. Field investigations have revealed a significant presence of loose solid materials within the basin, posing a high risk of re-triggering debris flows. To identify potential hazard zones and estimate the damage conditions of buildings under debris flow impacts, numerical simulation using MassFlow and finite element modeling are conducted in this study. In the absence of detailed building damage information, we established a response model of buildings subjected to debris flows, achieving a quantitative risk assessment for debris flow disasters in the Wudaogou area. Using finite element modeling, we constructed a numerical model for the single-story brick-wood structures widely present in rural Northeast China. By quantifying the building damage degrees under different debris flow intensity combinations using inter-story drift angles, we developed a building vulnerability function correlating structural damage with debris flow intensity indices. This vulnerability function is then used to estimate the degree and extent of building damage in the study area under potential debris flows. Experimental results show that such buildings exhibit poor disaster resistance. When the debris flow velocity exceeds 6 m/s or the debris flow thickness reaches 1 m, these buildings are likely subjected to moderate or higher degrees of damage. When the velocity reaches 10 m/s or the thickness exceeds 2 m, these buildings face a risk of collapse. Statistical data on the evaluation results reveal that the most severe damage occurs to buildings located on the eastern side of the river and near the gully mouth. Simulation of the most extreme debris flow disaster scenario shows that 57% of the buildings would suffer varying degrees of damage, and 14% would be destroyed by the debris flow. This comprehensive approach effectively generated debris flow risk maps and potential building damage degrees in the absence of detailed building damage information, providing valuable insights for debris flow risk assessment in the eastern Liaoning region.

Study area and Methodology

The study area is the Wudaogou debris flow basin in Fushun City, Northeast China, located at the junction of the Liaohe Plain and the Changbaishan Mountains, within the northeastern segment of the North China seismic belt. The region features complex terrain, geology, and a warm temperate monsoon climate. Average annual precipitation is about 900 mm, mostly concentrated in summer. On August 16, 2013, a major debris flow triggered by 276 mm of daily rainfall mobilized ~100,000 m³ of debris, causing severe damage near the basin outlet.

The basin covers ~0.73 km², comprising five tributaries and one main gully. The main gully is 1051 m long and ~90 m wide at the base, with a V-shaped profile and side slopes under 30°. The source area contains ~1 m of loose soil and soft rock, with sparse vegetation, creating favorable conditions for debris flow initiation. Residential buildings in the depositional area are mainly single-story brick–wood structures with brick strip foundations and timber roofs. Due to weak materials and lack of structural columns, these buildings are highly vulnerable to debris flow impact.

The methodology adopted in this study involves four key steps, and the work flow is shown in Fig.1. The first step entails preparation of the various input data required for numerical simulation. The parameters related to debris flow characteristics comprise debris flow density and blockage coefficient, etc. the hydrological parameters involve the peak debris-flow discharge and debris flow hydrograph. Parameters related to the materials of debris flows include friction coefficient and turbulence coefficient. In the second step, the debris flow disaster intensity (flow thickness and flow velocity) and impact range under different rainfall conditions is simulated using MassFlow, generating the debris flow hazard map. The third step involves construction of the numerical model for the buildings in the study area based on field investigations and structural design information. Using these models, a vulnerability function for the buildings under debris flow hazards are then established. Finally, according to the vulnerability function, the debris flow hazard map obtained via numerical simulation is converted to building vulnerability and classified into different damage degrees.

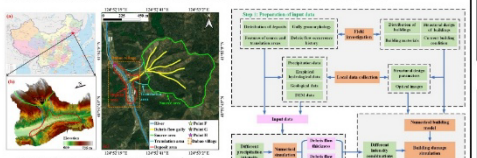


Fig.1 Study area of Wudaogou Debris Flow (WDF)

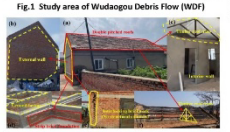


Fig.2 Structural design of a single-story brick-wood structure

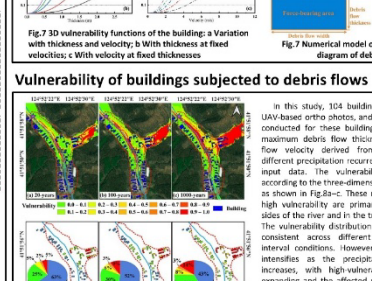


Fig.3 The methodological framework adopted in this study

Construction of the vulnerability function for buildings

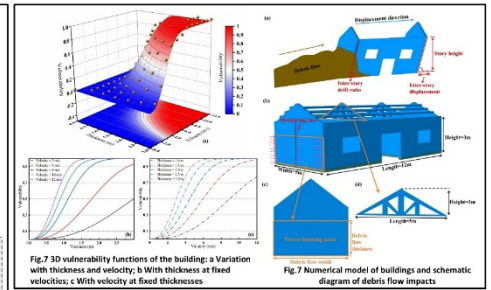


Fig.7 3D vulnerability functions of the building: a Variation with thickness and velocity; b With thickness at fixed velocities; c With velocity at fixed thicknesses

Fig.7 Numerical model of buildings and schematic diagram of debris flow impacts

Vulnerability of buildings subjected to debris flows

Fig.8 Distribution of building damage under different precipitation recurrence intervals

In this study, 104 buildings are extracted from the UAV-based ortho photos, and vulnerability assessment is conducted for these buildings. In the assessment, the maximum debris flow thickness and maximum debris flow velocity derived from the simulations under different precipitation recurrence intervals were used as input data. The vulnerability values are retrieved according to the three-dimensional vulnerability function, as shown in Fig.8a–c. These maps show that areas with high vulnerability are primarily distributed along both sides of the river and in the translation area of the WDF. The vulnerability distribution patterns remain relatively consistent across different precipitation recurrence interval conditions. However, the overall vulnerability intensifies as the precipitation recurrence interval increases, with high-vulnerability areas (red zones) expanding and the affected range widening. This aligns with the pattern that the debris flow intensity increases significantly with longer precipitation recurrence intervals. Since the vulnerability values vary for the same building at different locations, the maximum vulnerability value inside the building area is taken as the building's vulnerability value considering the worst-case scenario. Finally, according to the thresholds provided in Table 1, the vulnerability of the buildings is categorized into four levels (Fig.8d–f). The results indicate that the buildings near the gully outlet suffer from the most severe damage. Buildings on the western side of the river shows relatively lower levels of damage because of the higher elevation. The pie charts shown in Fig.15d–f record the area of damage to buildings under different precipitation recurrence intervals. And, the number of buildings at different damage levels under different precipitation recurrence intervals are shown in Table 8. An integrated analysis on the pie charts and Table 6 reveals consistent patterns. As the precipitation recurrence interval increases, both the area and the number of buildings experiencing complete damage increase significantly.

Debris flow simulation results

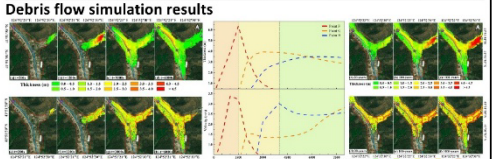


Fig.4 Dynamic process of the WDF under 1000-years precipitation recurrence interva

Fig.5 Dynamic variations of the thicknesses and velocities at different locations

Fig.6 Debris flow thickness and velocity under different rainfall scenarios

Table 1 Statistics on the damage degrees and damage areas of the buildings in WDF

Precipitation recurrence interval(years)	Debris flow area(m²)	Number of buildings at different damage levels				
		Complete	Severe	Moderate	Minor	No damage
20	42635.83	4	6	6	21	68
100	52556.32	7	8	8	32	52
1000	62131.01	14	7	9	30	43

Conclusions

The physical vulnerability of single-story brick-wood structures, which are widely distributed in northeastern China, has rarely been discussed in debris flow risk assessments. In this study, a comprehensive vulnerability assessment for buildings affected by debris flows in the Wudaogou area is conducted through numerical simulations. The study focuses on constructing a numerical building model and simulating the variation process of debris flows. Unlike many previous studies that primarily aim at quantifying vulnerability functions for different scales of debris flows, this study emphasizes determining damage levels based on the physical response characteristics of buildings under debris flow impacts. The relationship between debris flow intensity data (e.g., debris flow thickness and velocity) and vulnerability indices is characterized and statistically analyzed based on building damage process simulations.

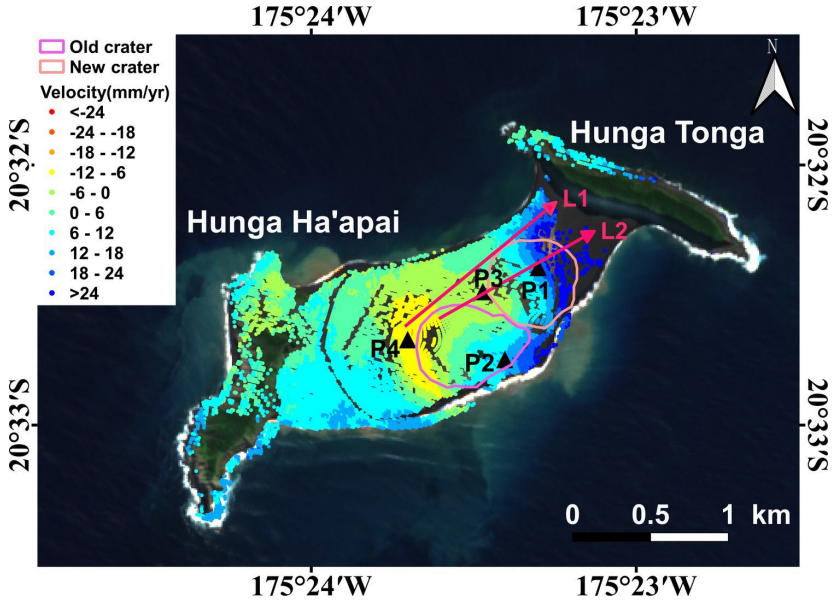
Retrieved results

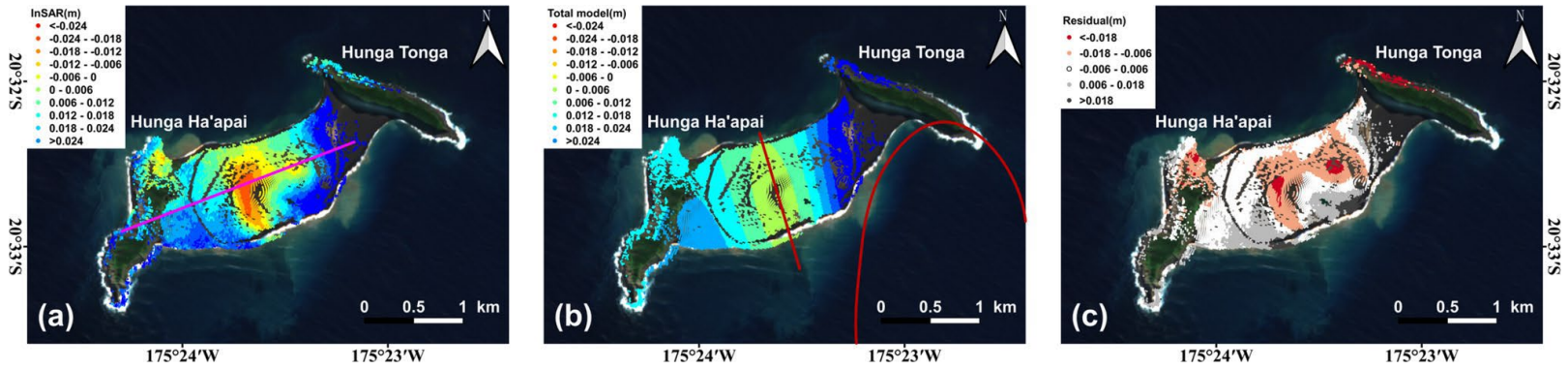
In the first year of the project, the European and Chinese teams have performed:

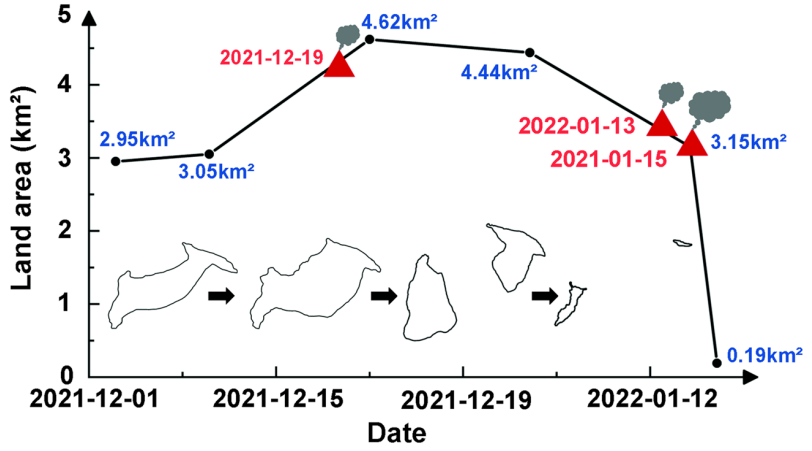
- A deep investigation of the Hunga-Tonga volcano eruption by means of the SBAS technique using S1 data;
- Update of the Fushun and analysis using InSAR techniques up to 2024 through S1 data;
- Completion of the Fushun pit mine study by using a new approach based on the **multi-temporal Offset Tracking technique (RS-POT)**;
- A preliminary investigation and interpretation of the Songliao Basin outcomes by using MT-InSAR technique (SBAS) and S-1 data.

Overview of the retrieved results

- On December 19, 2021, the Hunga Tonga-Hunga Ha'apai (HTHH) submarine volcano in the Tonga-Kermadec island arc initiated a new eruptive phase that lasted for approximately 1 month after 7 years of dormancy. A large-scale submarine explosive eruption occurred on 15 January 2022, The eruption completely upset the landscape of the island and triggered a tsunami in the Pacific Ocean.
- To reveal the evolution process of the 2021–2022 eruptive sequence of HTHH, three Sentinel-2A optical images, two Planet SkySat optical images, and 44 SAR C-band descending orbit Sentinel-1A images were collected.
- The MT-InSAR cumulated displacements are employed in an inversion framework using the VSM tool.
- The spheroid lies at 5000-m depth, its major axis (a =3500 m) is N-S oriented, and the minor axes are b =c=1000 m.
- The second source we include in the model is the dike that fed the eruption (Okada 1985). It is NNW-SSE oriented (strike equal to 15° from North counterclockwise), dip=90°.



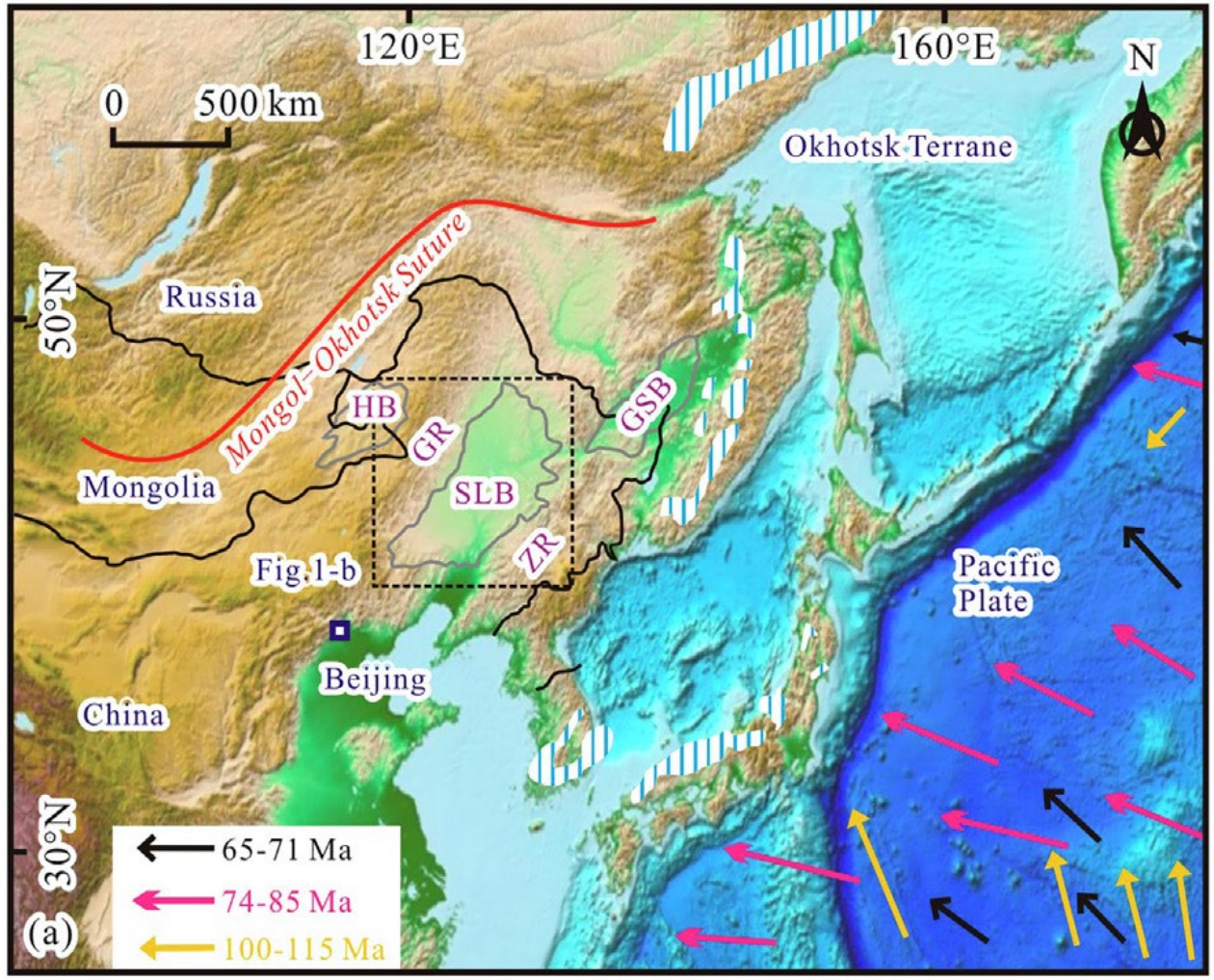




(Wei et al., Bulletin of Volcanology, 2025)

Overview of the retrieved results

Songliao basin (SLB) - NE China

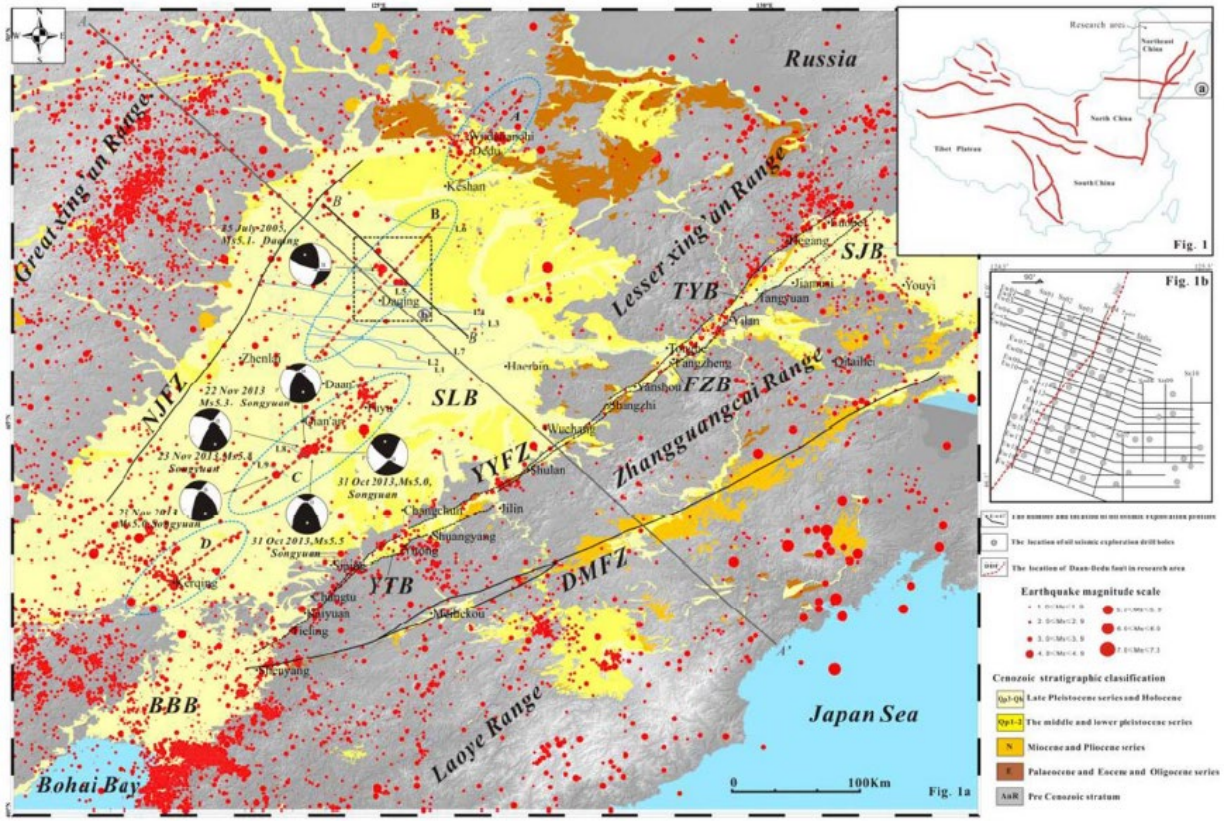


The **Songliao Basin** is one of the largest Mesozoic–Cenozoic continental sedimentary basins in East Asia.
The basin underwent three major evolutionary stages:

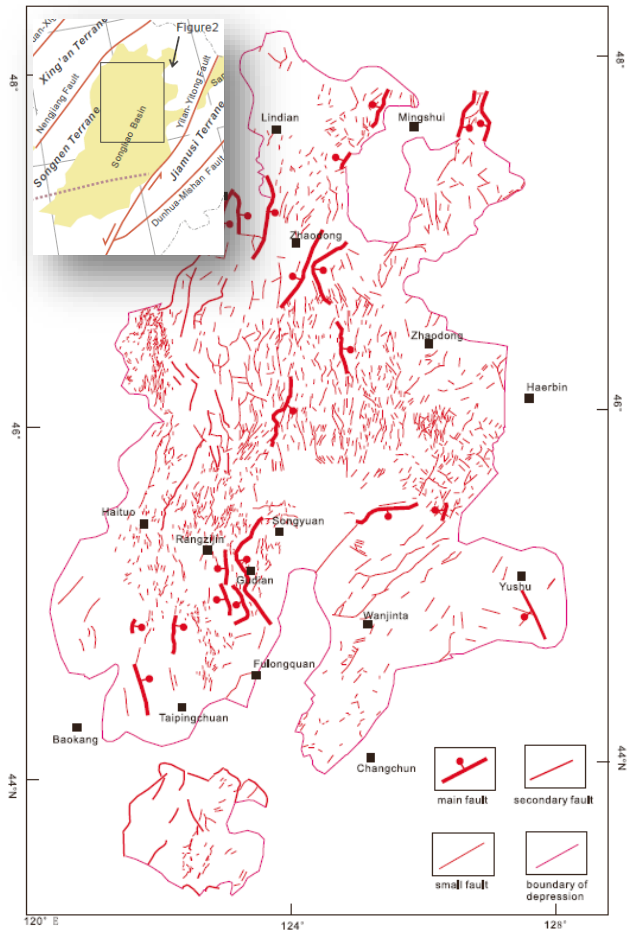
- **Rift Stage (Late Jurassic–Early Cretaceous)**: This phase involved intense faulting and volcanic activity, leading to the development of graben structures and thick volcanic-sedimentary sequences.
- **Post-rift Thermal Subsidence Stage (Late Cretaceous)**: The basin experienced thermal subsidence, allowing for the accumulation of vast lacustrine sediments, including oil-rich shales making the basin a major hydrocarbon reservoir.
- **Tectonic Inversion and Uplift (Paleogene to Present)**: Compressional forces related to the dynamics of the pacific plate led to structural inversion and uplift influencing hydrocarbon migration and entrapment.

Overview of the retrieved results

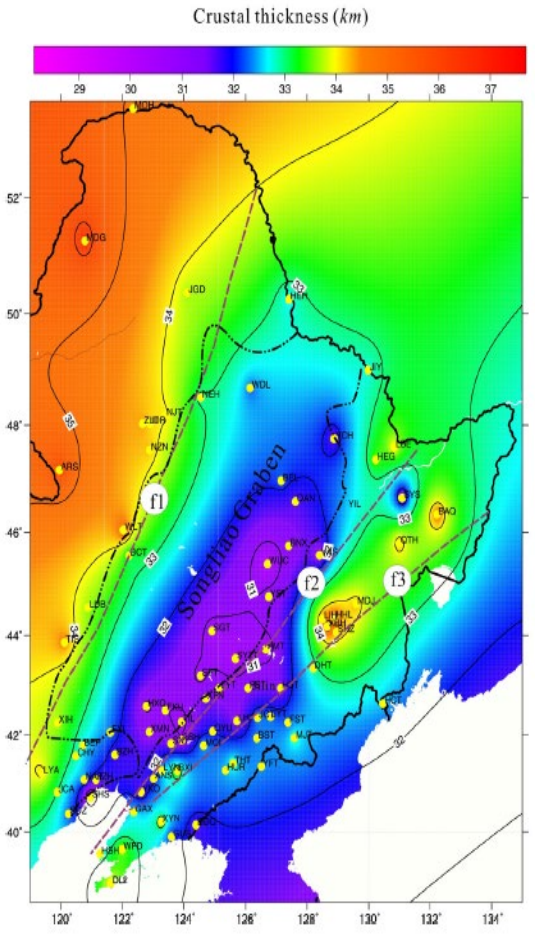
Songliao sedimentary basin Seismicity (maximum Magnitude 6.2)



Faults from seismic lines

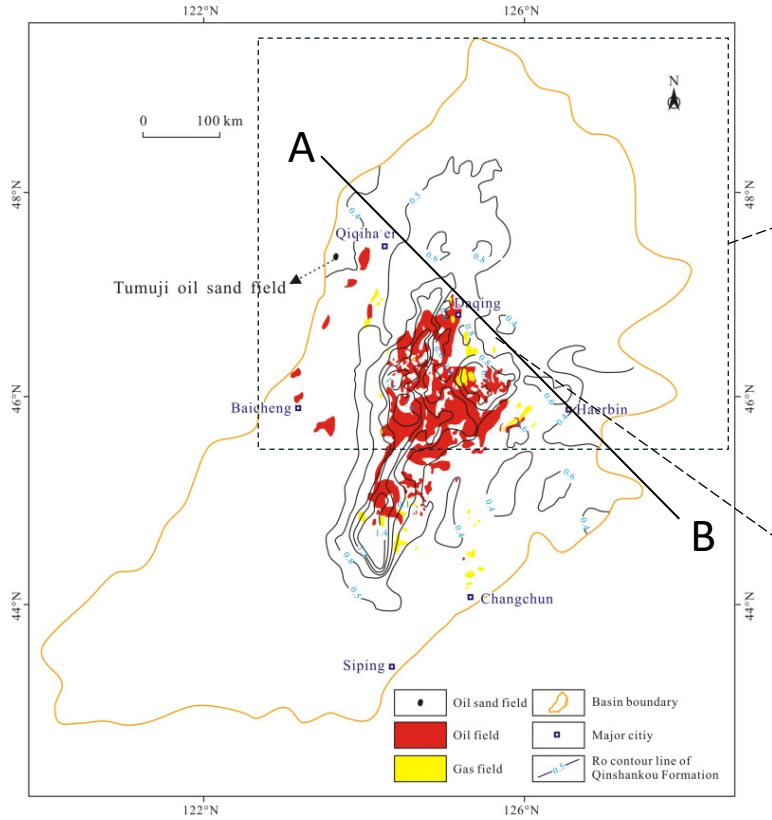


Crustal thickness

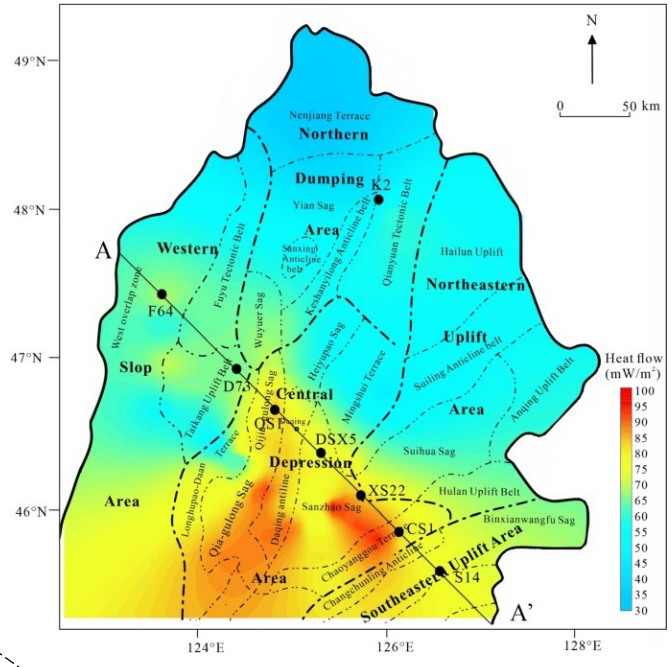


Overview of the retrieved results

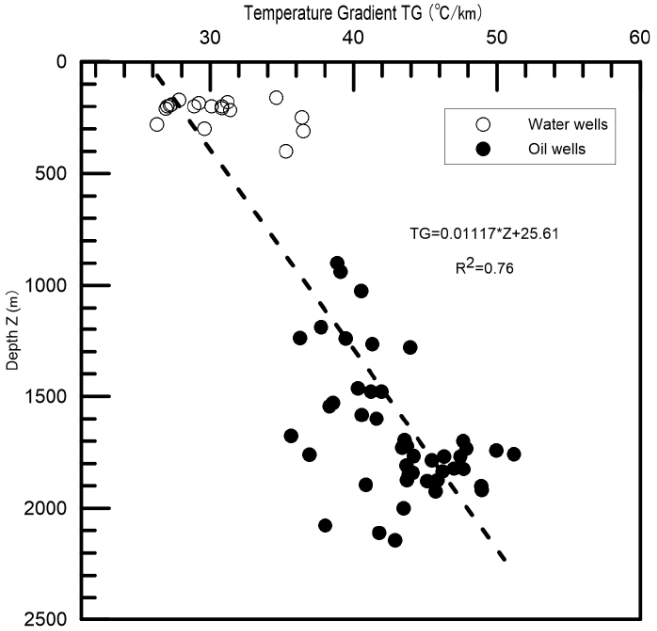
Songliao Basin Oil and Gas field and Daqing field

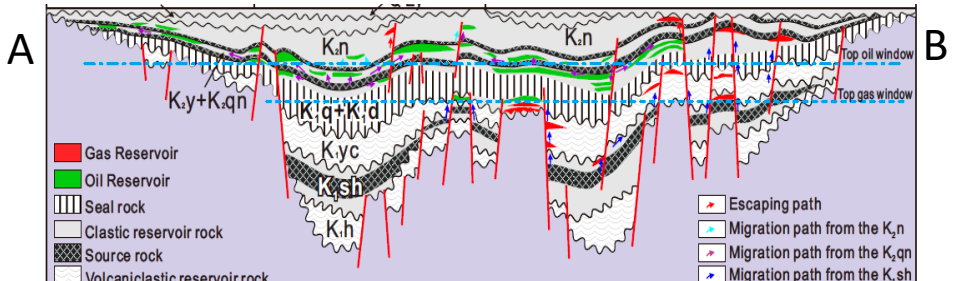


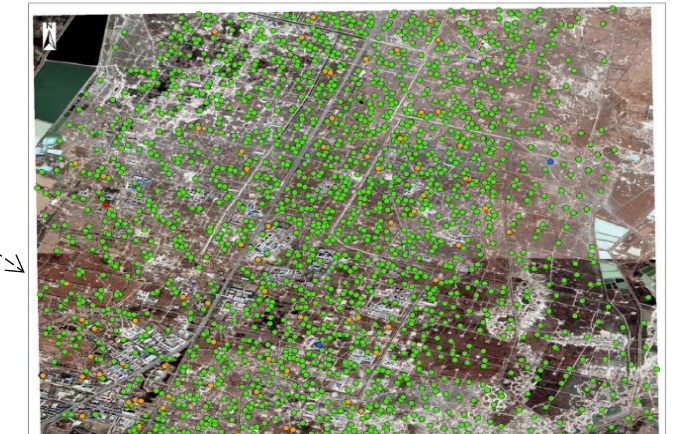
Heat flow



Temperature Gradient







Daqing Oil field consists of hundreds of wells

Overview of the retrieved results

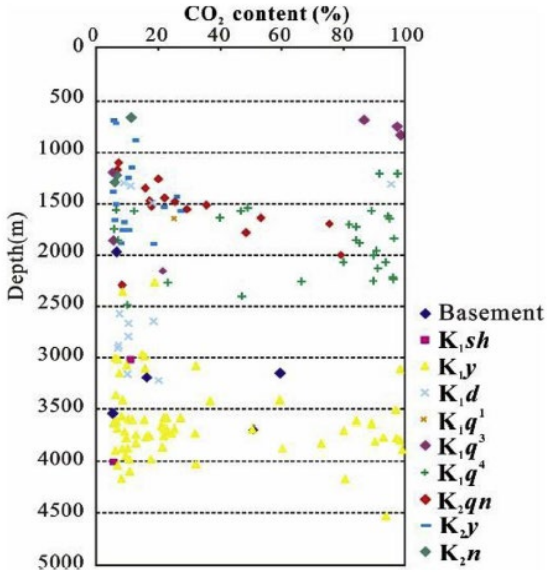
Passive Degassing at Daquing oil field

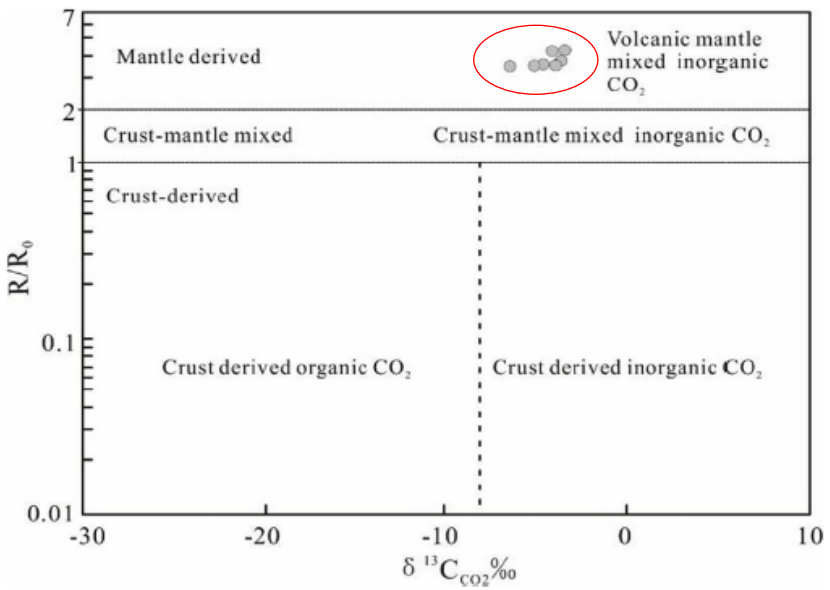
Most of the Daquing deep wells contains significant amount of carbon dioxide of magmatic origin probably released from the mantle because of the reduced crustal thickness

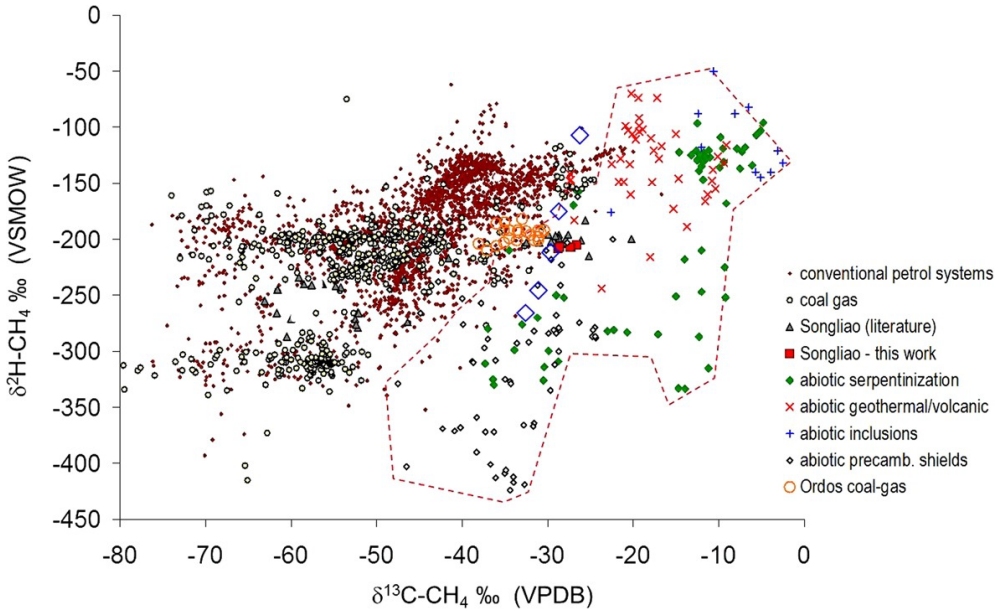
Most of the Daquing deep wells also contains methane of thermogenic origin related to high heat flow

CO_2

CH_4

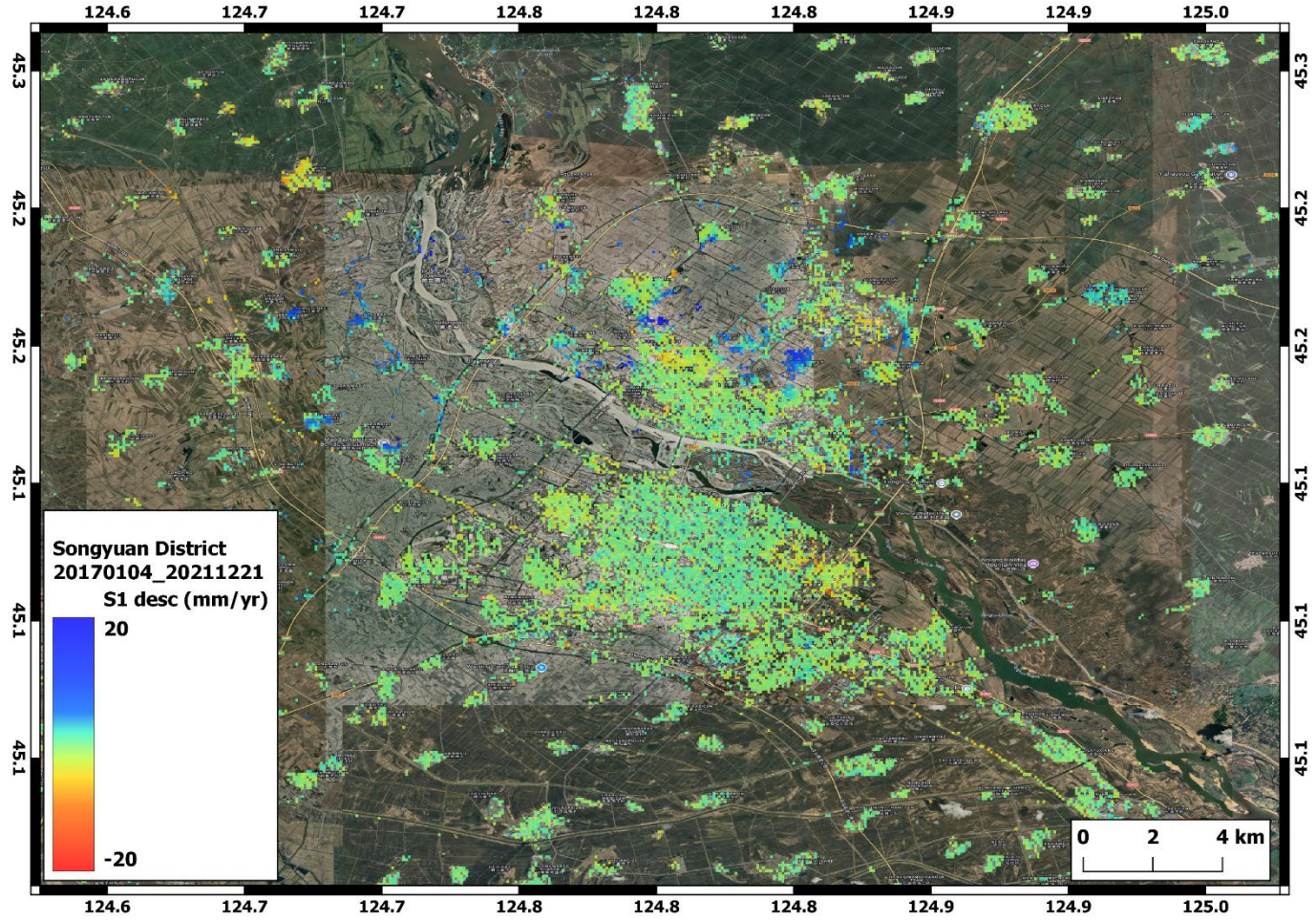






Overview of the retrieved results

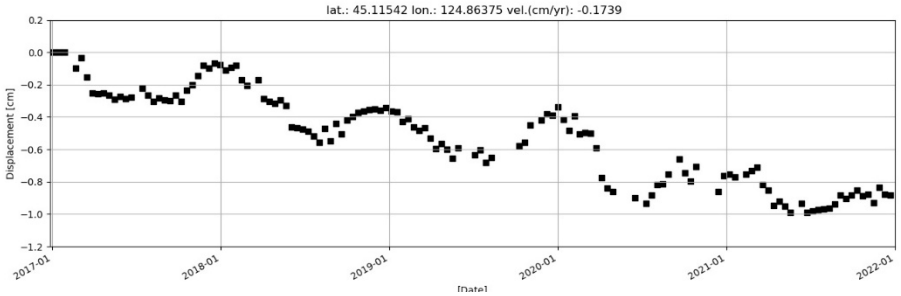
Retrieved deformation in the Songyuan City area (Songlaio Basin)

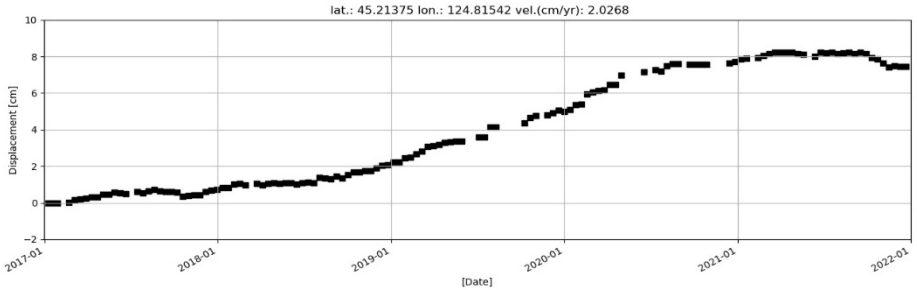


SBAS-InSAR using Sentinel-1 images in the temporal period Jan. 2017 – Dec. 2021.

Time series surface deformation results of Songyuan City district area.

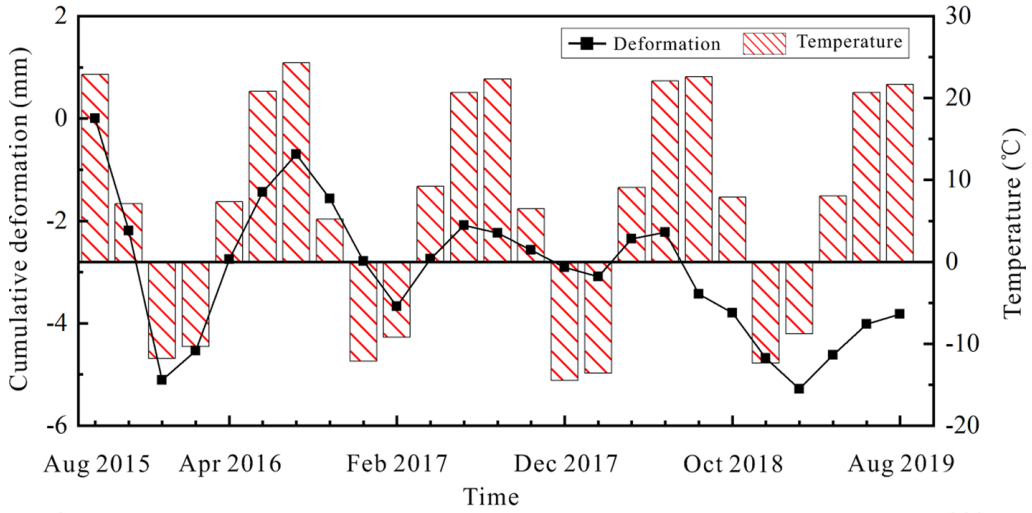
- Deformation shows a sort of annual cyclical “subsidence-uplift” motion with a subsidence trend.
- Maximum cumulative uplift observed in the oil production area.

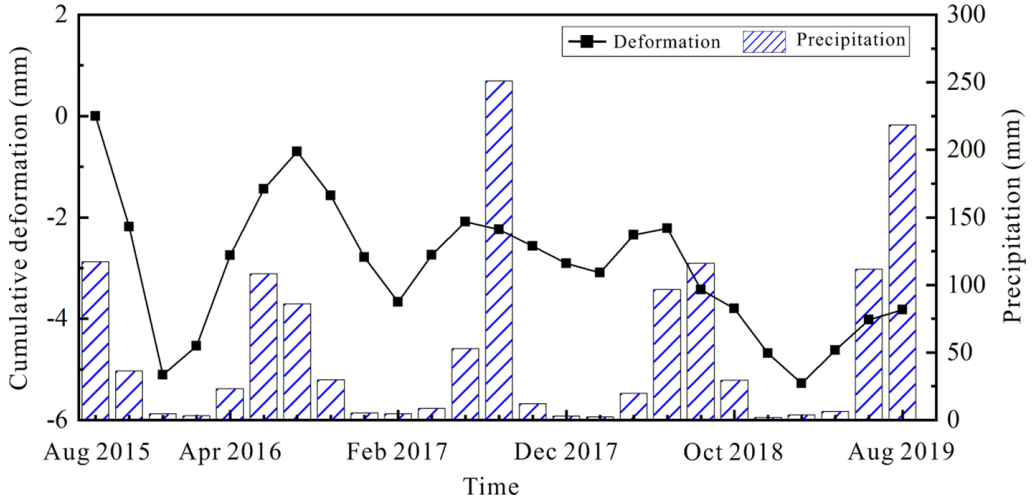




Overview of the retrieved results

Previous studies on deformation in the Songlaio Basin focused on the Songyuan City area





SBAS-InSAR using Sentinel-1 images as the data source

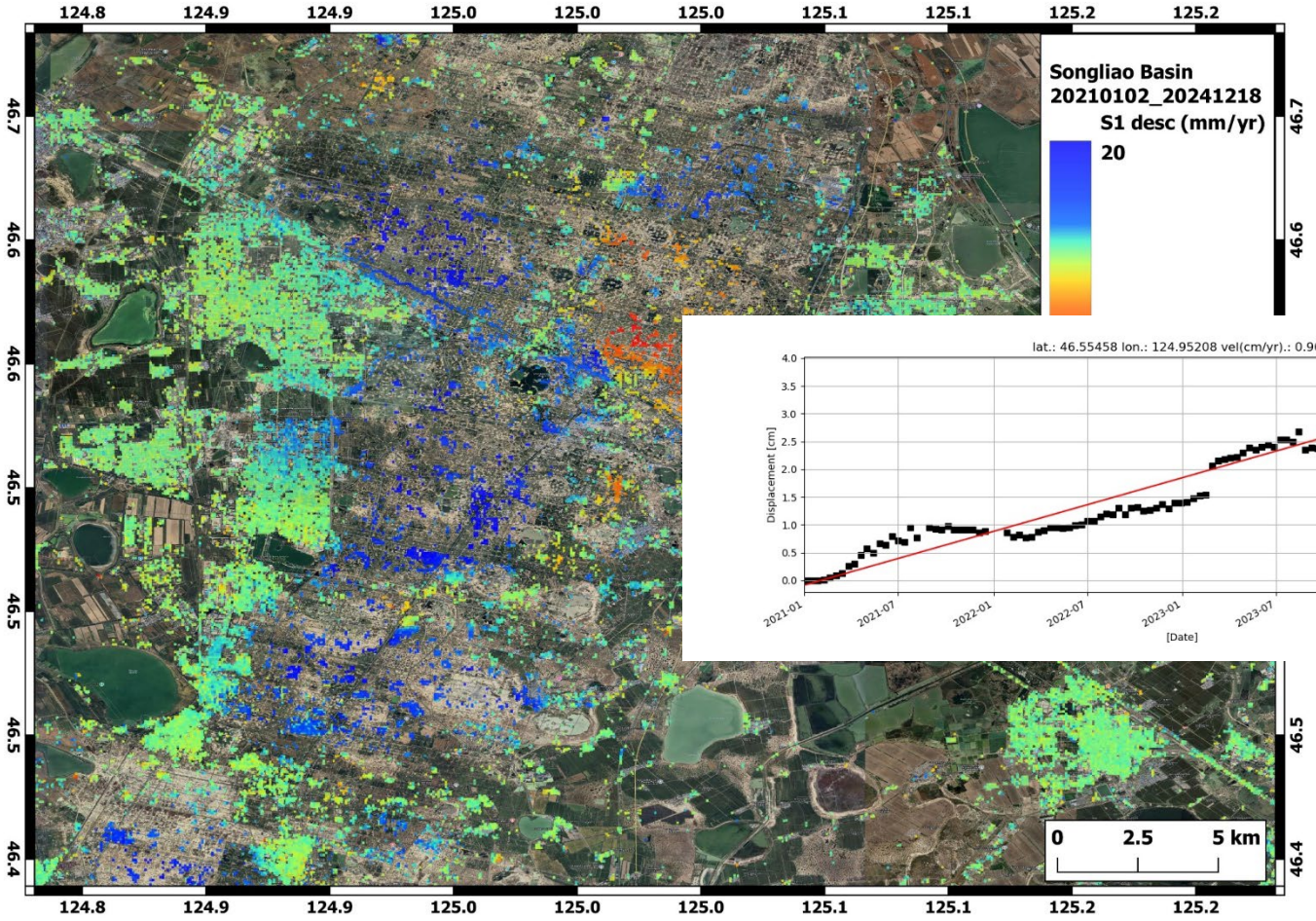
Time series surface deformation results of Songyuan City from August 2015 to August 2019.

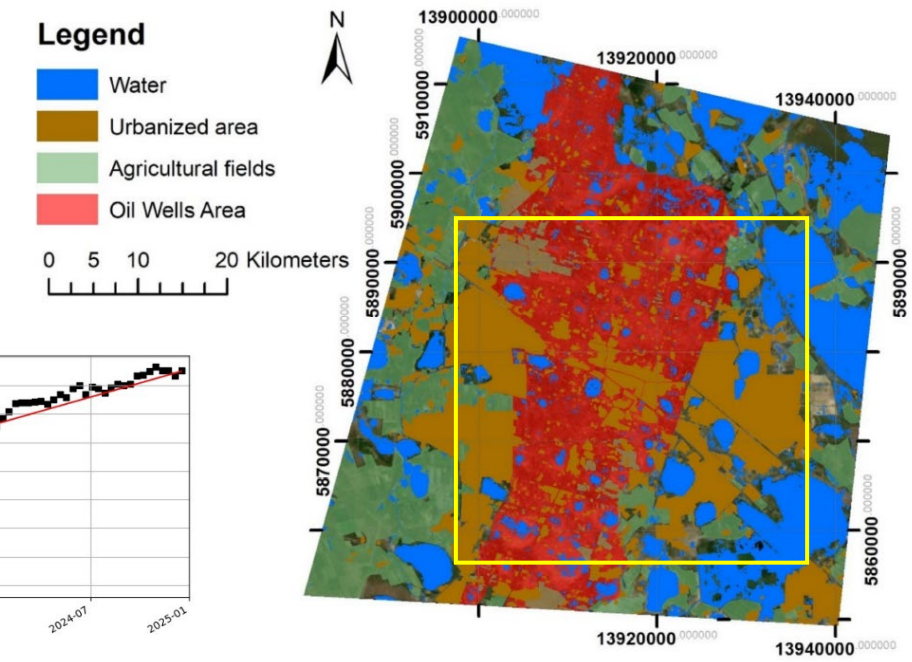
- Deformation shows an annual cyclical “subsidence-uplift” change.
- Maximum cumulative subsidence observed in the oil production area

Ding et al., 2023 Journal of the Indian Society of Remote Sensing https://doi.org/10.1007/s12524-023-01746-5

Overview of the retrieved results

Preliminary analysis of the ground deformation at Daquing oil field





Data show that every ton of crude oil produced in the oil field area, 2-3 tons of water collected from the neighboring areas (the water basins and the city) need to be re-injected and there are 36 879 m3/yr of oil polluted wastewater.

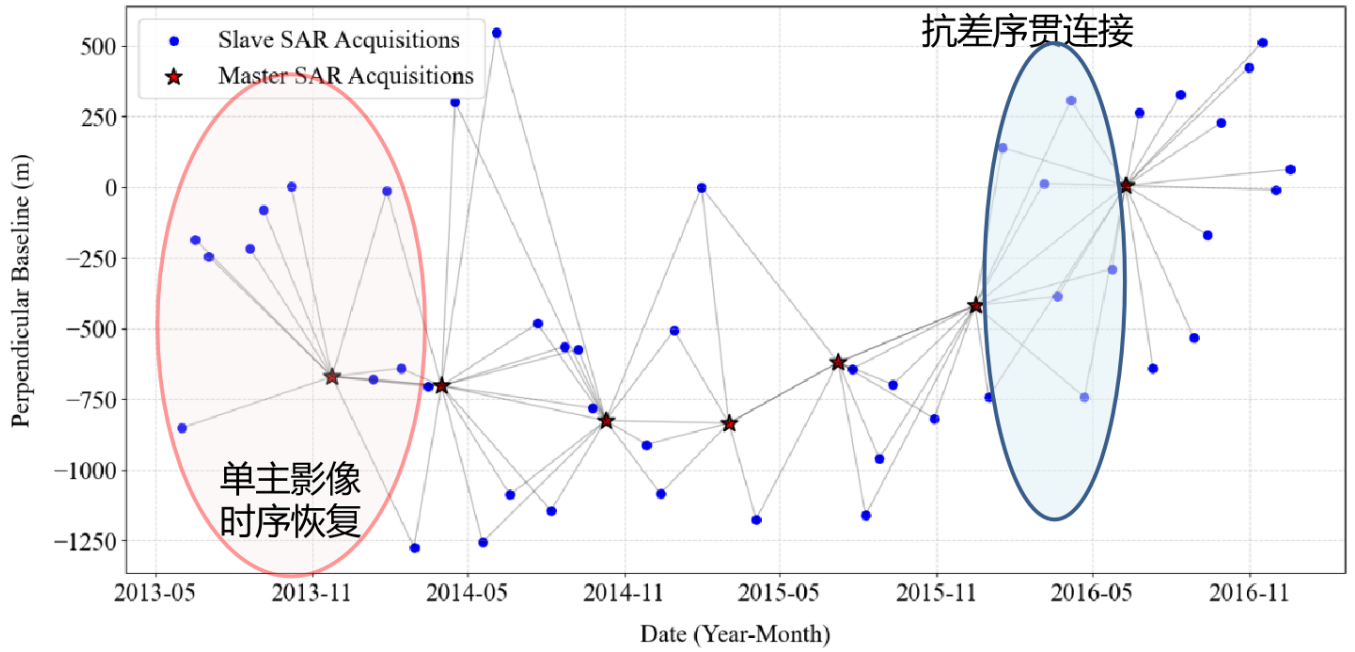
This implies the occurrence of pollution phenomena related to oil extraction activities and water injection

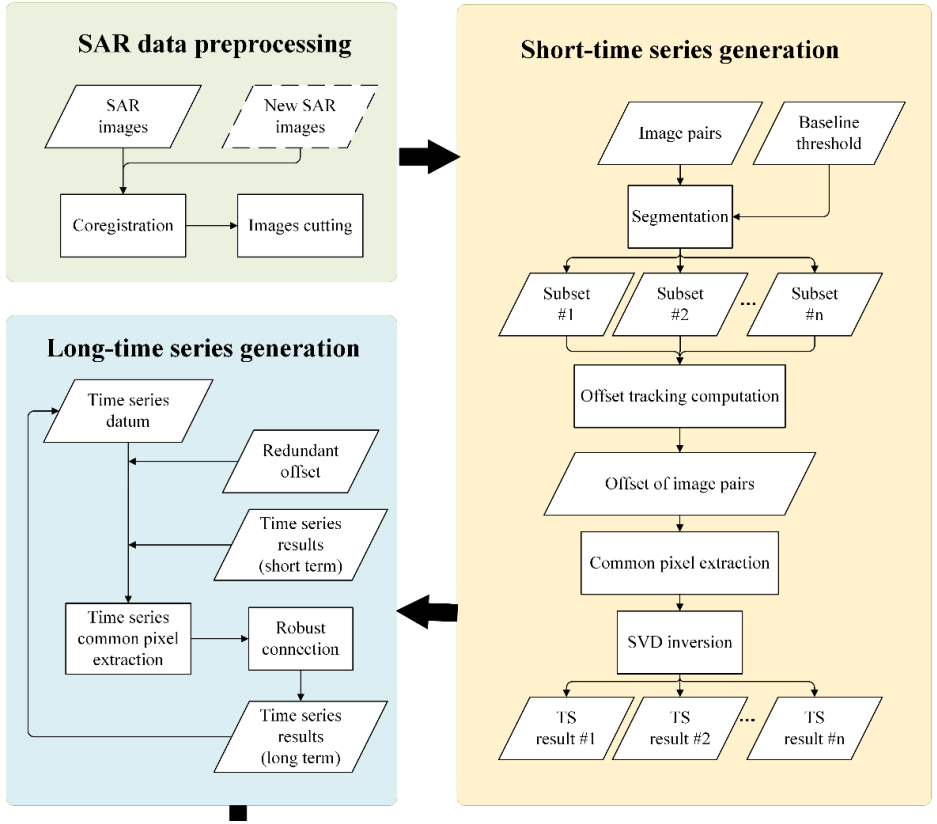
Overview of the retrieved results

Radar-Based Geohazard Monitoring

Case 1. Fushun West Open-Pit Mine

- POT-based Monitoring Framework for Large Ground Displacements

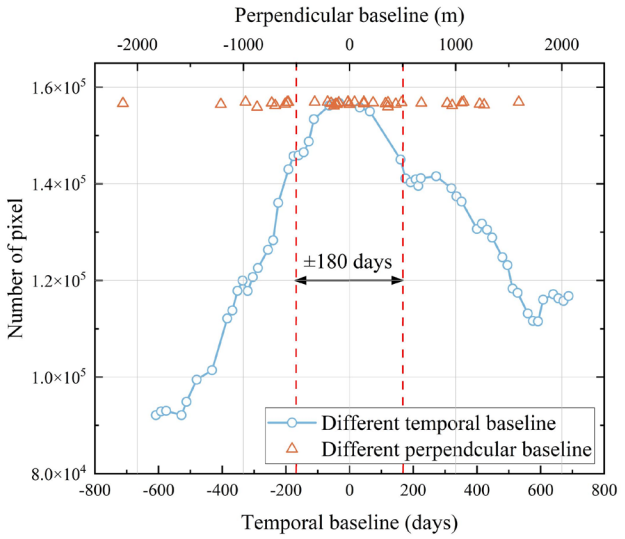




New Robust Sequential Pixel Offset Tracking (RS-POT) method effectively addresses decorrelation, displacement underestimation, and mismatching issues in large-deformation slope monitoring, achieving high-precision point-target tracking.

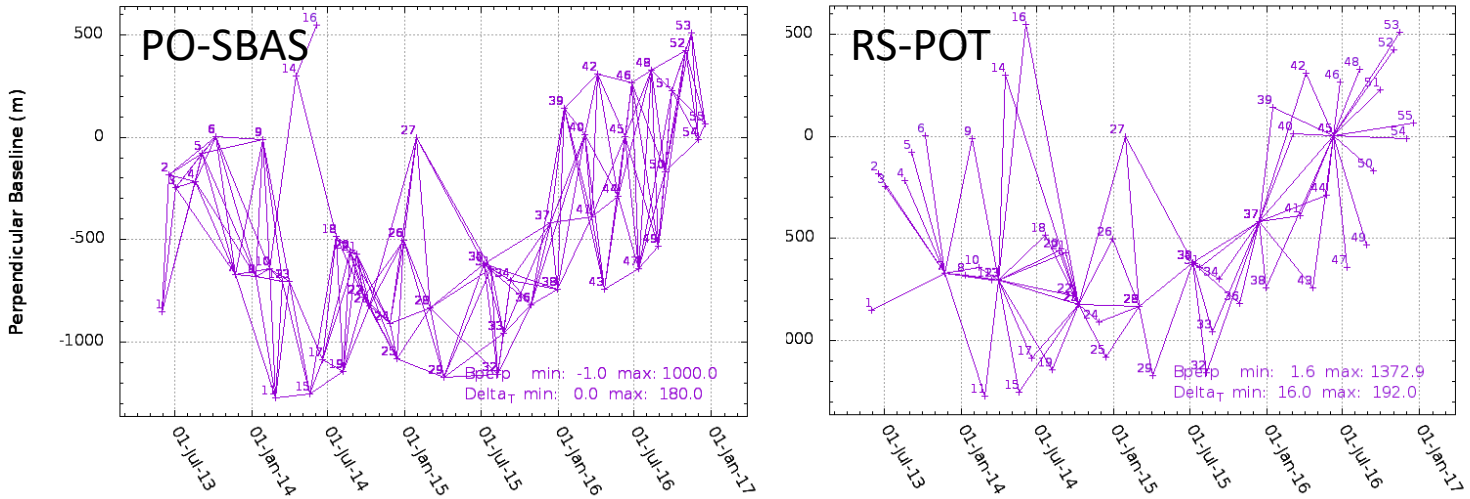
Overview of the retrieved results

Case 1. Fushun West Open-Pit Mine



No restrictions on the spatial baseline, temporal baseline threshold of 180 days

Spatio-temporal Baselines



189 image pairs

89 image pairs

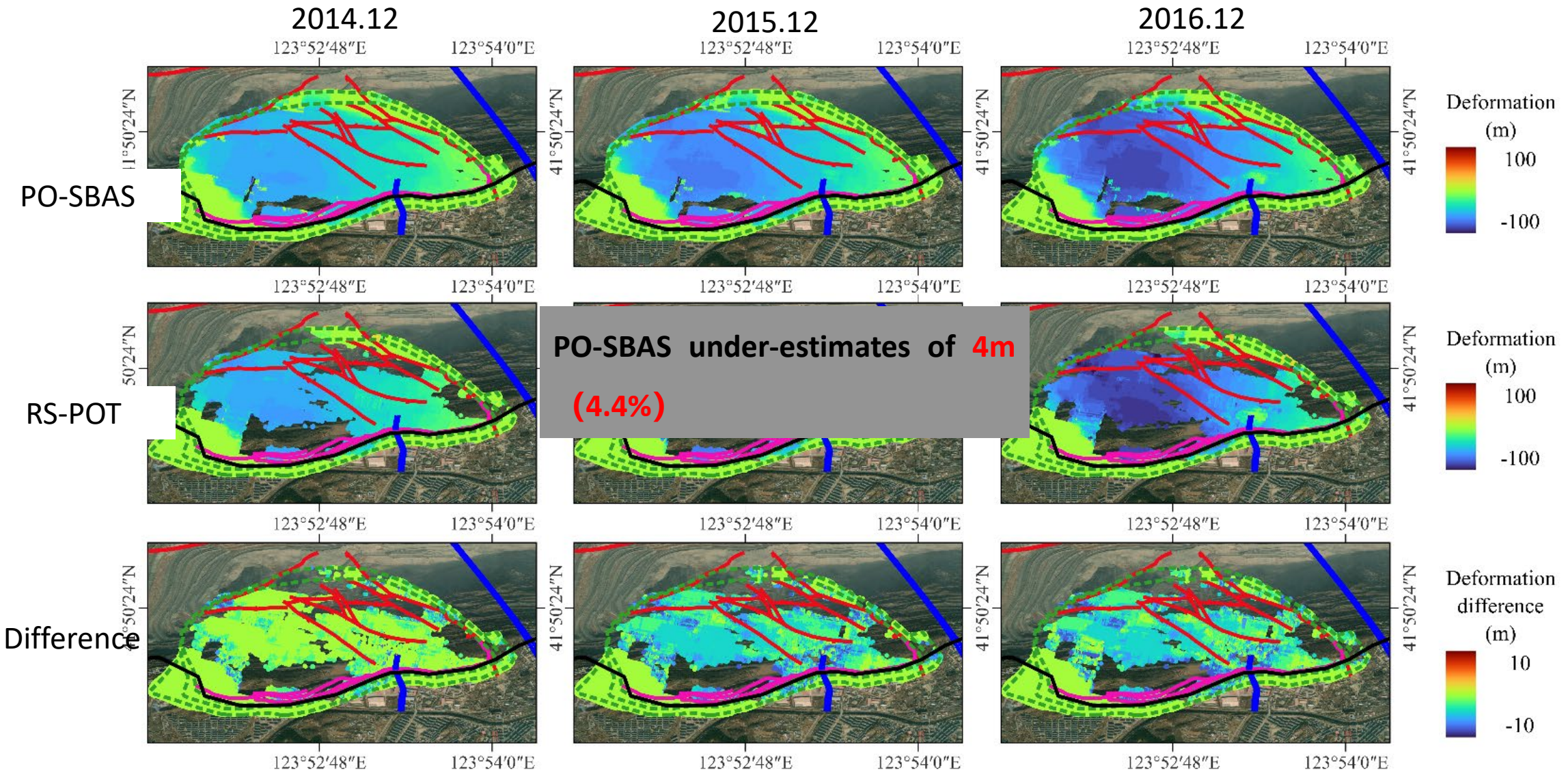
	Time for Offset Tracking	Time for Time Series Inversion	Time in Total
RS-POT	91.85h	1.97h	93.82h
PO-SBAS	207.47h	0.88h	208.35

- Computational cost reduction of 55%

(Wei et al., 2025, in preparation)

Overview of the retrieved results

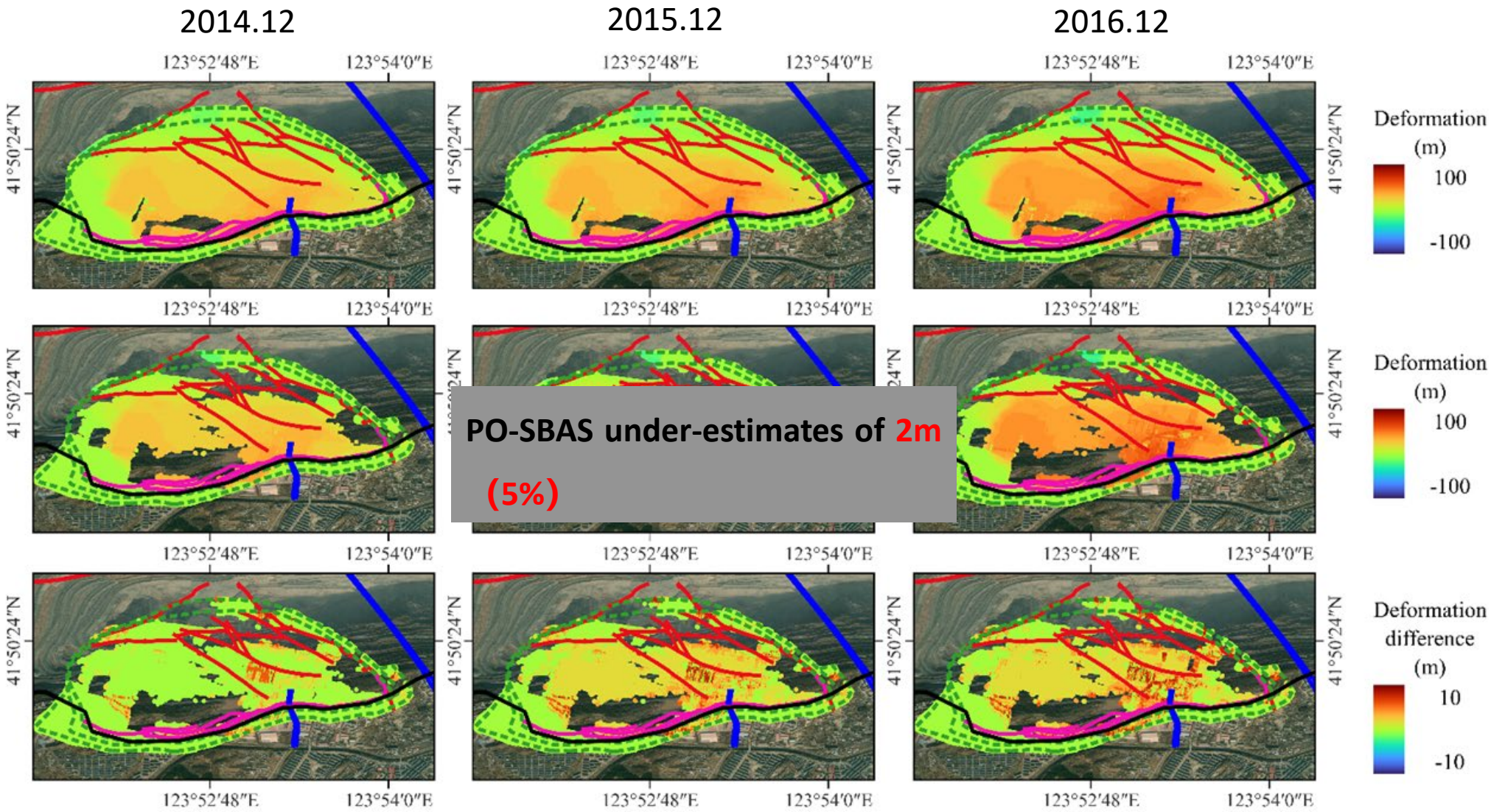
Cumulative Deformation in Azimuth direction



PO-SBAS under-estimates of 4m (4.4%)

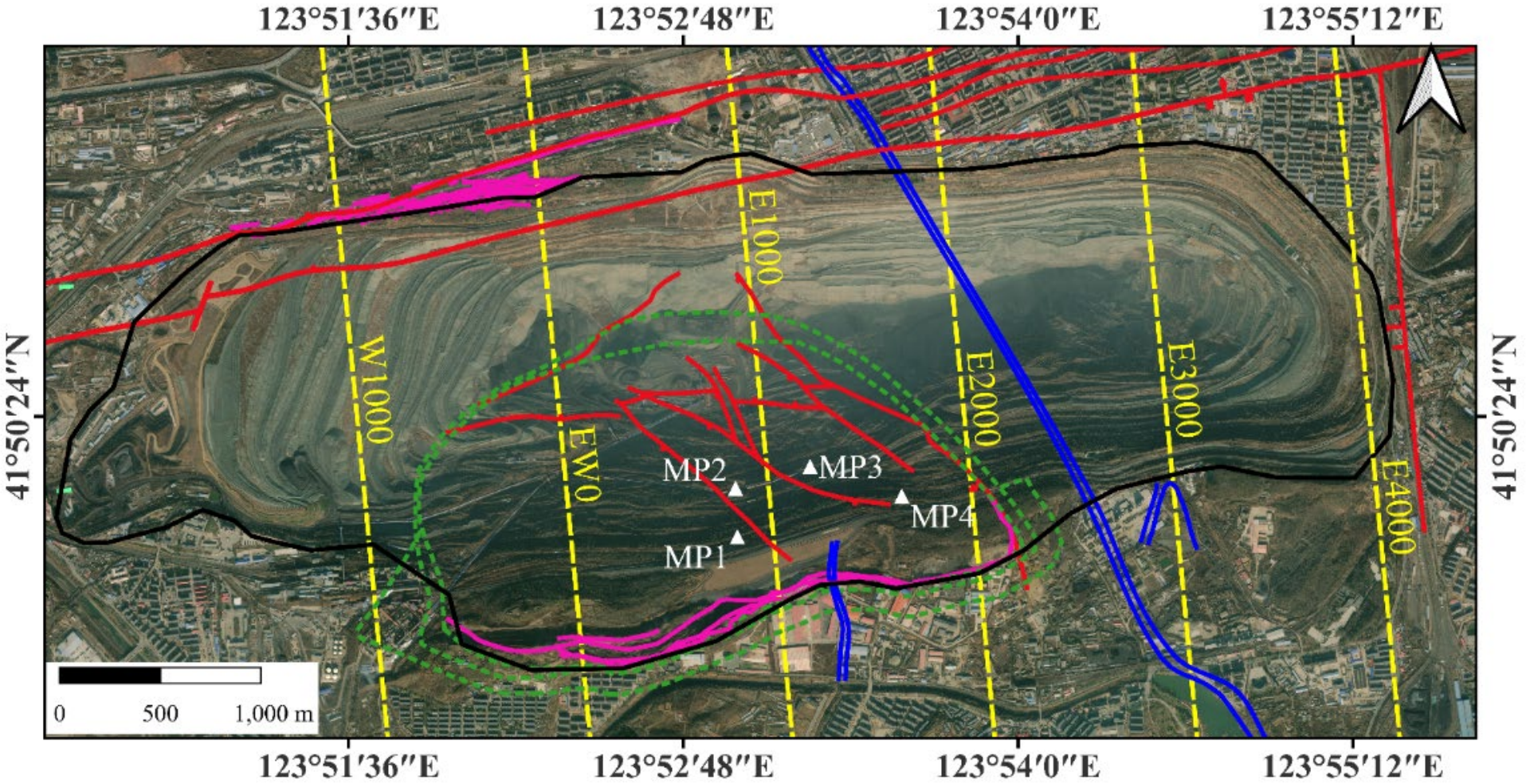
Overview of the retrieved results

Cumulative Deformation in Range direction

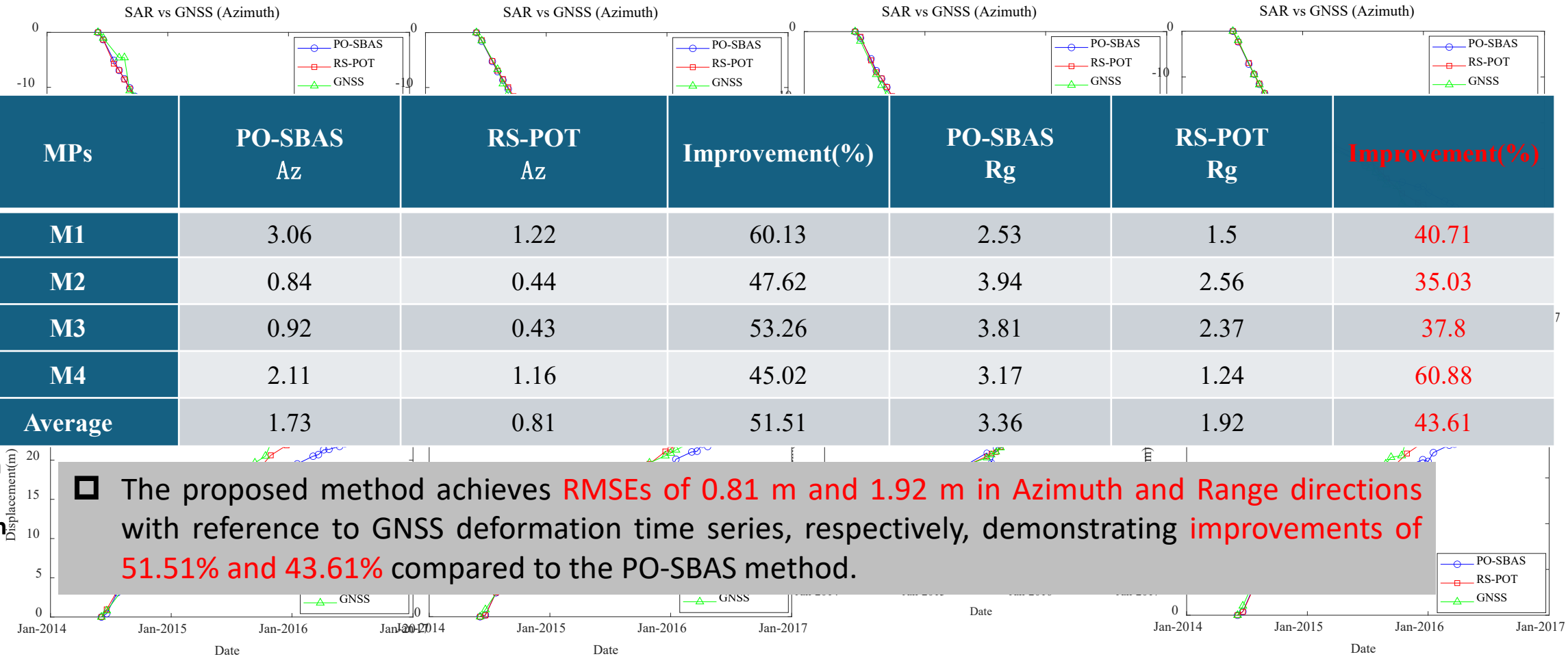


Overview of the retrieved results

Comparison with GNSS



Overview of the retrieved results



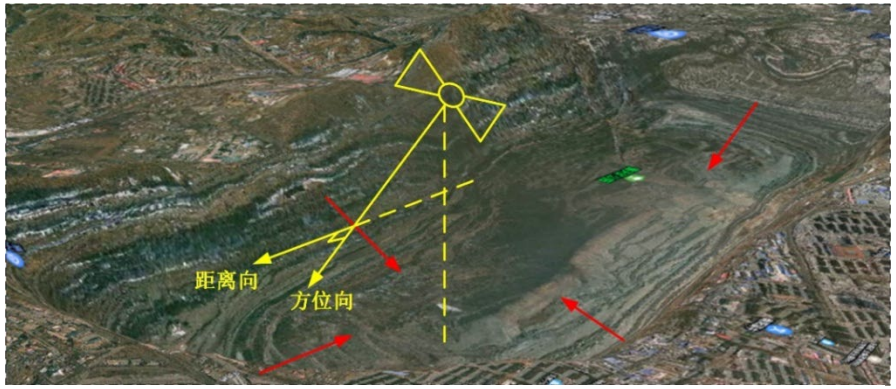
Azimu
Accur
Valida
Resu

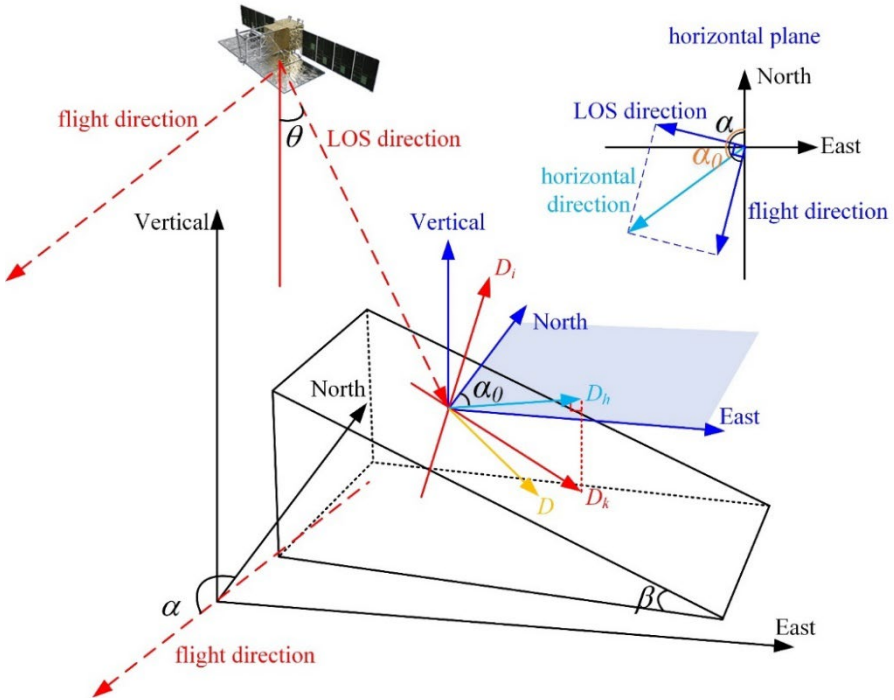
MPs	PO-SBAS Az	RS-POT Az	Improvement(%)	PO-SBAS Rg	RS-POT Rg	Improvement(%)
M1	3.06	1.22	60.13	2.53	1.5	40.71
M2	0.84	0.44	47.62	3.94	2.56	35.03
M3	0.92	0.43	53.26	3.81	2.37	37.8
M4	2.11	1.16	45.02	3.17	1.24	60.88
Average	1.73	0.81	51.51	3.36	1.92	43.61

Rar
Direction
Accuracy
Validation
Results

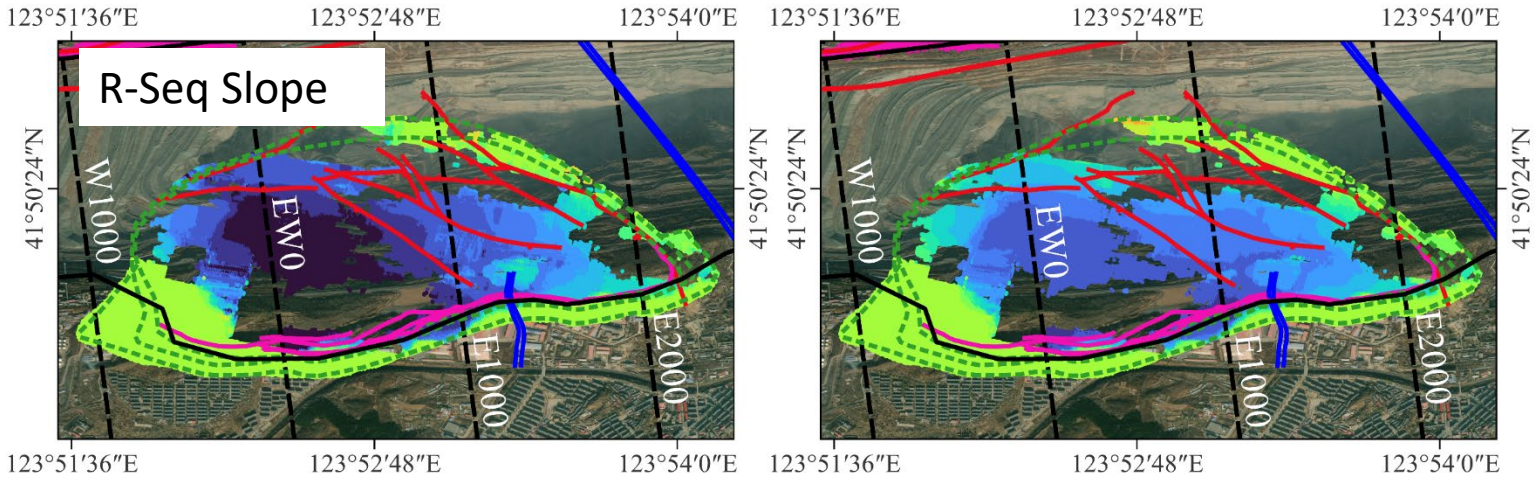
- The proposed method achieves RMSEs of 0.81 m and 1.92 m in Azimuth and Range directions with reference to GNSS deformation time series, respectively, demonstrating improvements of 51.51% and 43.61% compared to the PO-SBAS method.

Overview of the retrieved results





☐ Slope-Oriented Surface Deformation Results Based on RS-POT Method



2013.06~2016.12 Cumulative Displacement

$$\begin{cases} D_{az} = D_h \cdot \cos(\alpha - \alpha_0) \\ D_{\text{los\_h}} = D_h \cdot \sin(\alpha_0 - \alpha) \end{cases}$$

$$\begin{cases} D_{los\_h} = D_{los} \cdot \sin\theta \\ D_{los\_v} = D_{los} \cdot \cos\theta \\ D_{los\_v} = D_{K_v} - D_{l_v} \end{cases}$$

Slope-Oriented：

$$\begin{cases} D_k = \dfrac{D_{az} \cdot \cos\beta}{\cos(\alpha - \alpha_0)} + D_{los} \cdot \cos\theta \cdot \sin\beta \\ D_I = \dfrac{D_{az} \cdot \sin\beta}{\cos(\alpha - \alpha_0)} - D_{los} \cdot \cos\theta \cdot \cos\beta \end{cases}$$

Overview of the retrieved results

Geohazard Risk Assessment

Case 1.Debris Flow Risk Assessment in Fushun City

Debris Flow: A distinct type of sediment-laden flash flood occurring in steep mountainous gullies, typically triggered by heavy rainfall that mobilizes large volumes of mud, rocks, and debris.

Characteristics: Sudden onset, rapid velocity, high discharge, large sediment volume, and extreme destructive power.

Debris Flow Formation Conditions：

Topographic Conditions： Steep terrain with deep valleys, steep channel slopes, and open downstream deposition zones.

Material Conditions ： Abundant loose material prone to water erosion and transport

Triggering Conditions： Intense short-duration rainfall prone to generating torrential flows with tremendous impact force.

Supported Project: Remote Sensing Interpretation and Risk Assessment of Geological Hazards in Liaoning Province, 2022-2024

Study Area: Fushun City, Fuxin City, Chaoyang City ; Urban Dandong, Dongga City, Kuandian County, Huanren County

Target Hazards: Landslides, rockfalls, debris flows, land subsidence, collapse





Overview of the retrieved results

1.Risk Assessment Framework Development

Conditions for Debris Flow Disasters:

1.Debris flow occurrence

2.Resulting harm to human populations

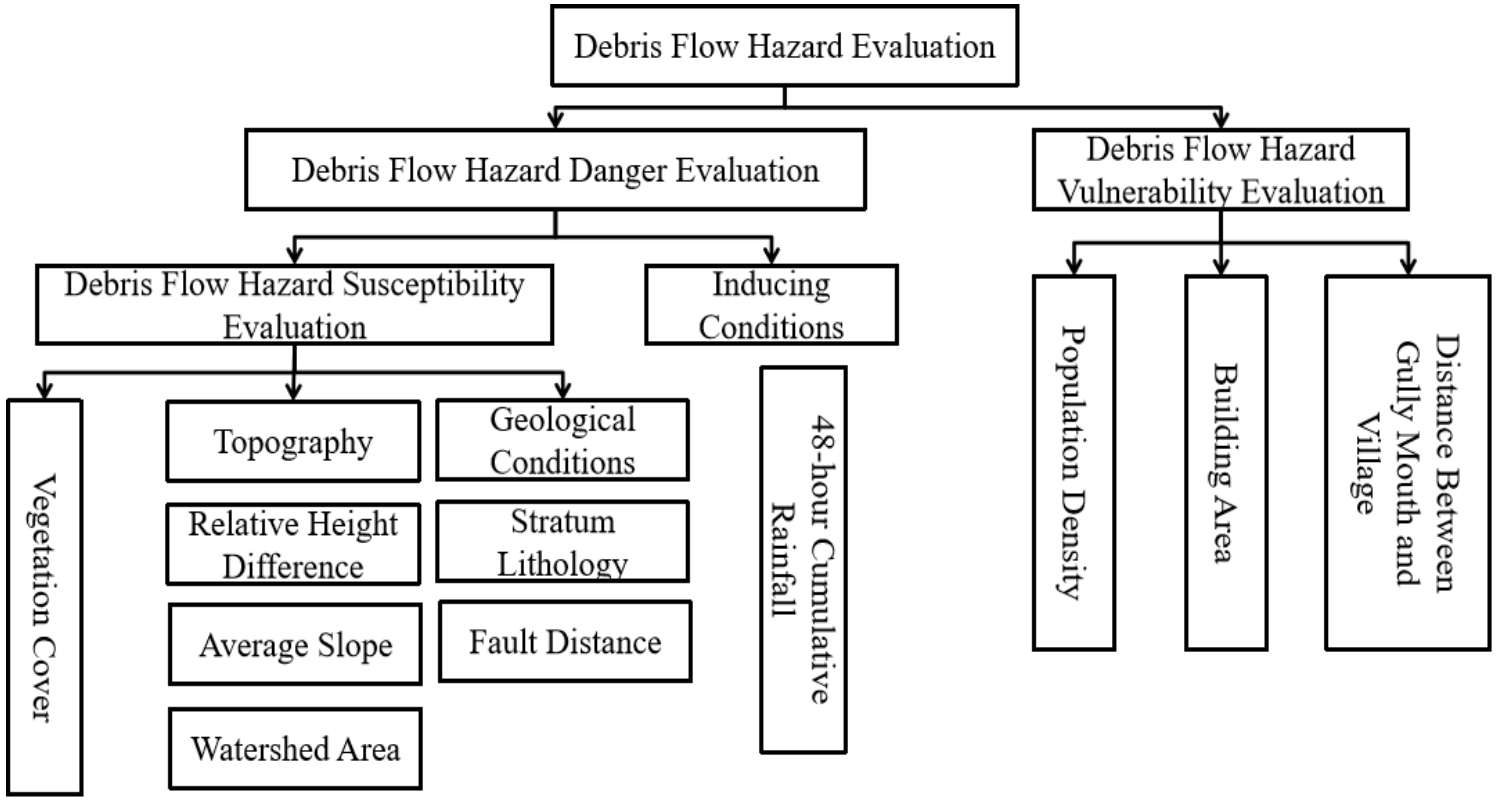
Debris Flow Risk Assessment Workflow:

1.Susceptibility Evaluation

2.Hazard Assessment

3.Vulnerability Analysis

4.Risk Quantification

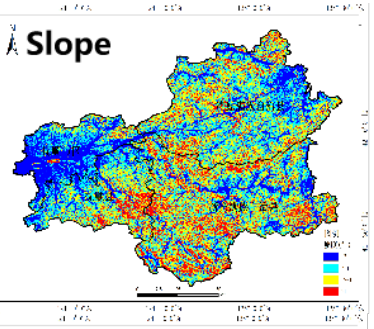


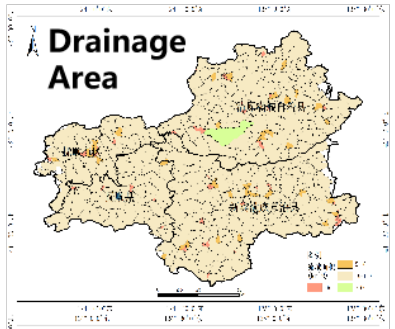
Risk Classification: Extreme, High, Medium, Low

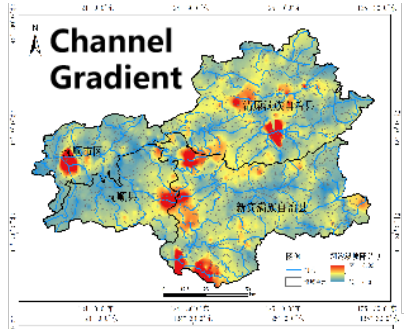
2. Evaluation Methods: Analytic Hierarchy Process (AHP), Information Value Method,

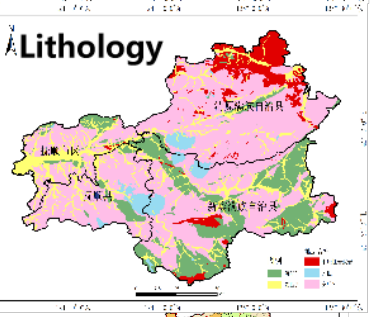
Machine Learning Approaches

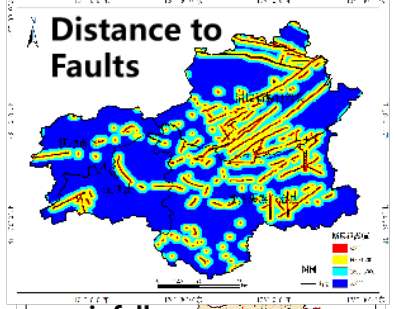
Overview of the retrieved results

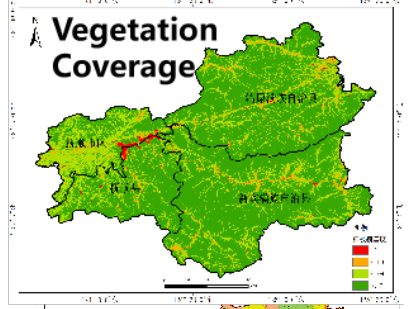


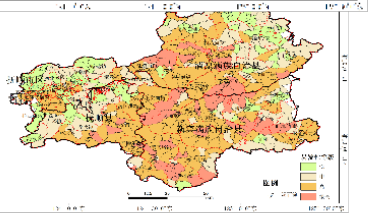


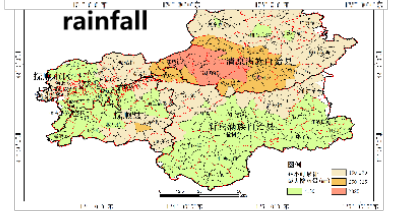


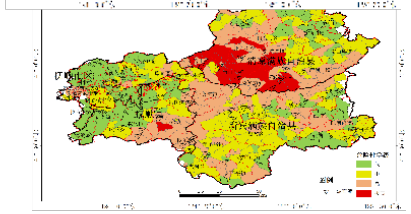


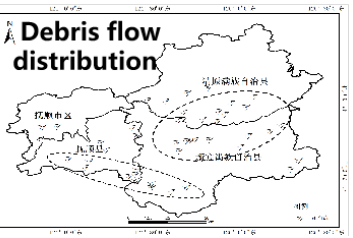


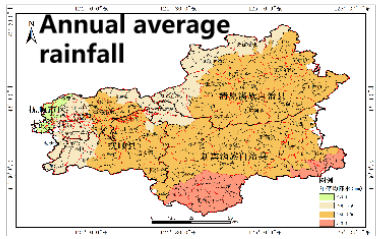


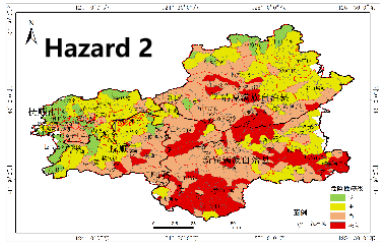


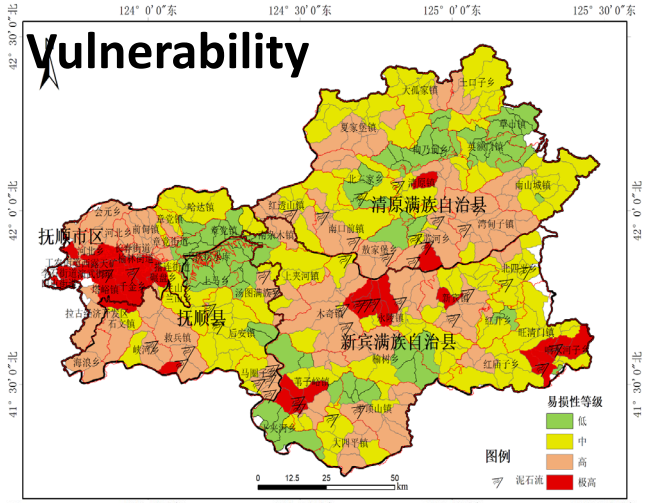


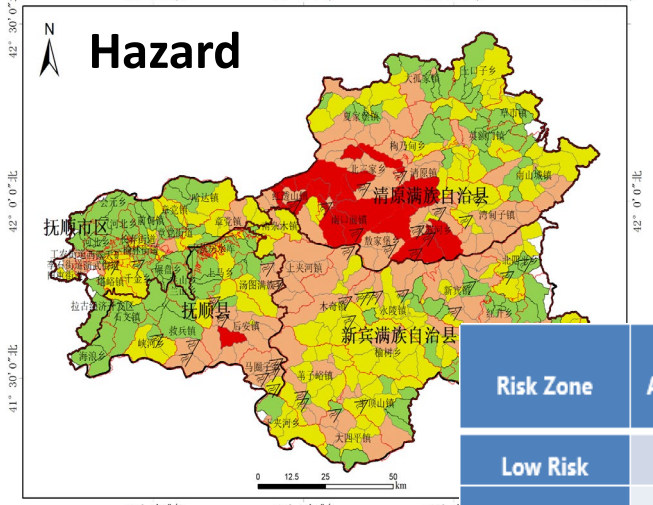


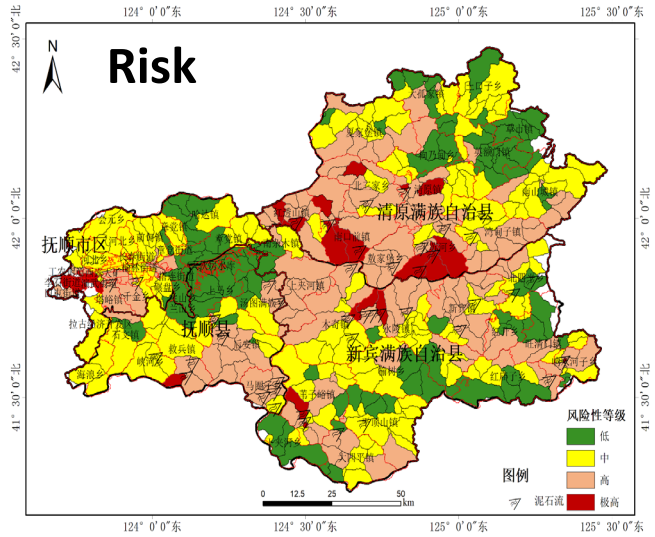












Risk Zone	Area (km²)	Percentage of Total Area	Recorded Debris Flow Points	Percentage of Total Points
Low Risk	2348.44	21.21%	3	7.14%
Medium Risk	4217.25	38.09%	7	16.67%
High Risk	3978.00	35.93%	25	59.52%
Extreme Risk	527.80	4.77%	7	16.67%

Overview of the retrieved results







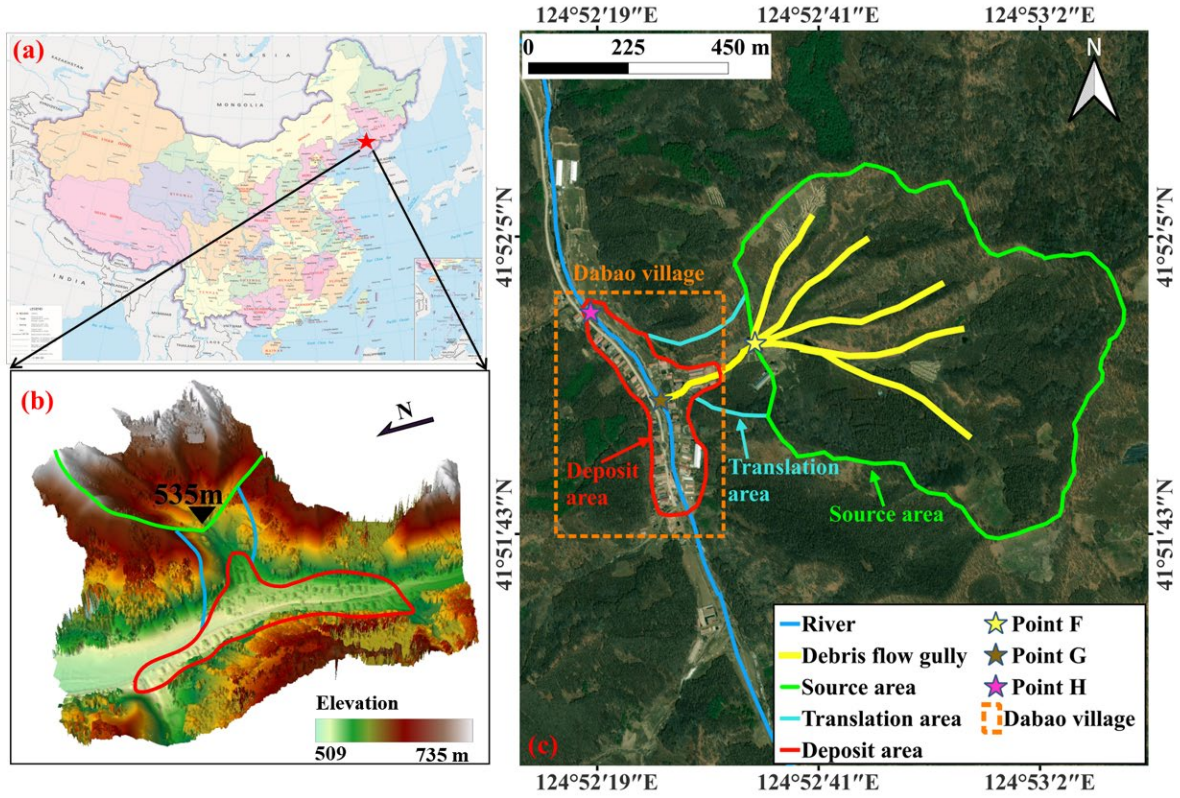


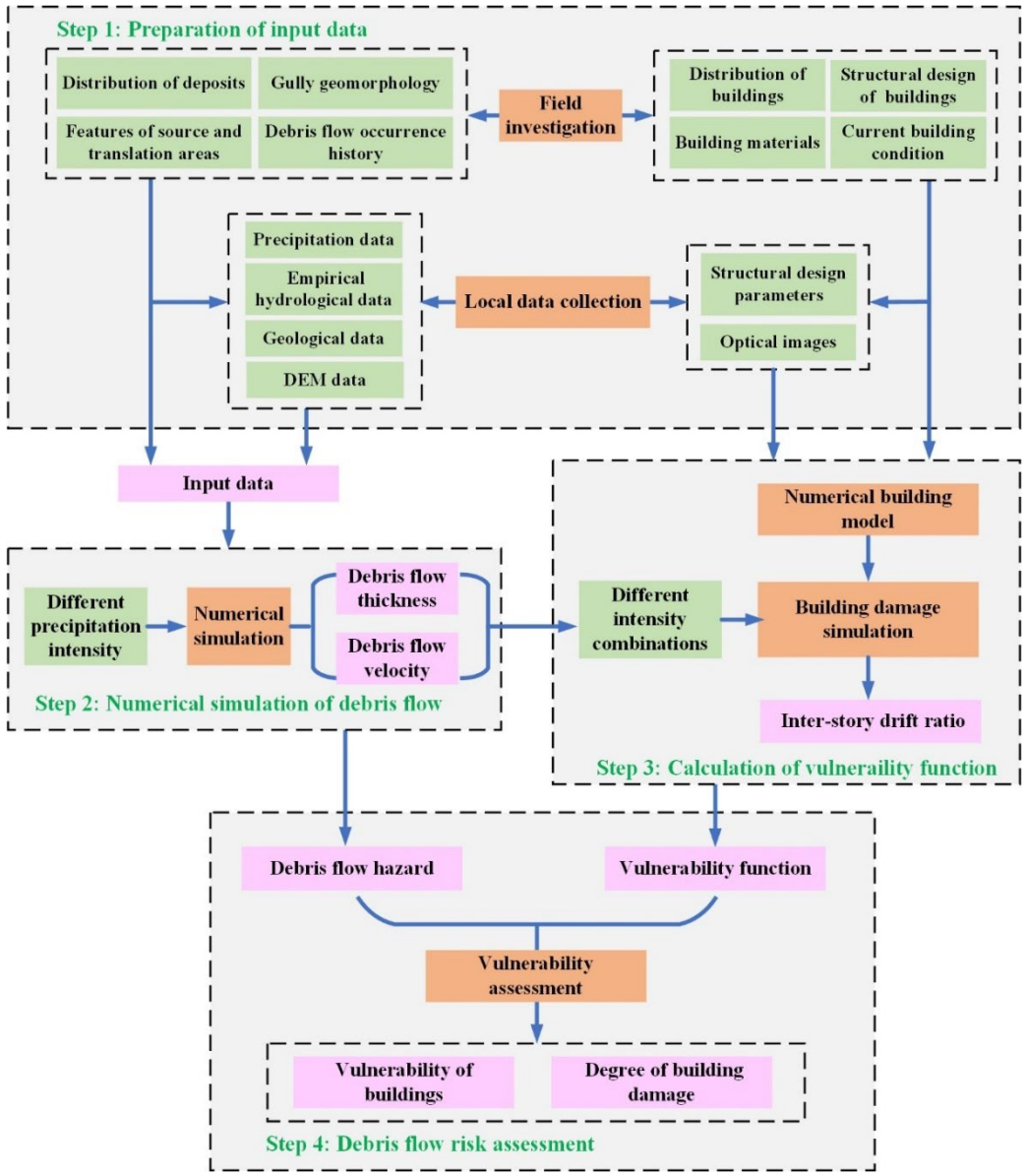




Overview of the retrieved results

Case 2.Debris Flow Simulation and Risk Assessment



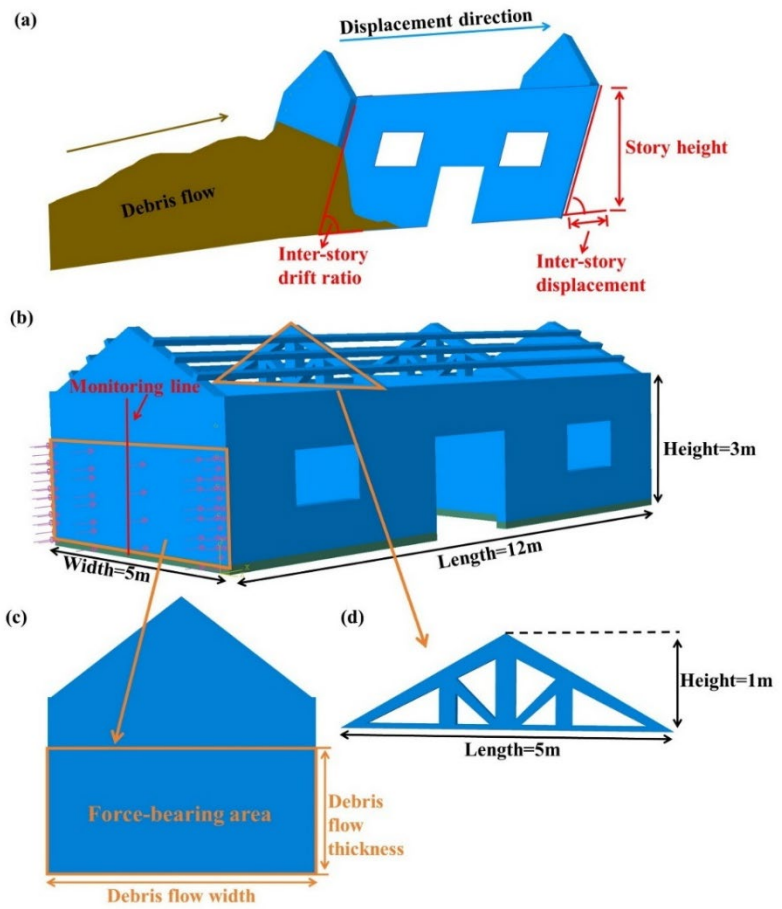


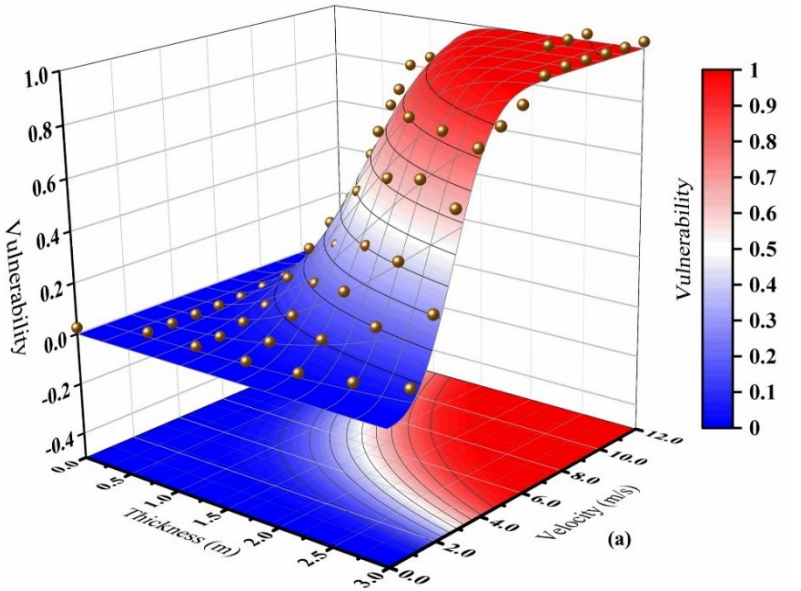
By integrating disaster simulation methods with finite element analysis of buildings, the damage status of structures under predicted disaster scenarios is obtained, enabling quantitative analysis of debris flow impacts on village structures and life/property losses.

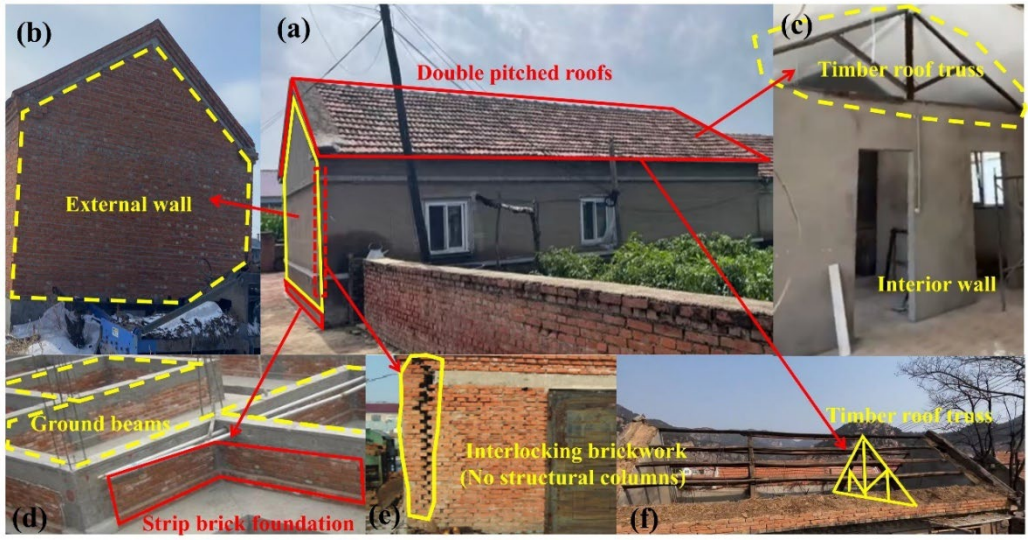
Overview of the retrieved results

1. Through field surveys and referencing regional building codes, the structural and material properties of buildings are determined to construct finite element models of local structures.

2. These models are then subjected to impact simulations using specified debris flow hazard scenarios to establish functional response relationships between building damage levels and debris flow intensity parameters.





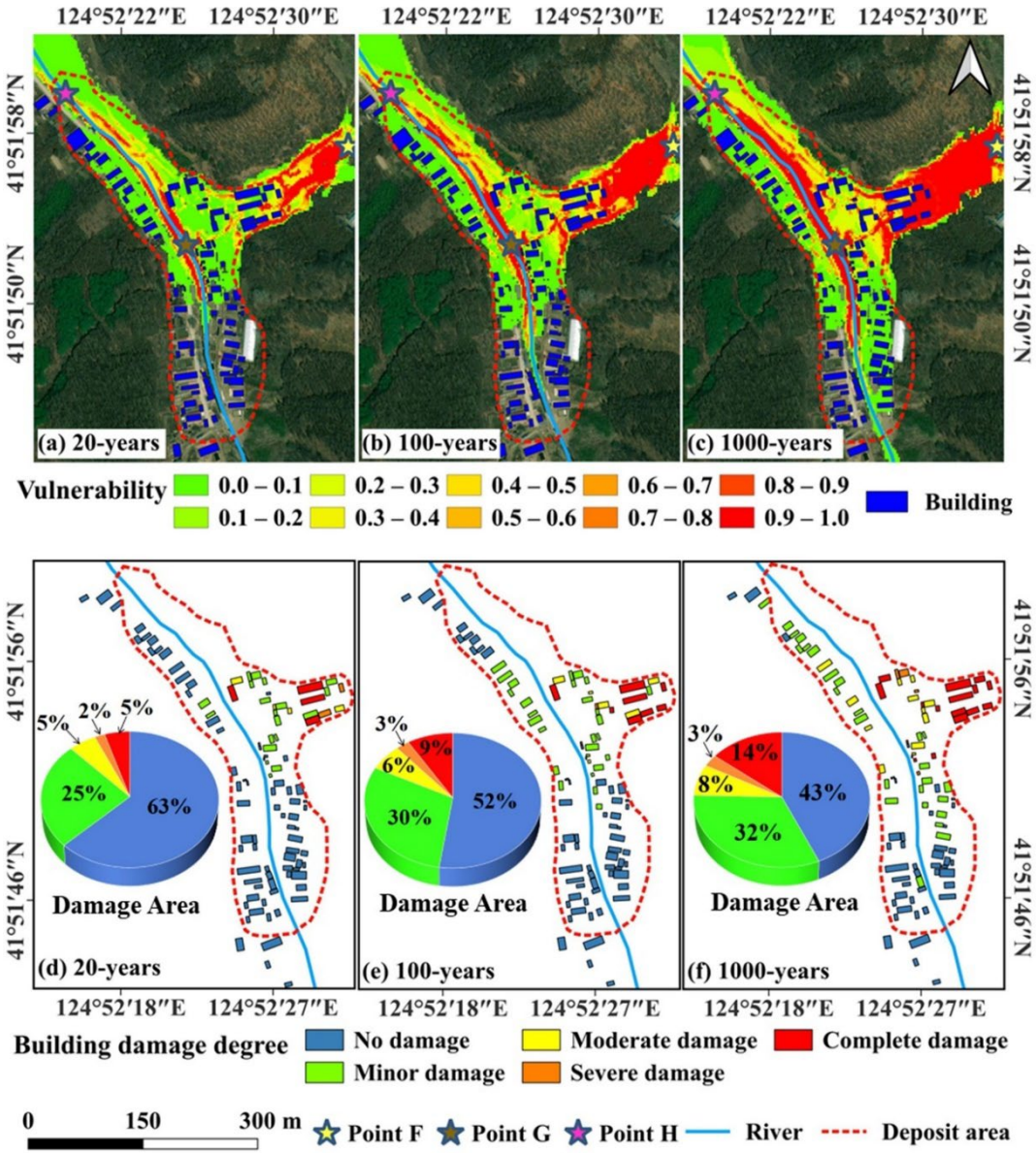


(Wei et al., 2025, Landslides)

Overview of the retrieved results

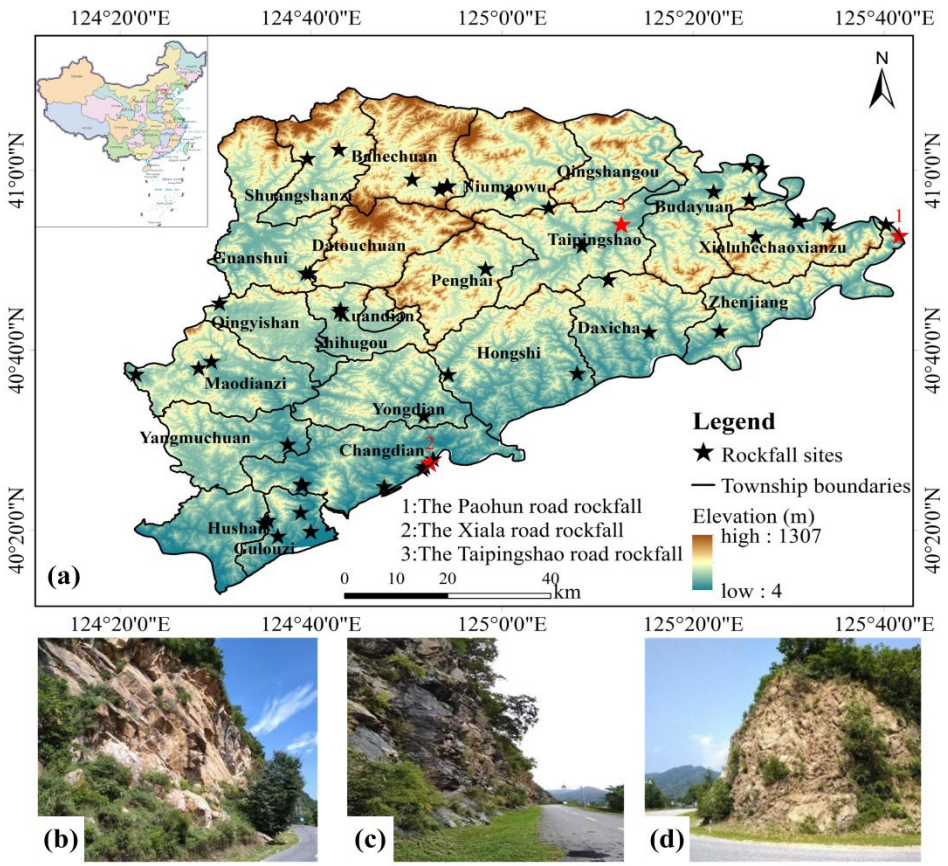
We have determined the potential damage scenarios of existing buildings in the area under varying intensities of debris flow impacts, and classified the disaster risk levels across different zones.

Precipitation recurrence interval (years)	Debris flow area (m^2)	Number of buildings at different damage levels				
		Complete	Severe	Moderate	Minor	No damage
20	42837.53	4	6	6	23	65
100	52556.32	7	5	8	32	52
1000	62131.31	14	2	9	36	43

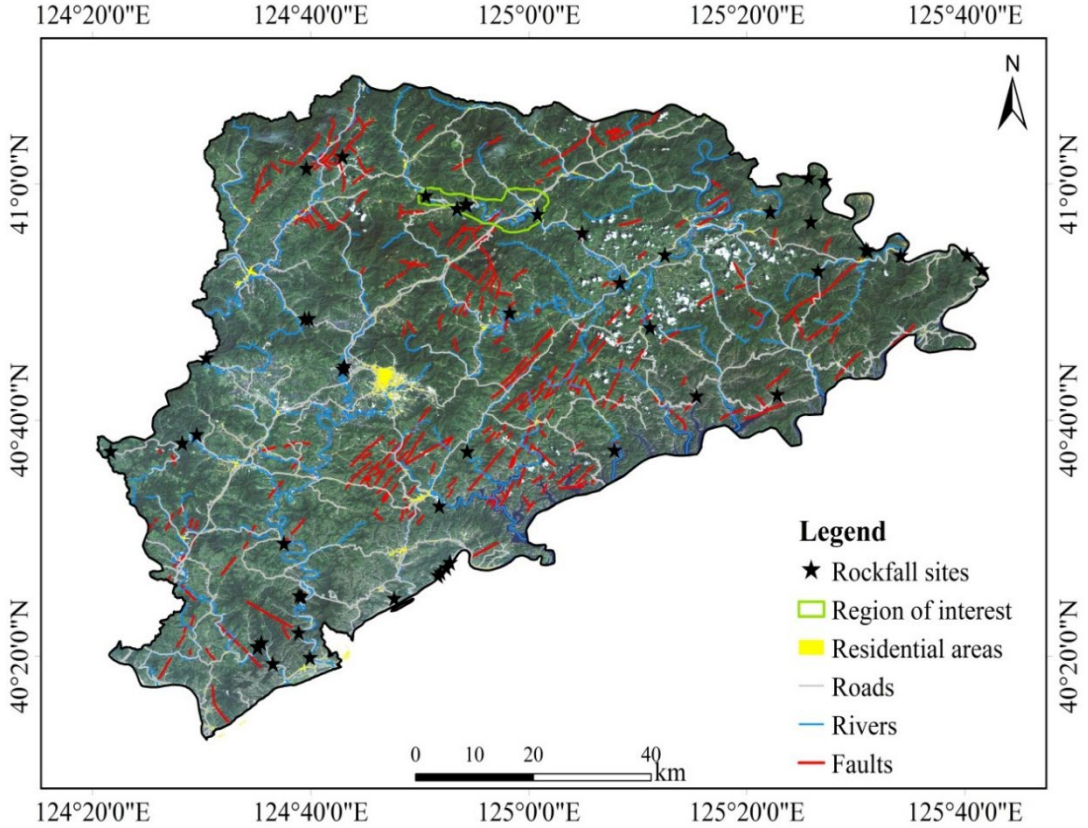


Overview of the retrieved results

Case 3. Rockfall Susceptibility Assessment in Kuandian County



Current Development Status of Landslide Hazards in Kuandian County

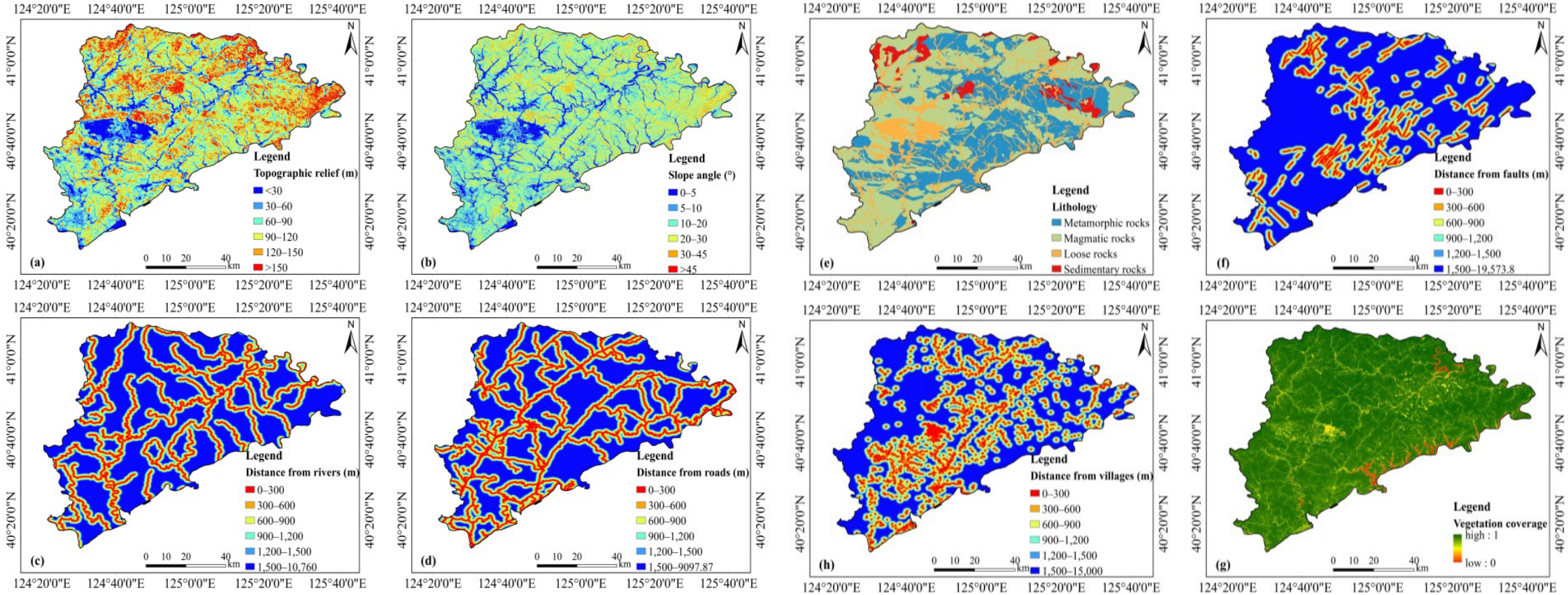


Data Collection for Assessment: Hazard points, Landsat imagery, villages, roads, rivers, geological maps, etc.

(Wei et al., Bulletin of Engineering Geology and The Environment, 2024)

Overview of the retrieved results

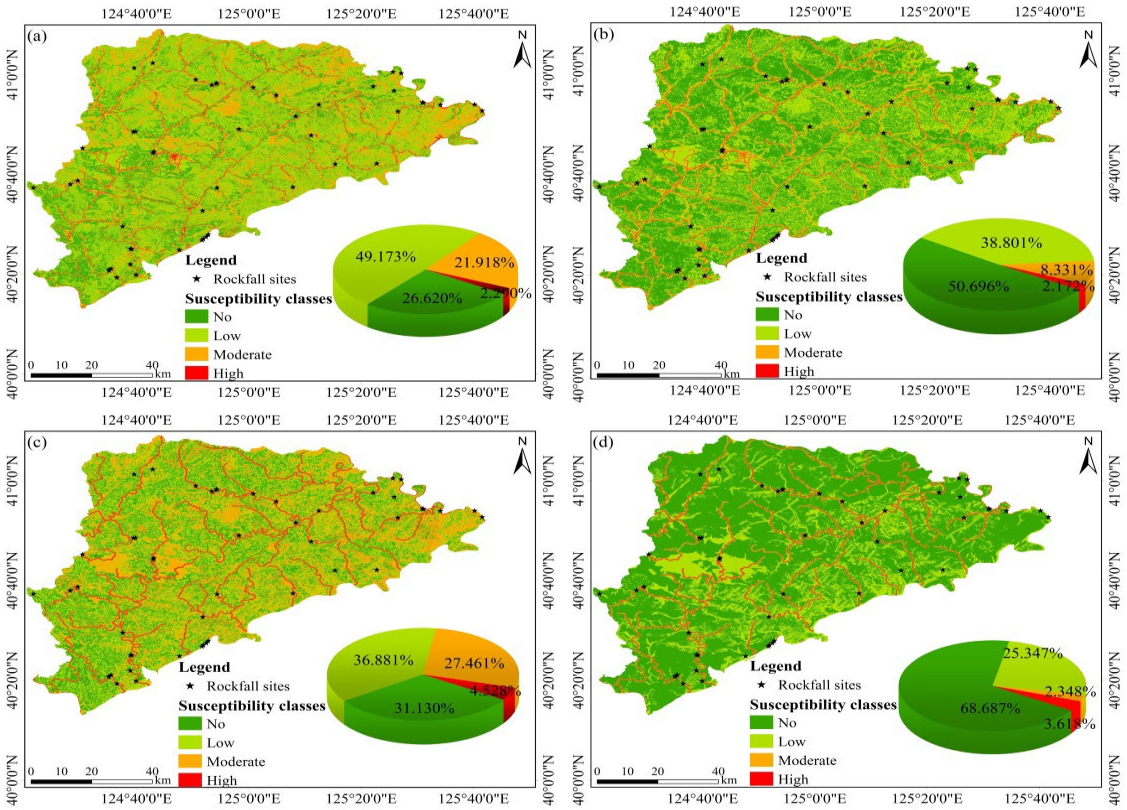
Evaluation Factors: Relative Relief, Slope Gradient, Lithology, Distance to Faults, Distance to Rivers, Distance to Roads, Distance to Villages, Vegetation Coverage

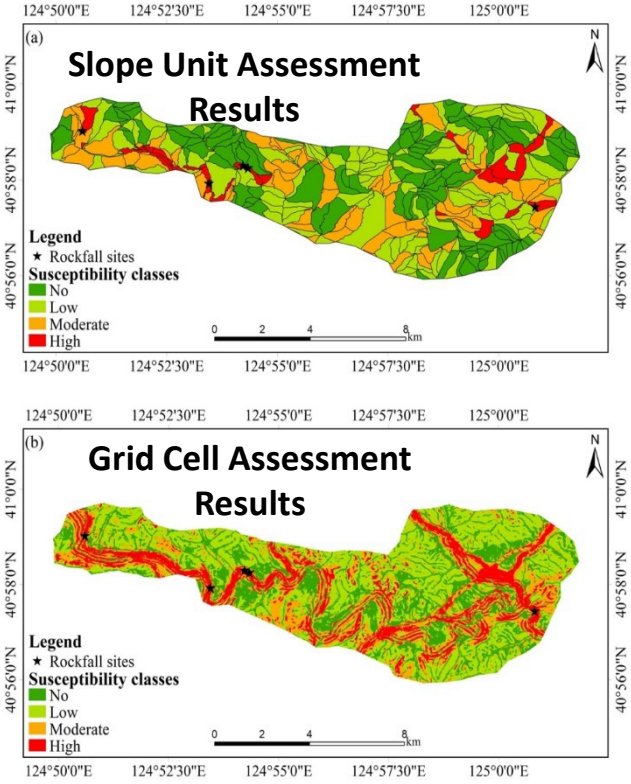


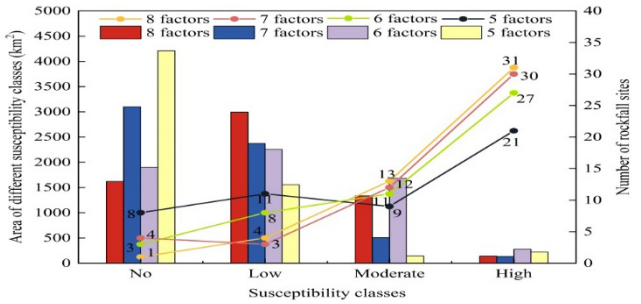
(Wei et al., Bulletin of Engineering Geology and The Environment, 2024)

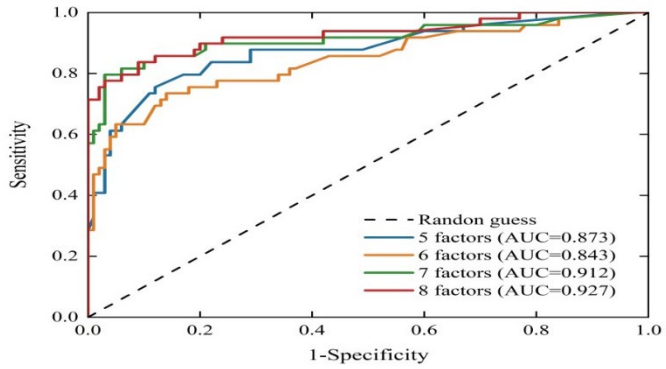
Overview of the retrieved results

Impact of Factor Selection on Results: **The evaluation accuracy progressively decreases when sequentially removing slope gradient, road distance, and relative relief.**









Related Publications

1. Lianhuan Wei, Xiangben Zhang, Huanan Zhang, Yaxin Xu, Meng Ao*, et al. Debris flow risk assessment via numerical simulation: A case study in Northeast China. Landslides, 2025, Published
2. Lianhuan Wei, Fang Wang, Cristiano Tolomei*, Shanjun Liu, Christian Bignami, Bing Li, Donglin Lv, Elisa Trasatti, Yuan Cui, Guido Ventura, Meng Ao, Stefano Salvi, Shiliu Wang, Xingyu Pan. Displacements of Fushun West Opencast Coal Mine Revealed by Multi-temporal InSAR Technology, Geo-spatial Information Science, 2024, Published
3. Lianhuan Wei, Yaxin Xu, Huashuo Cui, Donglin Lv*, et al. Rockfall Susceptibility Assessment over A Mountainous Area with Information Content Method and Analytic Hierarchy Process, Bulletin of Engineering Geology and the Environment, 2024， Published
4. Liu Shanjun, Liu Shiyao, Lv Donglin, Wei Lianhuan*, et al. Debris flow susceptibility and hazard assessment in Fushun based on hydrological response unit, Natural Hazards, 2024, Published
5. 刘善军，刘诗瑶，魏恋欢，吕东霖*. 基于子流域单元的抚顺市泥石流易发性及危险性评价，东北大学学报（自然科学版），2024.5，已见刊.
6. 魏恋欢，刘善军*，杨天鸿，赵晔. 联合高精度DEM与时序SAR的西露天煤矿特大型滑坡监测研究[J].东北大学学报(自然科学版)，2021.12，42(12): 1753-1760.
7. Wei, L., Pan, X., Trasatti, E. et al. Deformation and morphological changes before the 2021–2022 explosive eruption at Hunga Tonga-Hunga Ha’apai submarine caldera revealed by satellite remote sensing. Bull Volcanol 87, 17 (2025). https://doi.org/10.1007/s00445-025-01804-5
8. Lianhuan Wei, et al., Robust Sequential Pixel Offset Tracking, 2025, in preparation.
9. Lianhuan Wei, et al., Machine Learning Based Debris Flow Risk Assessment for Liaoning Province, 2025, in preparation

Conclusions and Future Plans

CONCLUSIONS

1. Geohazard monitoring with SAR data requires adaptive adoption of various methods (e.g., time series InSAR, pixel offset tracking, etc.), and sometimes improvements of existing algorithms are necessary for certain scenarios.
2. Deformation estimated by SAR is only one of the most important parameters of geohazards. Besides deformation, geological, geomorphological, meteorological and anthropogenic factors are also closely related to the occurence of geohazards. Conducting comprehensive assessment for geohazards using various parameters is necessary for disaster warning and prevension.
3. Exploitation of machine learning and deep learning models for geohazards risk assessment are the current development trend, although fine-tuning of the models are required.

FUTURE PLANS

1. Improvement of the Robust Sequential POT method by adopting adaptive thresholds for temporal baselines
2. Exploitation of domestic SAR satellite data (GF-3, LT-1, etc.) for geohazard monitoring
3. Deformation-constrained geohazard modeling and failure mechanism analysis
4. Near real-time geohazard early warning in Liaoning Province using multi-source remote sensing and meteorological data

Thank you for your attention!

Presenters: Lianhuan Wei & Cristiano Tolomei
Email：weilianhuan@mail.neu.edu.cn
cristiano.tolomei@ingv.it

Northeastern University, Shenyang, China
Istituto Nazionale di Geofisica e Vulcanologia, Rome, Italy

CSTEC
中国科学技术交流中心
China Science and Technology Exchange Center

esa
→ THE EUROPEAN SPACE AGENCY



2025 DRAGON 6 SYMPOSIUM

14-18 JULY 2025

PROJECT ID. 95348

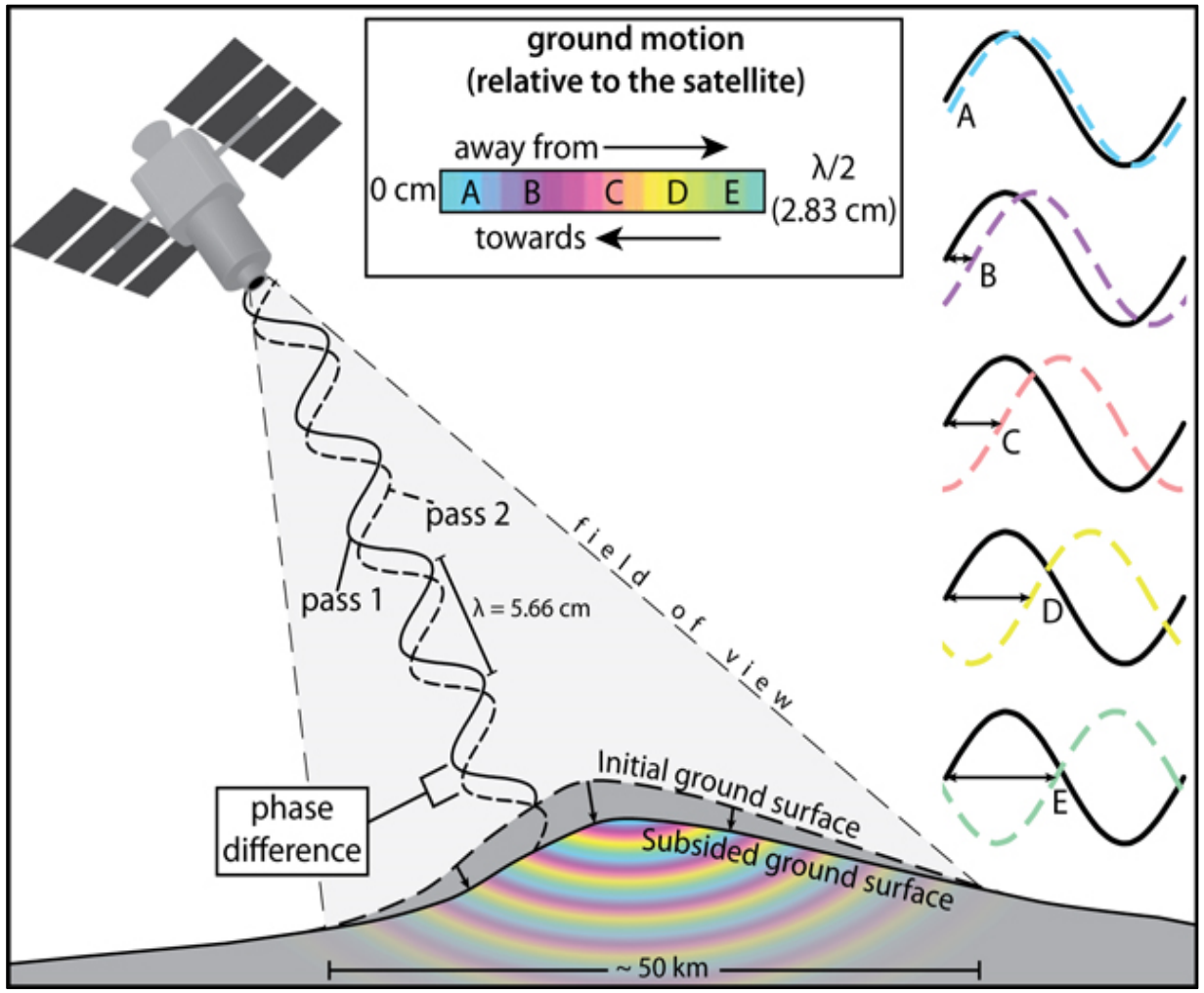
PHASE GRADIENT RATE-CONSTRAINED MINIMUM COST FLOW METHOD FOR ACCURATE PHASE UNWRAPPING IN LARGE GRADIENT DEFORMATION FIELDS





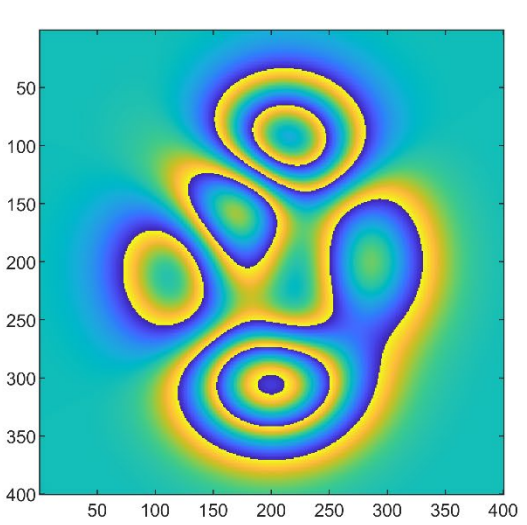


1. Research Background and Significance

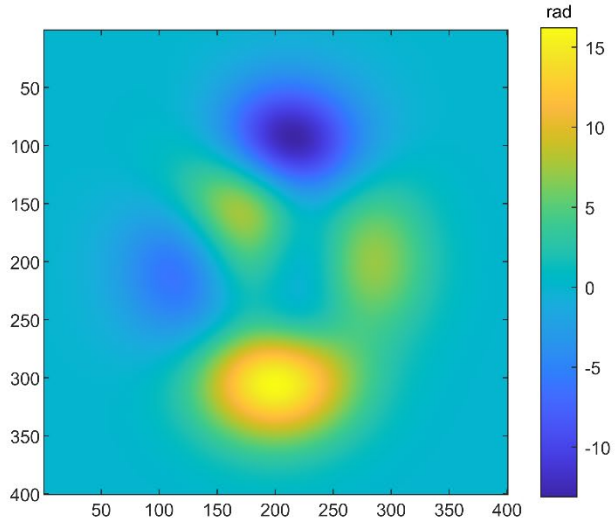


Surface deformation derived from phase interferometry

- InSAR retrieves surface deformation by interferometrically processing SAR images acquired over the same area at different times, enabling effective ground deformation monitoring.
- **Phase unwrapping** is a key step that restores the wrapped phase (within $[-\pi, \pi)$) to the true phase by adding integer multiples of 2π. **Its accuracy directly affects the reliability of InSAR deformation results.**

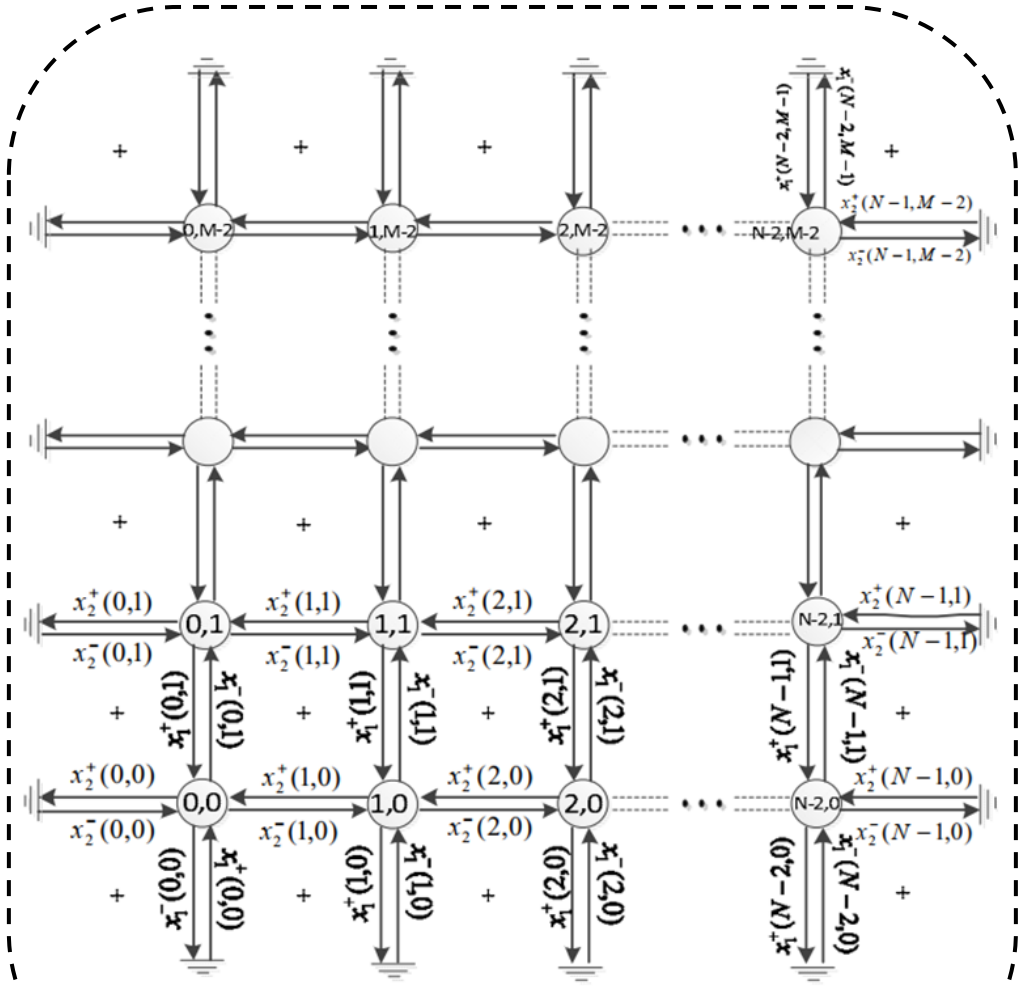


Wrapped phase



True phase

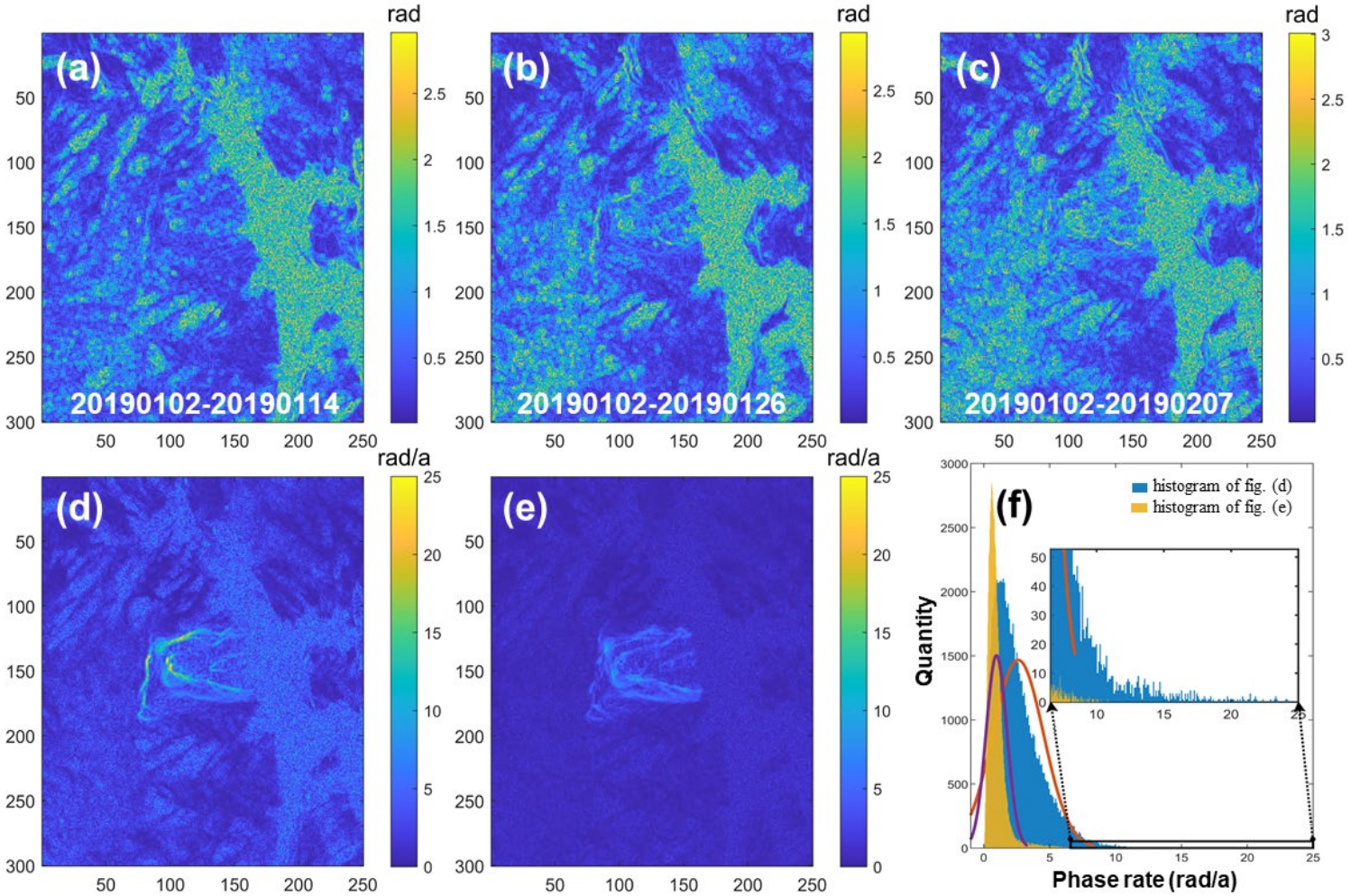
1. Research Background and Significance



Minimum Cost Flow Network

- The MCF method models phase unwrapping as a minimum cost flow problem, minimizing the difference between unwrapped and wrapped phase gradients to reduce error propagation in low-coherence areas and achieve a global optimum.
- When unwrapping arcs cross high-gradient deformation areas, their ambiguity is often underestimated, causing phase errors and reducing deformation monitoring accuracy.
- **To address this issue, we propose a Phase Gradient Rate Constrained Minimum Cost Flow (PGR-MCF) phase unwrapping method.**

2. PGR-MCF

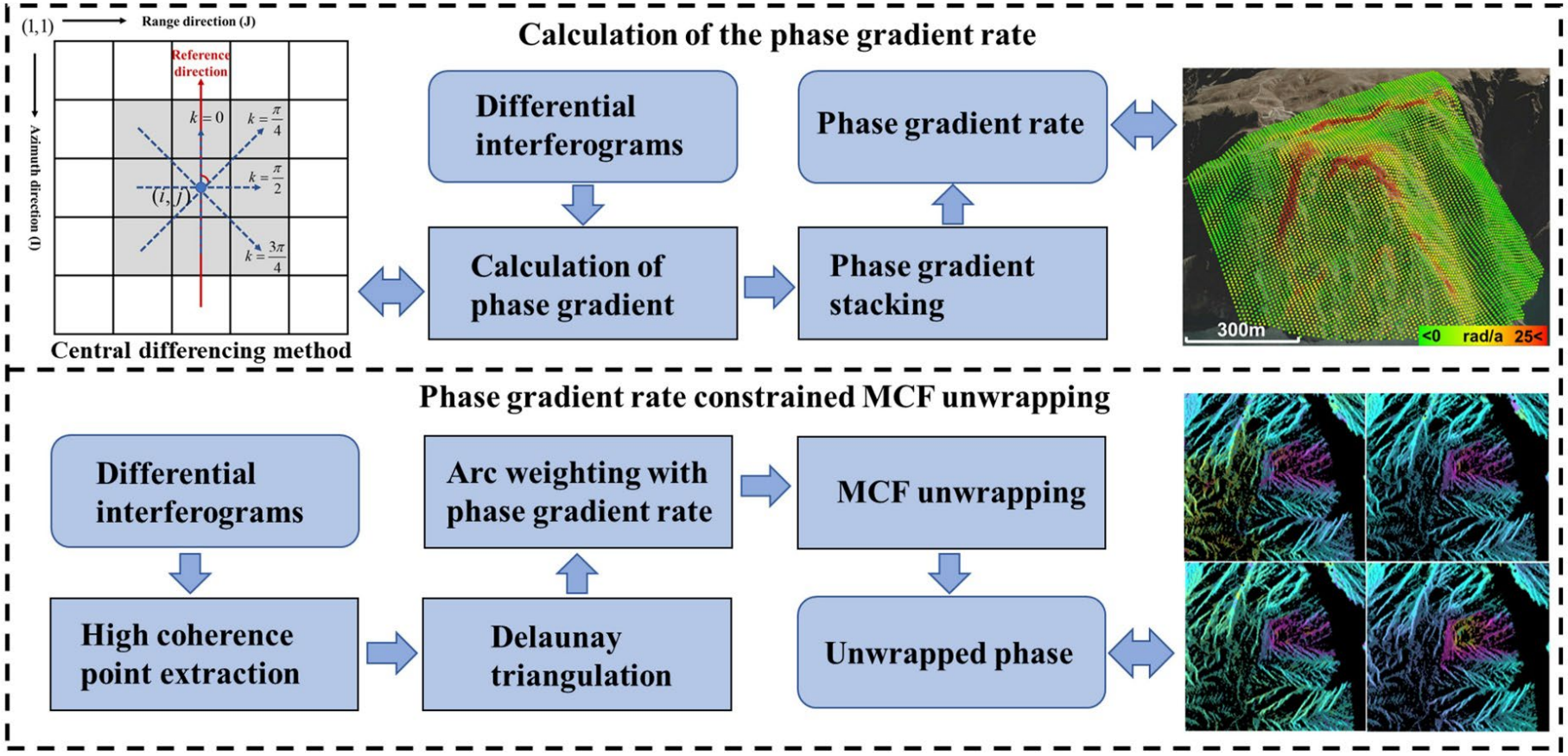


Phase gradient maps. (a-c) Wrapped phase gradients of single interferograms with 12-day, 24-day, and 36-day baselines, respectively. (d) Phase Gradient Rate calculated from the shortest temporal baseline interferograms. (e) Phase Gradient Rate calculated from the full temporal baseline interferograms. (f) Histogram of (d) and (e).

- The phase gradient of a single interferogram contains significant noise, while the phase gradient rate effectively suppresses this noise.
- The phase gradient rate calculated from the shortest temporal baseline interferograms is called the short-baseline phase gradient rate.
- The phase gradient rate calculated using all temporal baseline interferograms is called the full-baseline phase gradient rate.
- The full baseline phase gradient rate has lower noise, smaller magnitude, and more blurred boundaries.

2. PGR-MCF

- **Set the maximum full-baseline phase gradient rate as a threshold; arcs with short-baseline phase gradient rates exceeding this threshold are assigned zero weight.**
- **This guides the MCF unwrapping path to enter high-gradient deformation areas from low-gradient regions, avoiding unwrapping errors.**

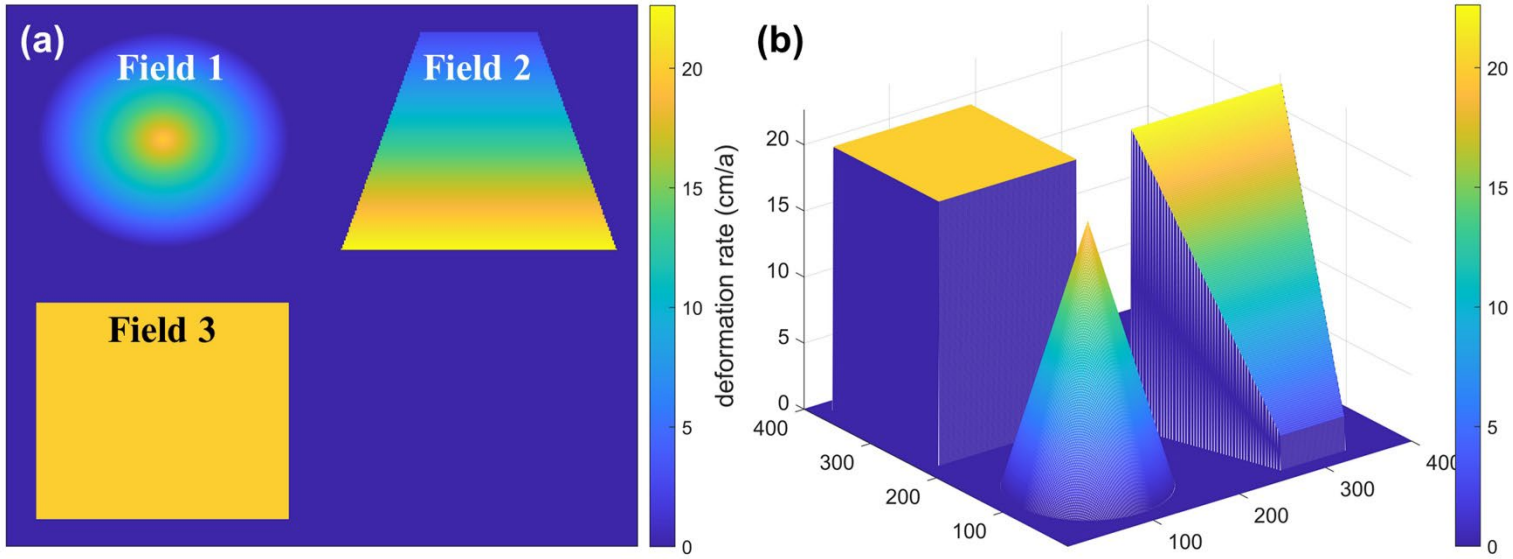


Technical Flowchart

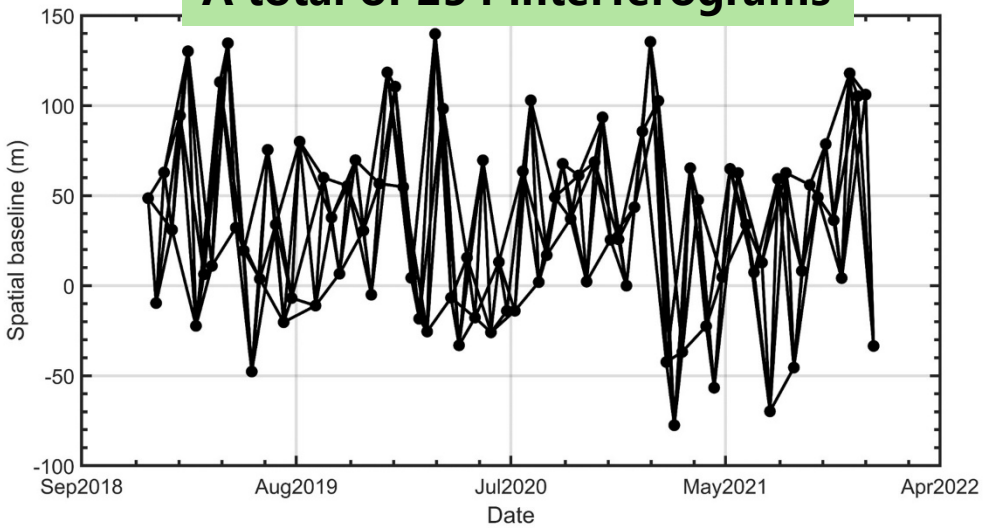
3. Simulation Experiment

Three deformation fields with a maximum deformation of 20 cm/a were simulated: a circular field, a trapezoidal field, and a rectangular field.

1. The circular field has no obvious boundaries.
2. The trapezoidal field shows clear deformation boundaries on the two sides and the bottom compared to stable areas, while the top side has no obvious boundary.
3. The rectangular field has distinct deformation boundaries compared to stable areas.

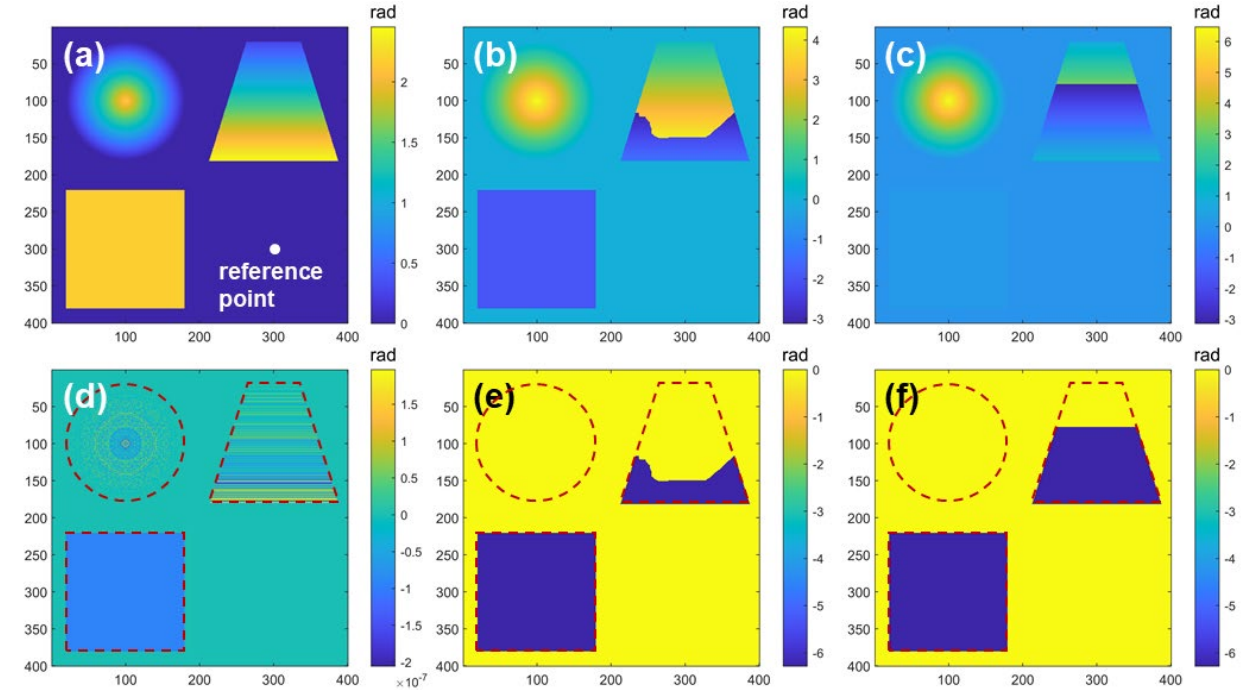


A total of 254 interferograms



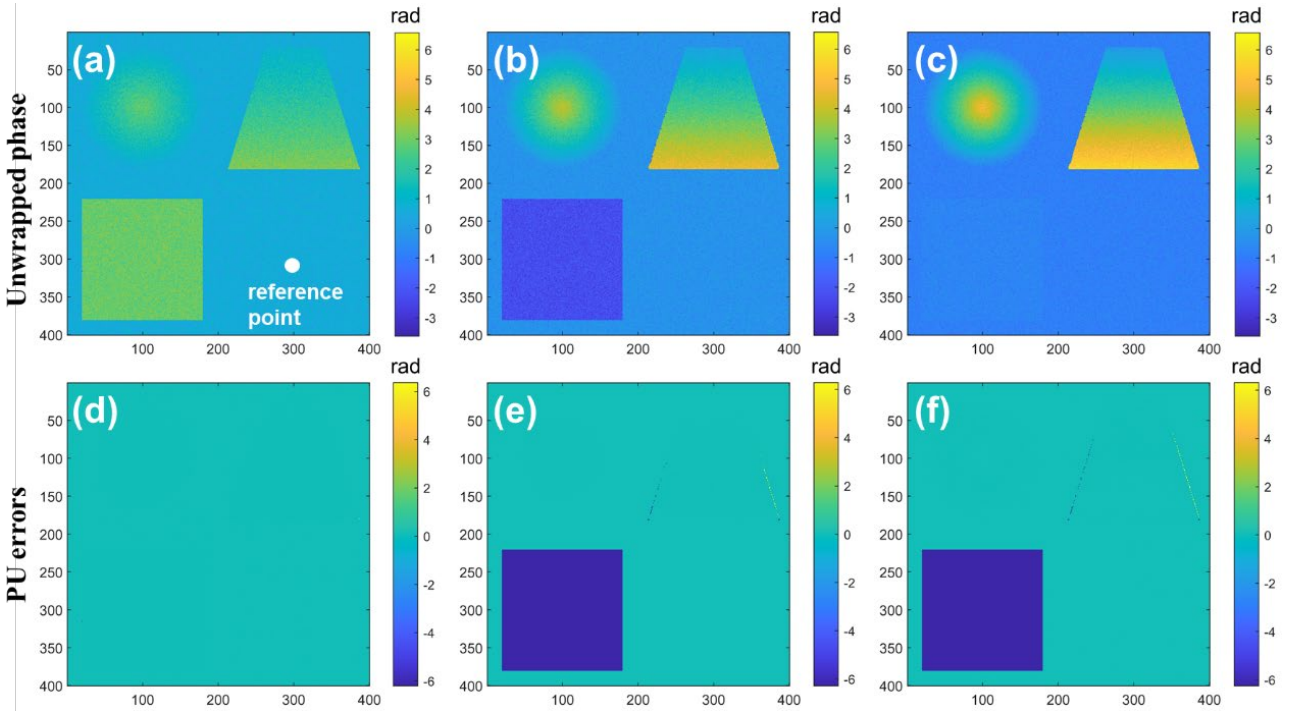
Baseline Diagram

3. Simulation Experiment



Unwrapped Phase Maps (Obtained by the MCF Method)

(a)-(c) Unwrapped phase maps; (d)-(f) Unwrapping error maps.

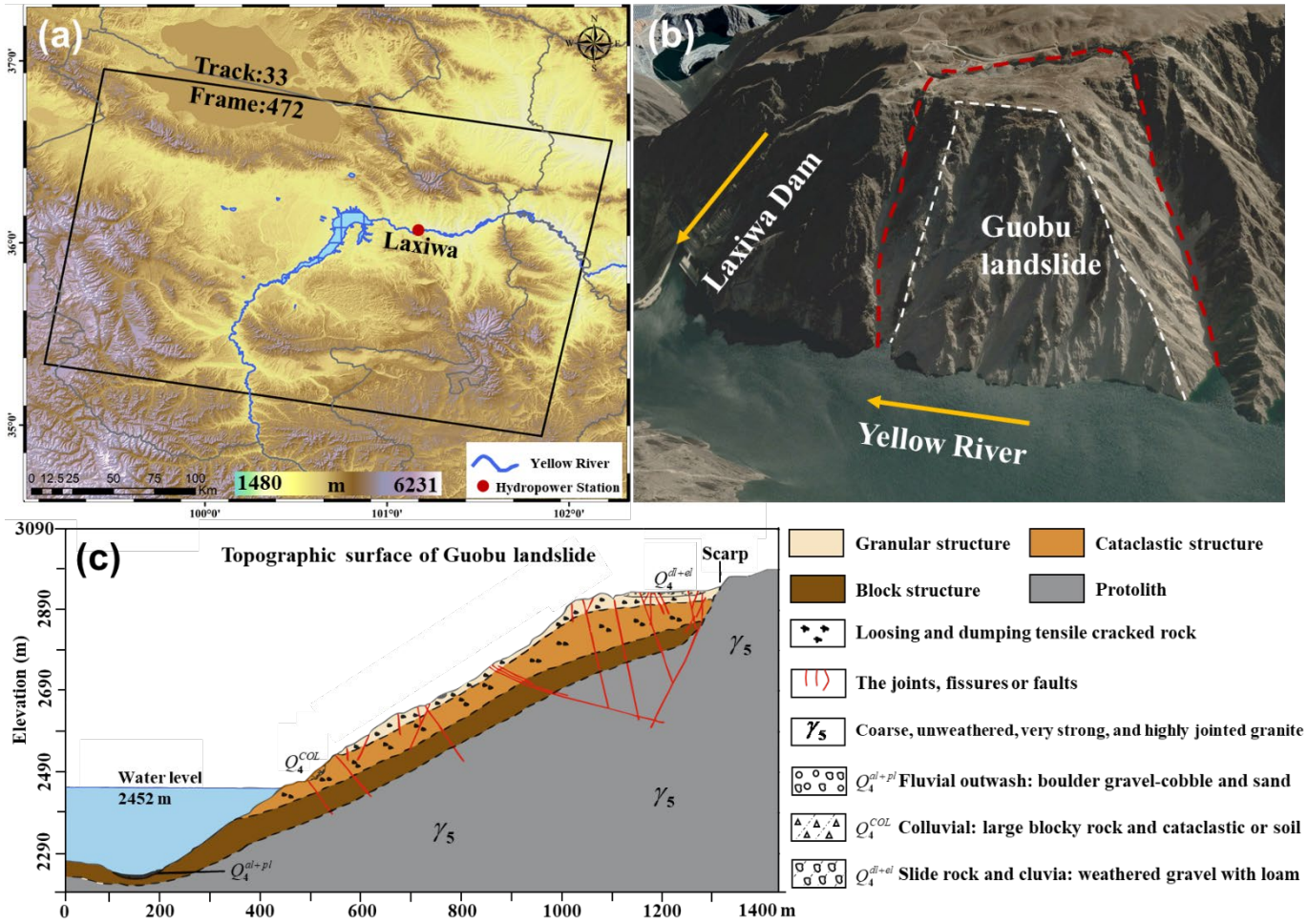


Unwrapped Phase Maps (Obtained by the PGR-MCF Method)

(a)-(c) Unwrapped phase maps; (d)-(f) Unwrapping error maps.

As the temporal baseline increased, traditional MCF failed in the trapezoidal and rectangular deformation fields, while PGR-MCF successfully unwrapped the trapezoidal region. However, due to the lack of low-gradient deformation areas in the trapezoidal region, PGR-MCF still encountered errors in this zone.

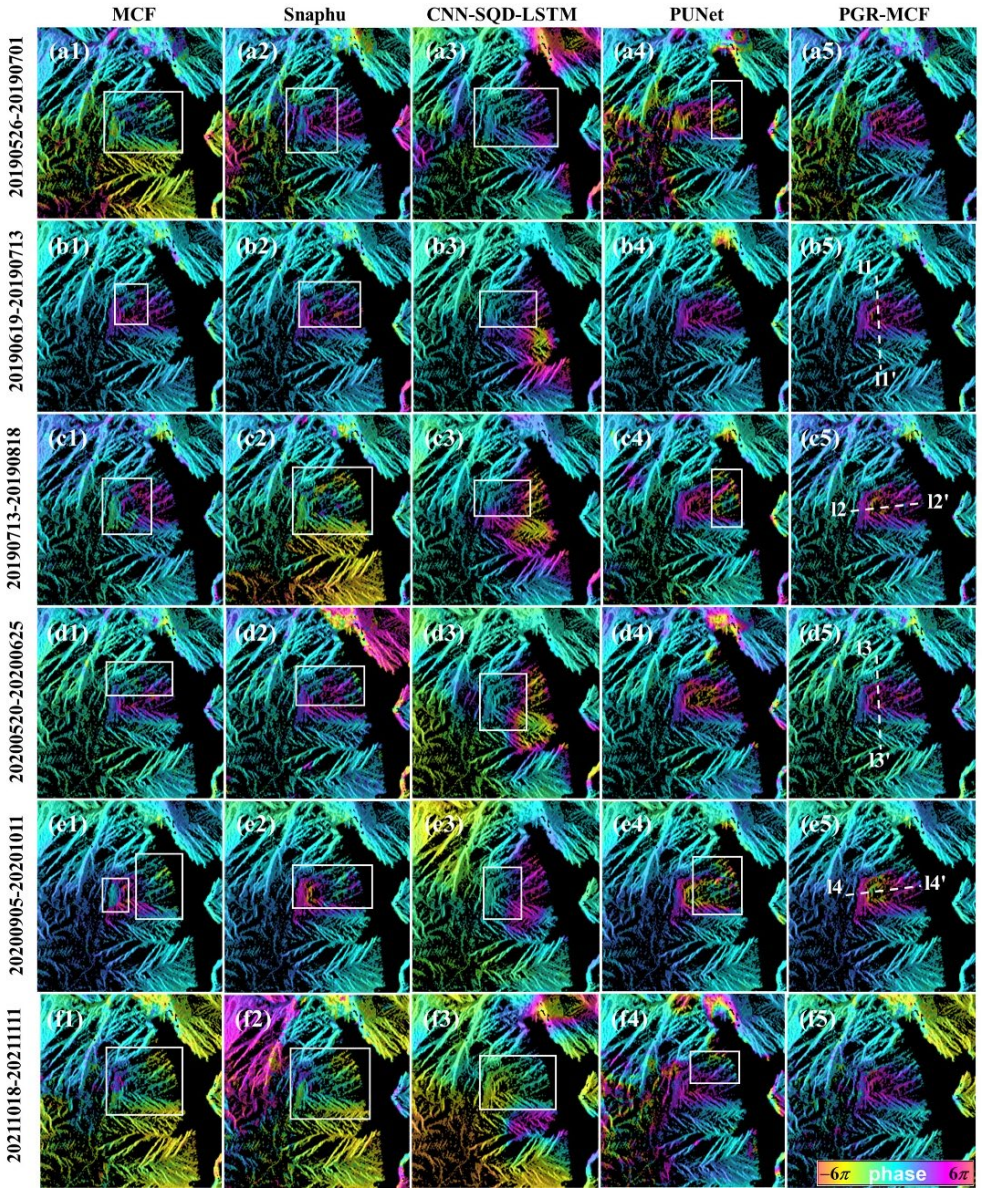
4. Guobu Landslide



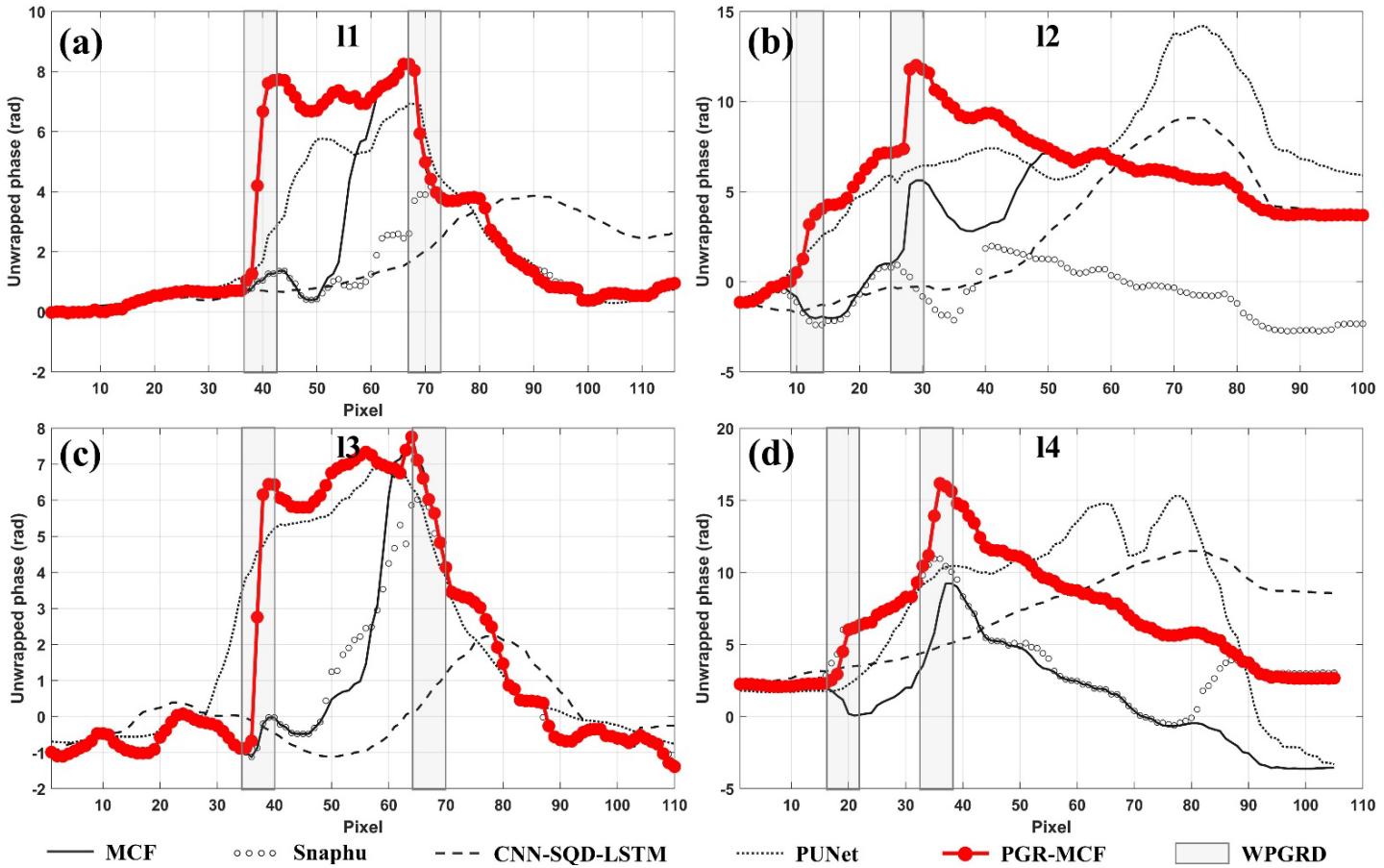
Study Area Overview: (a) Location of the Laxiwa Hydropower Station and the spatial coverage of the SAR imagery; (b) Panoramic photo of the Guobu landslide, where the red dashed line indicates the landslide boundary and the white dashed line outlines the strongly deformed zone of the Guobu landslide; (c) Geological cross-section of the Guobu landslide, adapted from (Lin et al. 2016; Shi et al. 2021; Shi et al. 2017).

- To validate the proposed algorithm's effectiveness in areas with large surface deformation gradients, we applied it to the Guobu landslide and compared it with existing phase unwrapping methods.
- The Guobu landslide is an active reservoir slope located just 500 meters from the Laxiwa Dam, with clear boundaries and visible cracks along the upper edge, indicating significant deformation compared to surrounding areas. This makes it an ideal test site for evaluating phase unwrapping methods.

4. Guobu Landslide

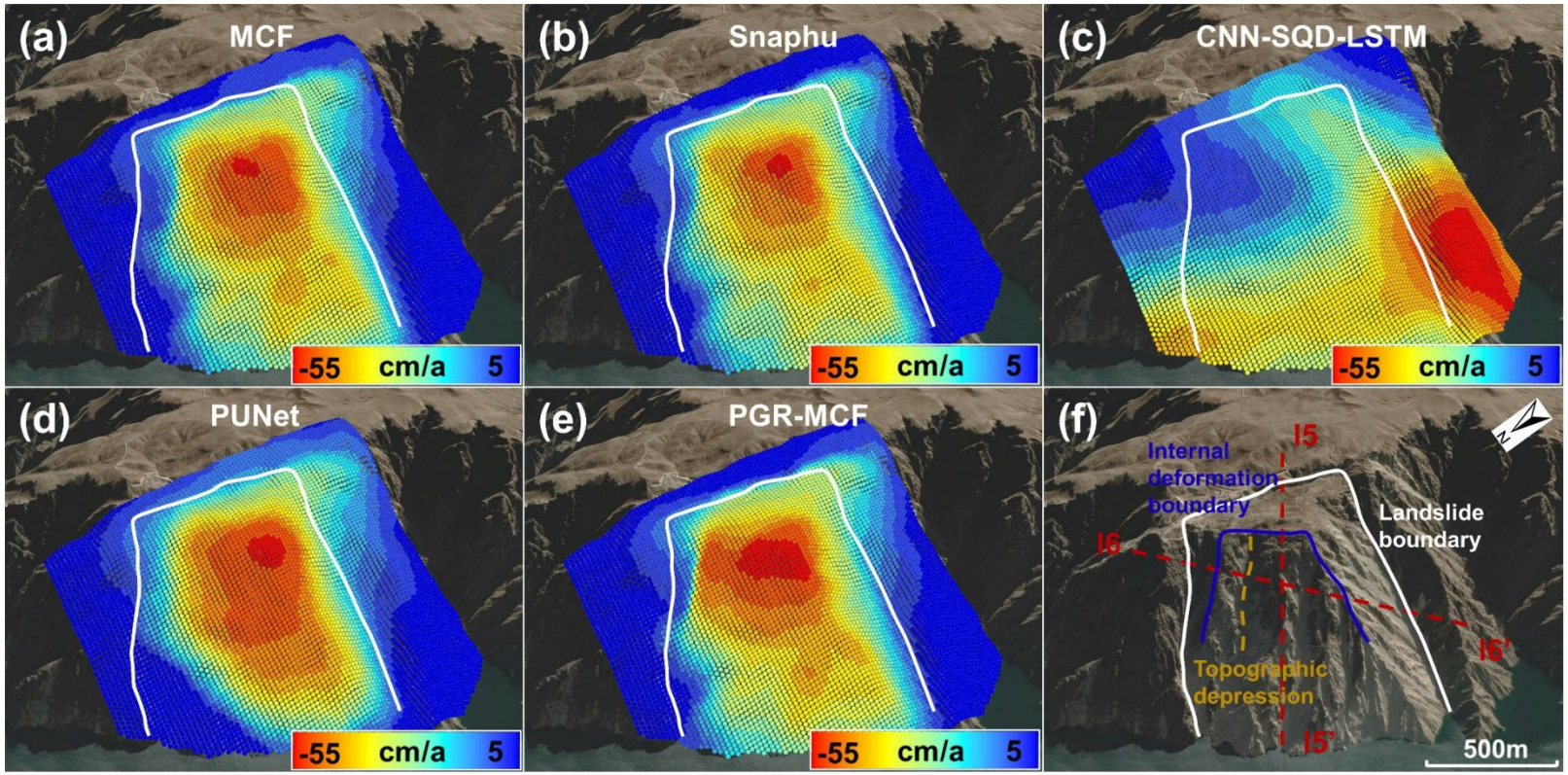


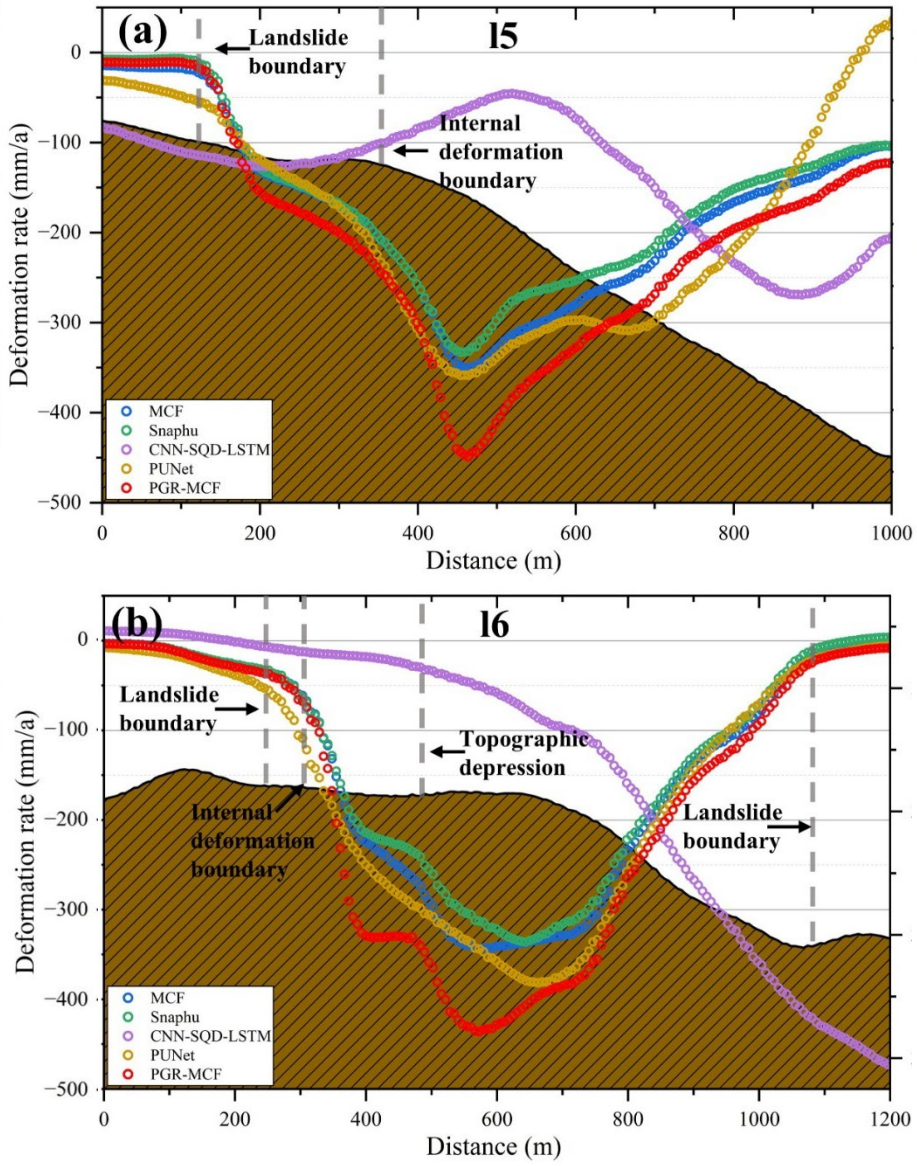
The left images show PU results from MCF, Snaphu, CNN-SQD-LSTM, PUNet, and PGR-MCF (left to right). White boxes highlight discontinuities, and white dashed lines indicate phase profile locations.



Phase Unwrapping Profile

4. Guobu Landslide





- **PGR-MCF produces continuous deformation fields with clear boundaries, while other methods tend to underestimate or oversmooth the deformation.**
- **The PGR-MCF method captures multi-stage deformation under complex terrain control: low-velocity deformation in the rear stable zone; gradual acceleration within the landslide body; and intense deformation beyond internal deformation boundaries.**

5. Method Advantages

1. PGR-MCF identifies high deformation gradient areas and optimizes the unwrapping path selection, effectively avoiding PU errors caused by large-gradient boundaries, making it especially suitable for high-gradient deformation scenarios.

2. Unlike traditional methods that require strict short temporal baselines and small deformation rate differences, PGR-MCF only needs boundary regions that meet these conditions to achieve correct unwrapping, thereby alleviating temporal baseline limitations in high-gradient deformation areas.

3. During unwrapping, PGR-MCF preserves the true phase structure of high-gradient regions and maintains clear boundaries, which helps enhance the physical interpretation of geological mechanisms.

4. It does not rely on external models, offering strong adaptability for unknown or sudden deformation areas.

Thank you for your attention!

Presenters: Xiaosong Feng

Email：2410440@stu.neu.edu.cn

Northeastern University, Shenyang, China

2025 DRAGON 6 SYMPOSIUM

14-18 JULY 2025

PROJECT ID. 95348

DEBRIS FLOW RISK ASSESSMENT VIA NUMERICAL SIMULATION: A CASE STUDY IN NORTHEAST CHINA

PUBLICATION:LANDSLIDES





1. Research Background and Significance



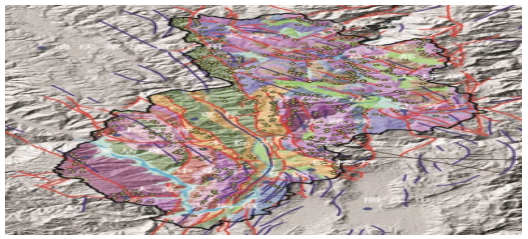
Debris flow is a common natural disaster in mountainous areas, usually accompanied by severe casualties and property losses.

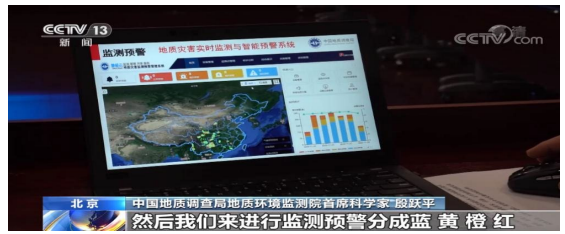
Climate change (extreme rainfall) is reshaping the pattern of debris flow disasters, leading to a large number of emerging debris flows occurring in traditionally non-high-risk areas.

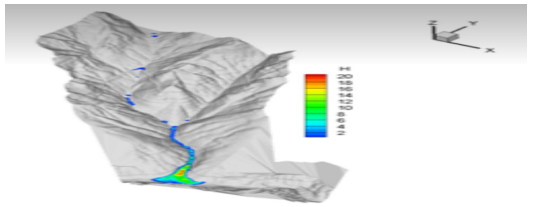
Assessing the risk of newly emerging high-risk debris flow areas, and realizing disaster deduction and damage assessment in these high-risk zones, are key directions for debris flow prevention and mitigation efforts.

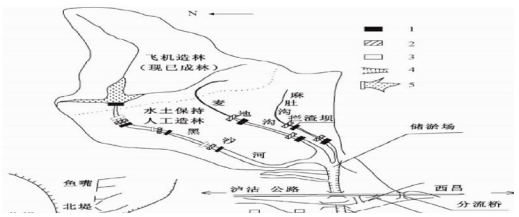
Aug 16-17, 2013: Heavy rains hit Fushun , triggering 18 debris flows and 294 suspected hazard points. 1 dead, traffic disrupted, losses at 660,000 yuan.

Aug 19-23, 2024: Rare heavy rains hit Jianchang, Liaoning, causing flash floods and debris flows in towns—10 dead, 14 missing, over 4,200 households flooded.









1. Research Background and Significance

- **Common methods:** Flow-2D, Massflow, SPH, OpenLISEM
- **Current status:** These models can finely reconstruct the entire debris flow process. However, complex models have high parameter requirements, hindering their promotion in data-scarce areas.
- **Advantages:** Complete simulation of physical processes, high spatial resolution, and support for deduction under different rainfall scenarios.
- **Limitations of existing methods:** Lack of simulation for building damage, vulnerability assessment relying on detailed damage information, and absence of response mechanisms for brick-wood structures in Northeast China.
- **Research focus of this paper:** Acquisition of input parameters in data scarcity, and complementation of simulation for building damage and losses.



Aerial photo: Guangxi "6·22" debris flow & landslide

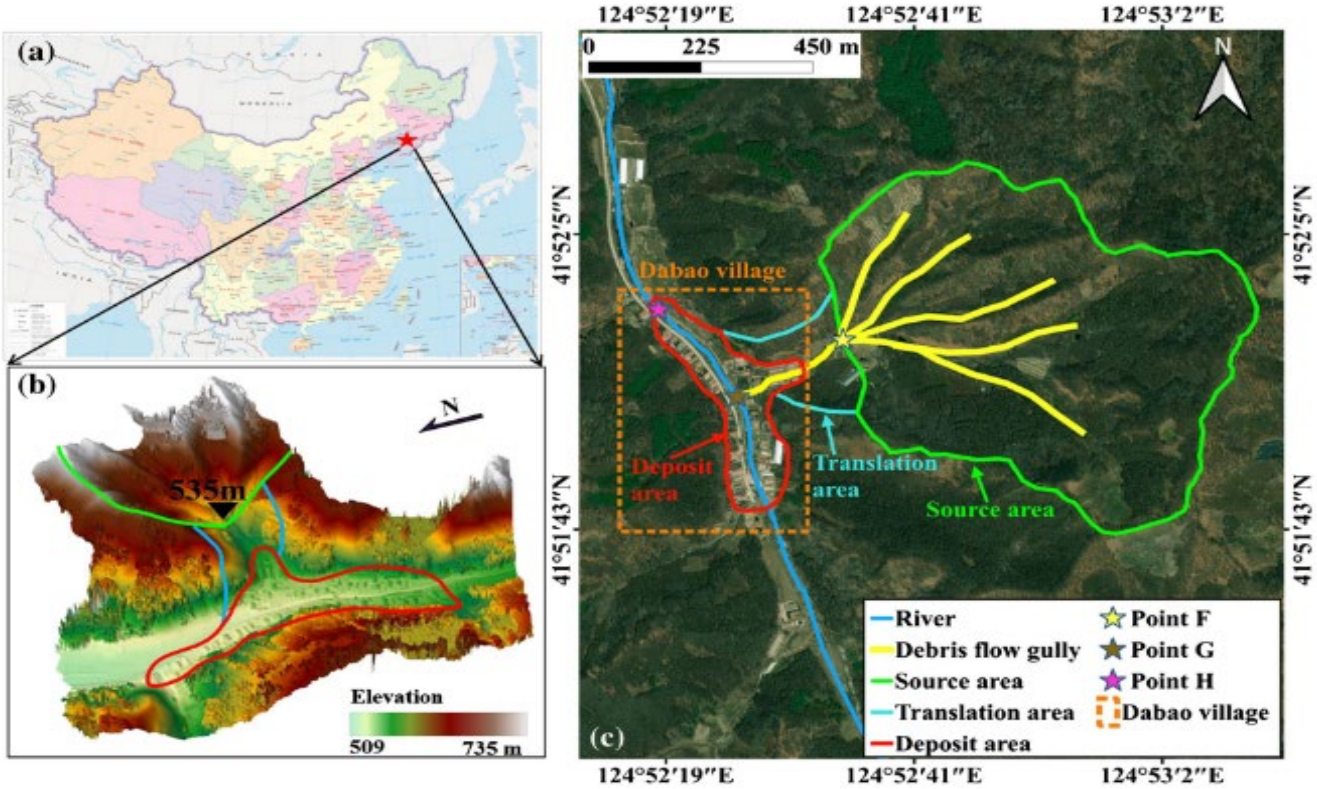


Damaged or destroyed houses in Jianchang

2.Study Area



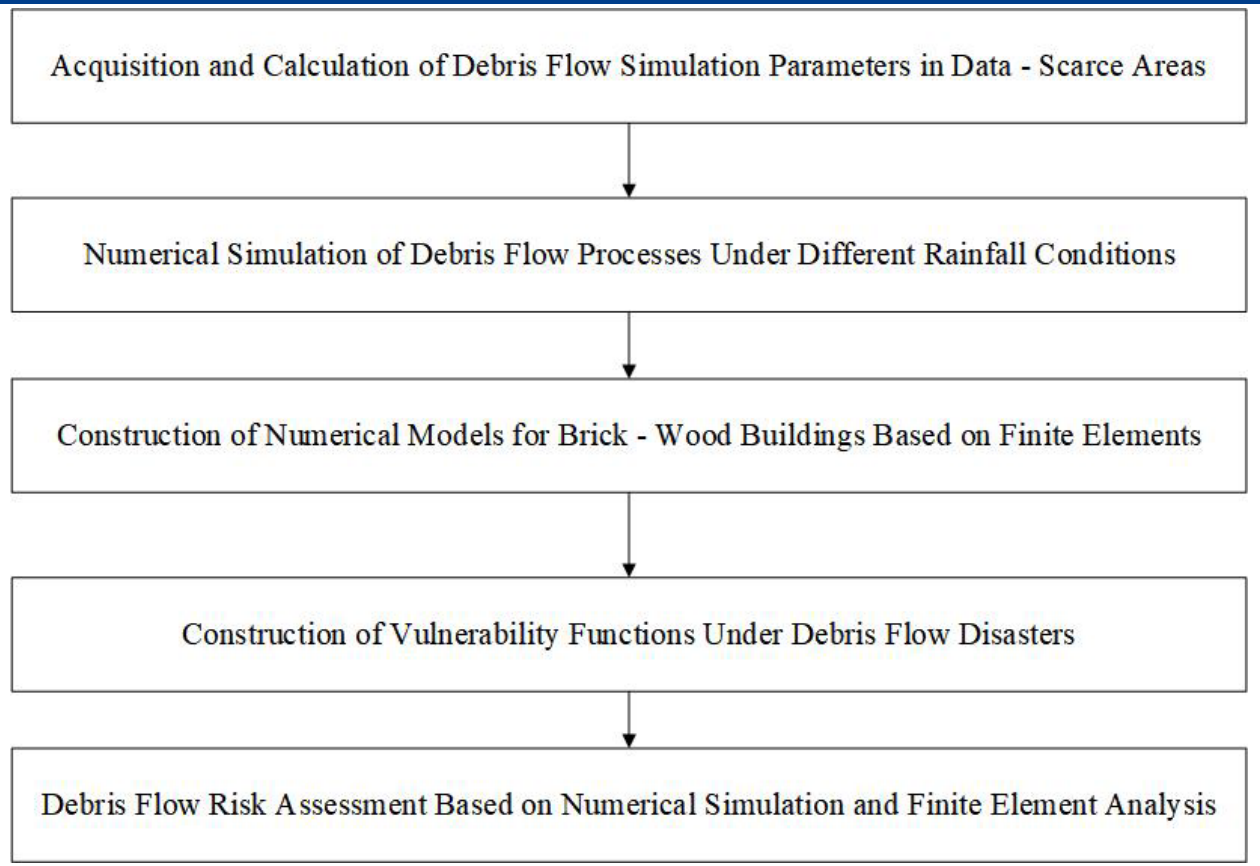
Actual photos of debris flow disaster sites in Liaodong



Schematic diagram of Wudaogou debris flow

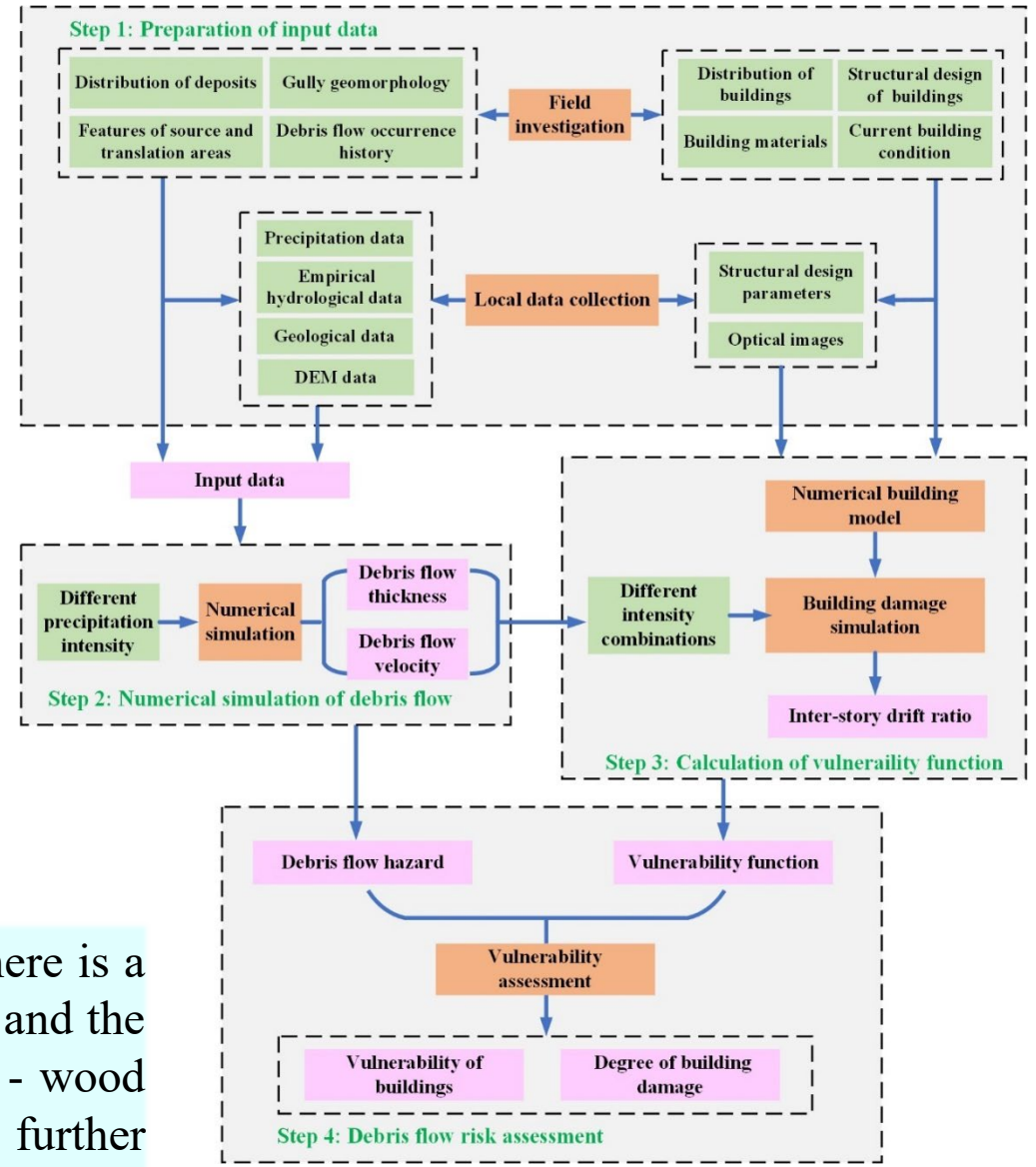
The Liaodong mountainous area is a debris flow hotspot in Northeast China, with many buildings along gullies facing high impact risk. Our study area, Fushun's Wudaogou, has been hit by frequent debris flows over the past decades. Field investigations reveal abundant loose solid materials in the basin, posing a high risk of re-triggering.

3.Methods and Technical Routes



Research workflow

To assess the damage of buildings under debris flow impact. When there is a lack of building damage information, combined with numerical simulation and the finite element model of buildings, the vulnerability of single - story brick - wood structure buildings under debris flow disasters is evaluated, and further quantitative risk assessment of debris flow is carried out.



The methodological framework adopted

4.1 Results: Acquisition and Calculation of Parameters

Based on the debris flow dynamic model, carry out the numerical simulation of the debris flow catastrophic process. The depth - integrated continuous medium model is adopted for the numerical simulation of debris flow. The mass and momentum equations of this model are:

$$\frac{\partial \mathrm{h}}{\partial t}+\frac{\partial \mathrm{hu}}{\partial x}+\frac{\partial \mathrm{hv}}{\partial y}=0$$

$$\frac{\partial \mathrm{hu}}{\partial t}+\frac{\partial(\mathrm{hu}^2+\mathrm{k}_{ap}gh^2/2)}{\partial x}+\frac{\partial \mathrm{huv}}{\partial y}=-k_{ap}gh\frac{\partial z_b}{\partial x}-\frac{(\tau_{zx})_b}{\rho}$$

$$\frac{\partial \mathrm{hv}}{\partial t}+\frac{\partial \mathrm{huv}}{\partial x}+\frac{\partial(\mathrm{hv}^2+\mathrm{k}_{ap}gh^2/2)}{\partial y}=-k_{ap}gh\frac{\partial z_b}{\partial x}-\frac{(\tau_{zy})_b}{\rho}$$

Formula for fluid impact and hydrological calculation

$$F_\delta=\lambda\frac{\gamma_c}{g}V_c^2 \qquad \tau=\mu\rho gh+\rho g\frac{U^2}{h\xi}$$

$$t_d=x(L_c/\sqrt{J})^y \qquad F=m\frac{dv}{dt}$$

$$S=h\cdot W$$

Rainfall-flood method and morphological survey method:

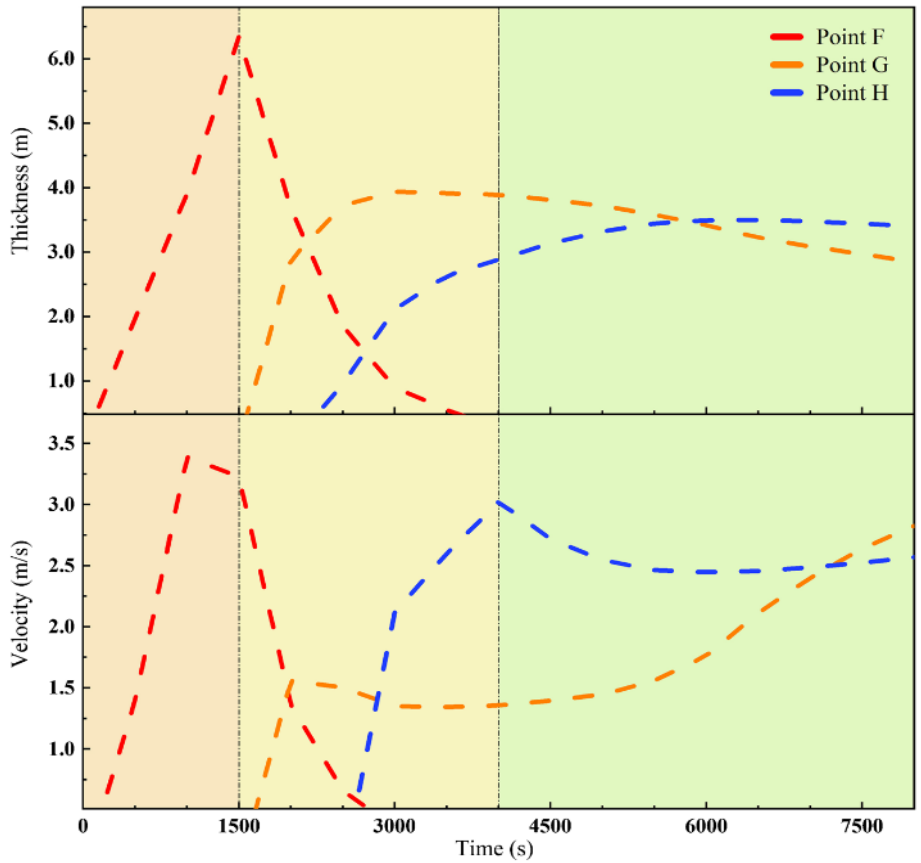
$$P_m=1-(1-\frac{1}{T})^m \qquad \varphi=(\gamma_c-\gamma_w)/(\gamma_H-\gamma_c)$$

$$Q_C=(1+\varphi)Q_pD \qquad \gamma_c=\frac{\gamma_wV_w+\gamma_HV_H}{V_w+V_H}$$

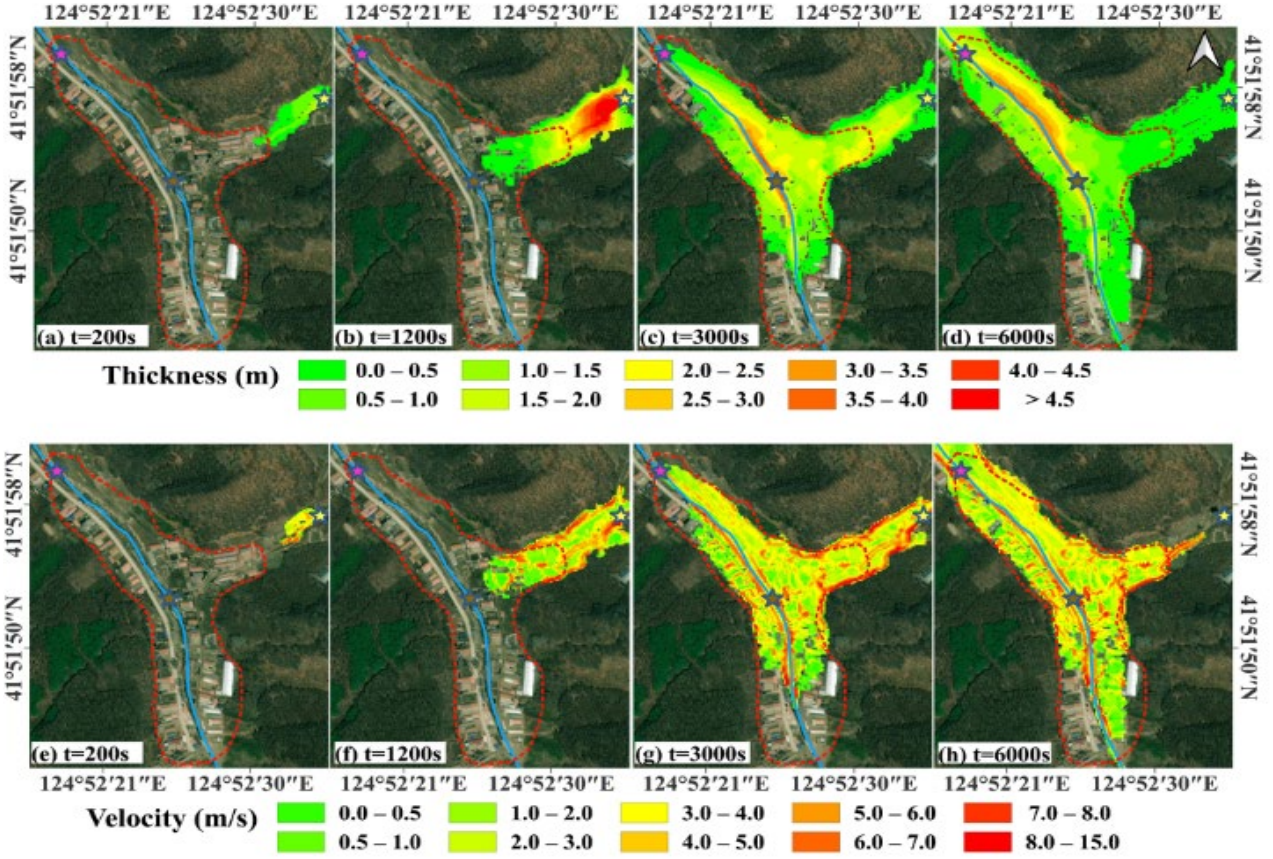
$$Q_P=0.278\psi\frac{P_\tau}{t_d}F$$

Numerical simulation of debris flows is realized based on the SCS - CN soil hydrological curve and the Massflow model. Effective acquisition of key parameters such as debris flow density, flood peak discharge, debris flow peak discharge and base friction coefficient is determined by adopting the morphological survey method, empirical formula (hydrological manual) method, rainfall - flood method and parameter inversion method.

4.2 Results: Numerical Simulation of Debris Flow



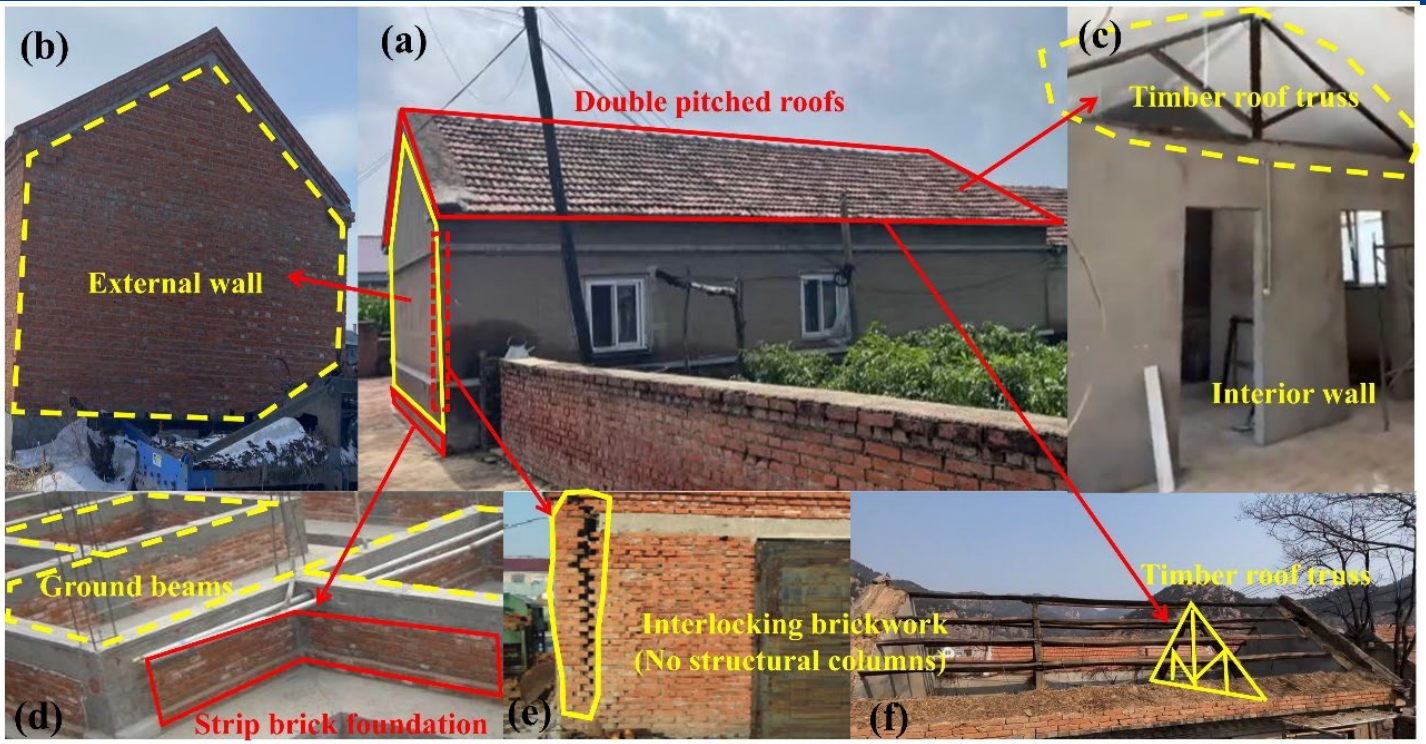
Key point: curve of flow thickness and velocity



Distribution of debris flow thickness and velocity at different times

Without the use of ground station data and field survey materials (for emerging disaster sites with scarce simulation data), the 2013 debris flow disaster process in this area was simulated and reconstructed based on satellite rainfall data and open-source hydrogeological information. The simulated flow velocity and accumulation thickness distribution are basically consistent with the actual disaster situation.

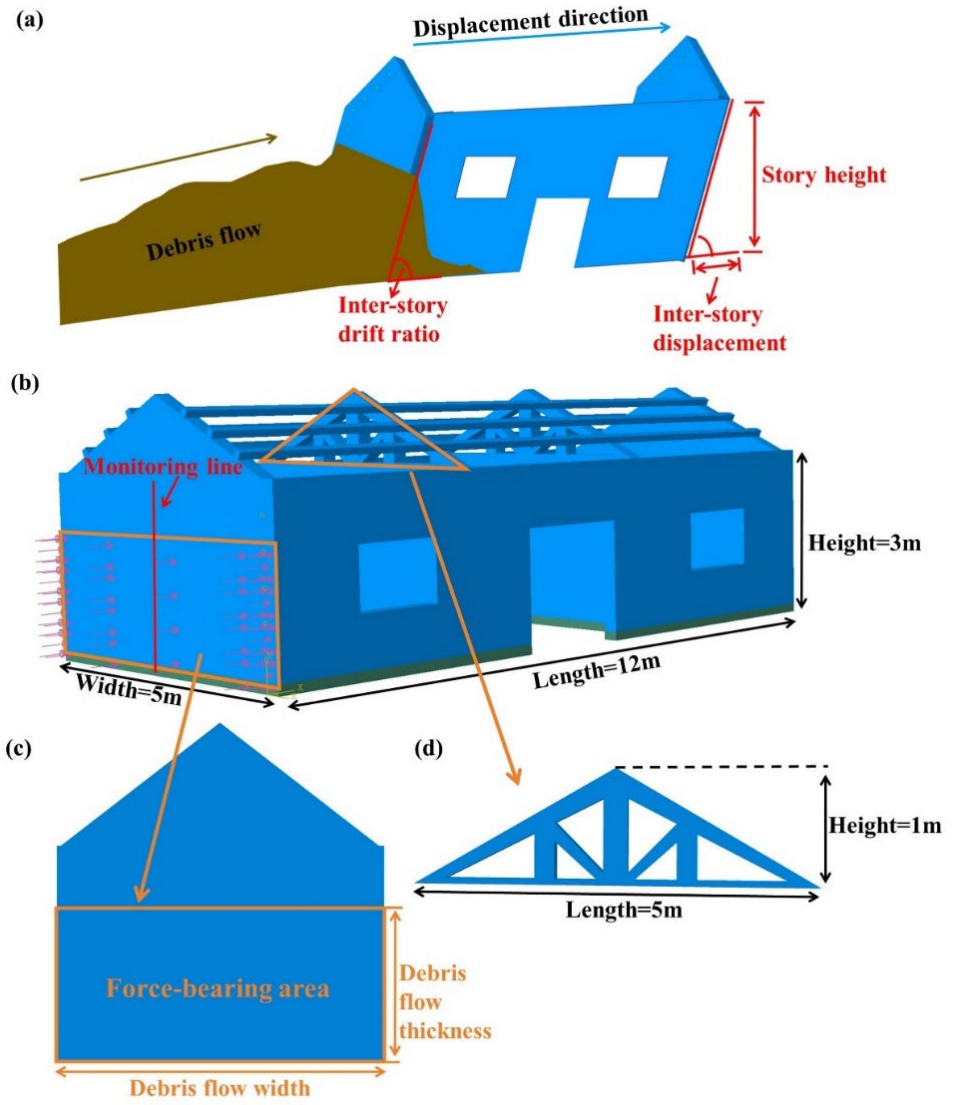
4.3 Results: Construction of Models for Buildings



Structural schematic diagram of single-story brick-wood structure buildings

To analyze the response of buildings under the impact of debris flows, a finite element model of the buildings was constructed. The structural dimensions and material parameters of the model were determined based on on-site inspections and relevant standards.

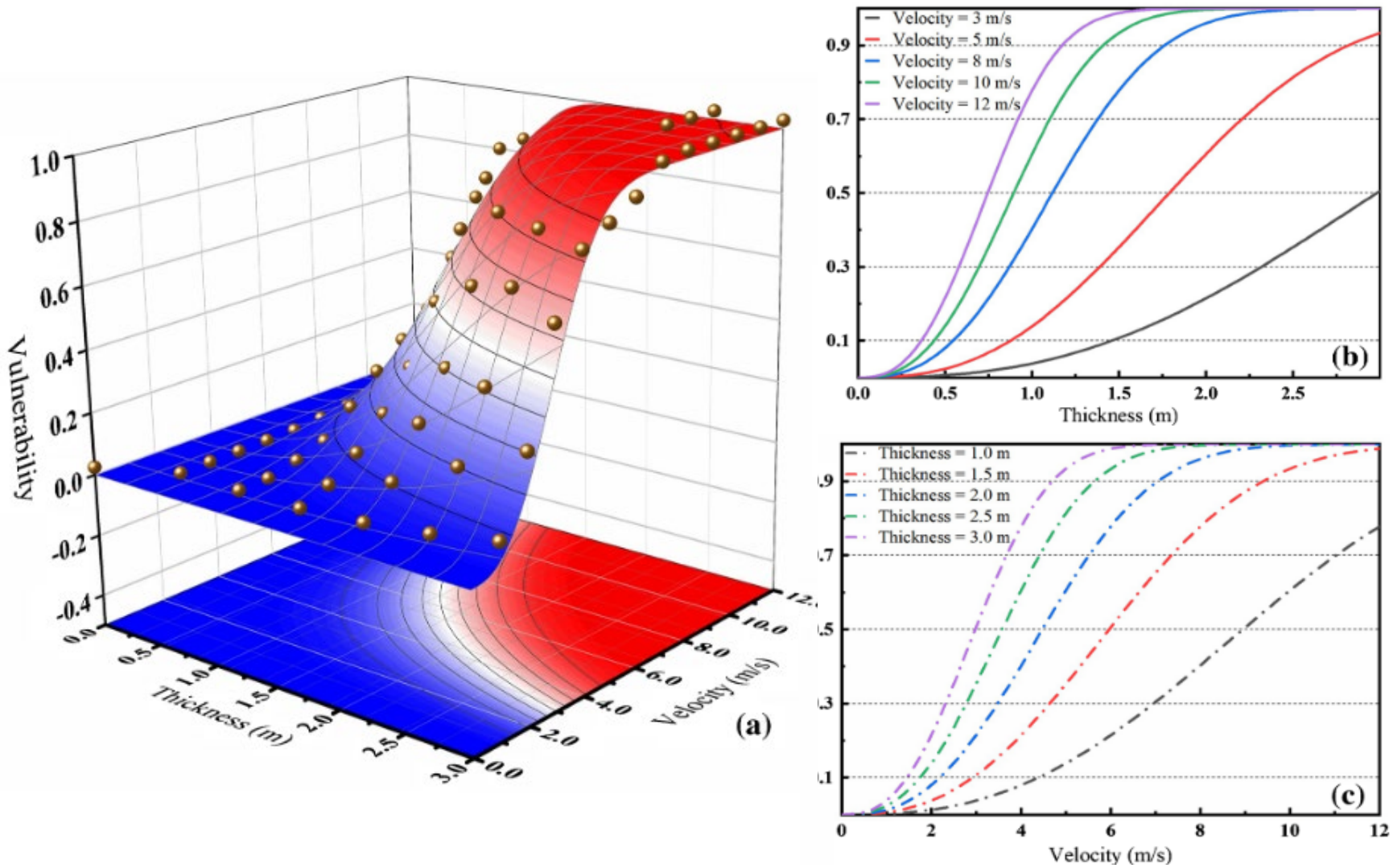
The inter-story drift angle was used to quantify the damage state of buildings caused by debris flow impact.



Schematic diagram of the building finite element model

4.3 Results: Construction of Vulnerability Functions

Seventy-two combinations of debris flow intensity are adopted to construct a three-dimensional vulnerability function of buildings with respect to debris flow thickness and velocity. This function comprehensively depicts the disaster-affected response characteristics of buildings, can reflect the impact resistance performance of brick-wood structures, and significantly improves the applicability and accuracy of physical vulnerability assessment for buildings.

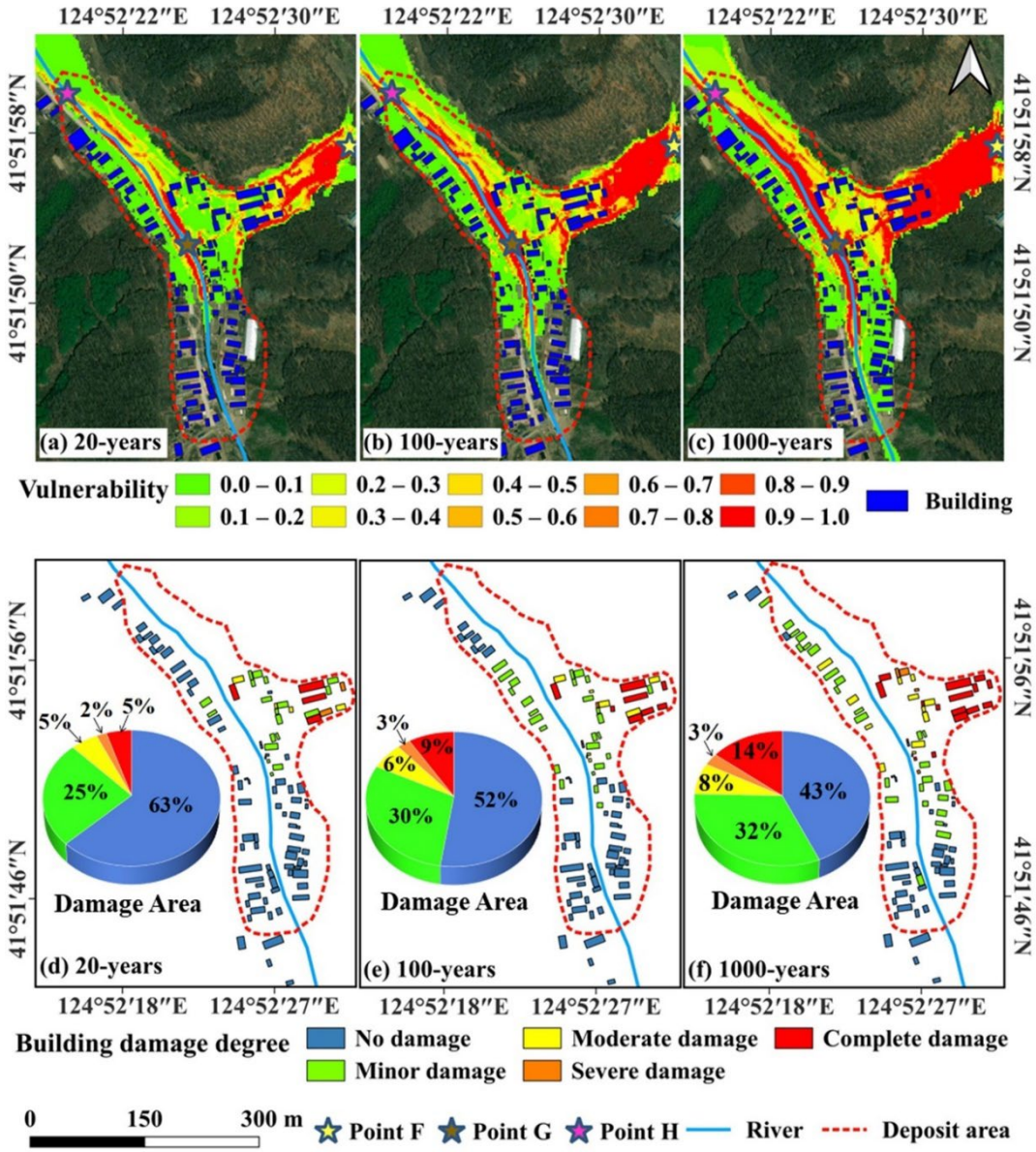


Three-dimensional vulnerability functions of the building: a three-dimensional vulnerability variation diagram ; b vulnerability variation associated to thickness; c vulnerability variation associated to velocity

4.4 Result : Debris Flow Risk Assessment

We have determined the potential damage scenarios of existing buildings in the area under varying intensities of debris flow impacts, and classified the disaster risk levels across different zones.

Precipitation recurrence interval (years)	Debris flow area (m^2)	Number of buildings at different damage levels				
		Complete	Severe	Moderate	Minor	No damage
20	42837.53	4	6	6	23	65
100	52556.32	7	5	8	32	52
1000	62131.31	14	2	9	36	43



5 Conclusion

This study explores the under-discussed physical vulnerability of single-story brick-wood structures in NE China under debris flows, using numerical simulations in the Wudaogou area.

- **Effective Outputs in Information-Limited Scenarios**

  Debris flow parameters (such as density, peak flood discharge, and peak debris flow discharge) are determined through morphological investigation, empirical equations, and rainfall-runoff methods. The simulation results for the 1000-year precipitation recurrence interval show high consistency with the 2013 catastrophic debris flow data.

- **Advantages of 3D Vulnerability Function**

  A 3D vulnerability function considering debris flow thickness and velocity is established for typical local structures. Notably, this simulation method does not require actual building damage information, offering a reference for vulnerability analysis in regions lacking historical disaster records.

Thank you for your attention!

Presenter: Xiangben Zhang
Email：2301122@stu.neu.edu.cn
Northeastern University, Shenyang, China